Fatty liver disrupts homeostatic functions of Kupffer cells in liver regeneration

Doctoral thesis

to obtain a doctorate (PhD)

from the Faculty of Medicine

of the University of Bonn

Ioannis Panetas

from Athens, Greece

2022

Written with authorization of

the Faculty of Medicine of the University of Bonn

First reviewer: Prof. Dr. Zeinab Abdullah

Second reviewer: Prof. Dr. Kathrin Paeschke

Day of oral examination: 24.03.2022

For the Institute of Molecular Medicine and Experimental Immunology (IMMEI)

Director: Prof. Dr. Christian Kurts

Table of Contents

List of abbreviations

ALT	Alanine aminotransferase
ALR	AIM2-like receptor
ALI	Acute liver injury
ANOVA	Analysis of Variance
BM	Bone marrow
BM-KC	Bone marrow differentiated Kupffer Cells
BM-MΦ	Bone marrow derived Macrophages
BW	Body weight
CCL	Chemokine (C-C motif) ligand
CCNA2	Cyclin A2
CDC	Centers for Disease Control and Prevention
CDK1	Cyclin-dependent kinase 1
CFP	Cyan fluorescent protein
CFSE	Carboxyfluorescein succinimidyl ester
Chrm3	Cholinergic Muscarinic Receptor 3
CLEC4F	C-Type Lectin domain Family 4 Member F
CLR	C-type lectin receptors
C-Met	Tyrosine-protein kinase Met
CSF1r	Colony stimulating factor 1 receptor
CT	Computed tomography
CYP2E1	Cytochrome P450 Family 2 Subfamily E Member 1
DAMPS	Damage-associated molecular patter molecules
DILI	Drug induced liver injury
ECM	Extracellular Matrix
EGF	Epidermal Growth Factor
EMP	Erythromyeloid progenitors
Em-KC	Embryonically derived Kupffer Cells
FFA	Free fatty acid
FOXM1	Forkhead Box M1

GEO	Gene expression omnibus
GFP	Green fluorescent protein
HB-EGF	Heparin binding epidermal growth factor
HCC	Hepatocellular Carcinoma
HFD	High Fat Diet
HGF	Hepatocyte Growth factor
HMGB1	High mobility group box 1
HSC	Hepatic stellate cell
Id3	DNA-binding protein inhibitor ID-3
IL-6	Interleukin 6
JAM-A	Functional Adhesion Molecule A
KC	Kupffer Cells
LiMAx	Liver function capacity test
LPS	Lipopolysaccharide
LSEC	Liver sinusoidal endothelial cell
LW	Liver Weight
LXRα	Liver X receptor α
MCD	Methionine-choline deficient diet
MEF	Mouse embryo fibroblasts
MFSD2A	Major Facilitator Superfamily Domain Containing 2A
MYD88	Myeloid differentiation primary response 88
NAFLD	Non-alcoholic fatty liver disease
NASH	Non-alcoholic steatohepatitis
ND	Normal diet
NF-kB	Nuclear factor 'kappa-light-chain-enhancer' of activated B-cells
NPC	Non-parenchymal cell
NLR	Nucleotide-binding oligomerization domain-like receptors
PAMPS	Pathogen-associated molecular patterns
PhX	2/3 Partial Hepatectomy
RFP	Red fluorescent protein

ROS	Reactive oxygen species
STAT3	Signal transducer and activator of transcription 3
TAM	Tamoxifen
TGFα	Transforming growth factor-alpha
Timd4	T-cell immunoglobulin and mucin domain containing 4
TLR	Toll-like receptors
TNFα	Tumor necrosis factor α
TNFR-I	Tumor necrosis factor receptor 1
YFP	Yellow fluorescent protein
YS	Yolk Sac

1. Introduction

1.1 Innate immunity from liver homeostasis to progression of obesity-induced inflammation

The liver is the largest solid organ of the human body. Its wide range of functions are related with the removal and addition of compounds from and to the bloodstream, while circulating through the microanatomical functional units (lobules). The liver is the main secretion source of unique body components, such as the bile, that supports the digestion of lipids in the small intestine, albumin as the main protein component of the human blood plasma and blood coagulation factors secreted by hepatocytes (Heinz and Braspenning, 2015).

In addition to the secretion of compounds, the liver also possesses the unique capacity of detoxifying the blood by modifying and transforming compounds in a less toxic form, which can be eliminated or tolerated by the body. In contrast, other compounds are not modified or eliminated, but are stored in the liver. Examples are some classes of carbohydrates (glycogen, etc.), vitamins, iron but also fat.

The liver is located on the frontline of the body, being the first organ that encounters bacteria, viruses and food antigens derived from the gut which can reach the liver through the portal vein. Elimination of dead erythrocytes and tumor cells also takes place in the liver.

Two large vessels supply the liver with blood. Those are the portal vein and the hepatic artery, which supply the liver with blood from the gastrointestinal tract and the heart, respectively. The nutritious and antigen-containing blood from the portal vein, merges with the oxygenated blood from the hepatic artery and flows along the capillaries, known as sinusoids (Fig 1). Sinusoids are constituted by lined liver sinusoidal endothelial cells (LSECs). Liver-resident macrophages (Kupffer cells) reside along the sinusoids and together with LSECs constitute the most powerful scavenger system of the body (Sørensen *et al.,* 2015).

The position of the liver in the frontline of immune activity, attributes to its microarchitecture design, with Kupffer cells having the mission to detect, capture and clear antigens, as well as maintaining a tolerogenic function to regulate inflammation. The importance of those functions are reflected in the liver innate immune system,

containing the largest pool of phagocytes in the human body and their potential to promote, among other properties, antigen-specific tolerance (Heymann *et al.*, 2015; Robinson *et al.*, 2016).

1.1.1 Features and origin of Kupffer Cells in liver homeostasis

A tight balance between tolerance and immunity is required for the homeostatic function of the liver. Innate immune cells and specifically liver macrophages are the immune cell population that has the potential to maintain this balance.

Among the different macrophages that can be found in the liver, Kupffer cells (KC's) represent the liver-resident macrophages, which reside in a strategic position along the sinusoids, with unique properties in clearance of foreign and altered-self substances from the bloodstream, in liver injury and metabolism (Nguyen-Lefebvre and Horuzsko, 2015). Kupffer cells are the most abundant immune cell population in the liver during homeostasis, located within the sinusoidal wall, while being in contact *via* their protrusions with the space of Dissé (space between the epithelium and the sinusoids) (Bouwens *et al*., 1986; Frevert *et al*., 2006; Motta, 1984). Recently, establishment of direct interactions of the latter with hepatocytes and hepatic stellate cells has been documented (Bonnardel *et al*., 2019).

A lot of research has been focused on the expression of transcription factors of liver resident KC that "program" their identity and adaptation in the liver microenvironment. By obtaining such an identity, Kupffer cells perform their homeostatic functions in the liver. For instance, inactivation of Id3 impairs Kupffer cell development leading to their deficiency in adults (Mass *et al*., 2016). Furthermore, Kupffer cells are also characterized by increased expression of genes associated with uptake, modification, and export of cholesterol when compared with other tissue-resident macrophages. Such genes are under control of the transcription factor LXRα expressed in Kupffer cells (Joseph *et al*., 2003).

Till date, there is a debate concerning the origin of the tissue-resident macrophages. Sheng *et al*. (2015) indicated an exclusive origin of tissue macrophages from fetal liver HSCs. However, this view has changed since it was indicated that proportions of tissue-resident macrophages such as F4/80^{hi} Kupffer cells, are derived from EMP (erythron-myeloid precursors) that emerge in the yolk sac at E8.0 (Gomez Perdiguero *et al*., 2015; Schulz *et al.*, 2012; Stremmel *et al*., 2018). Specifically, the tissue-resident

Kupffer cells arise *via* the MΦ ancestor populations A1 ($CD45^+$c-$kit^{lo}CX_3CR1^{lo}F4/80^{lo}$) and A2 ($CD45^+$c-$kit^-CX_3CR1^{hi}F4/80^{hi}$) in the yolk sac. After birth, YS derived macrophages are partially displaced by fetal liver derived HSCs, but a proportion of YS Kupffer cells remain in adult life (Sheng *et al*., 2015, Hagemeyer *et al*., 2016; Hoeffel *et al*., 2012). Kupffer cells are self-maintained through adult life with no contribution of bone marrow cells to the macrophage pool in homeostatic conditions (Hashimoto *et al*., 2013; Yona *et al*., 2013).

Together with universal markers (F4/80, Tim4, CD64, etc.), which are expressed in most tissue-resident and bone marrow-derived macrophages (BM-MΦ), Kupffer cells are also characterized by the unique expression of the C-Type Lectin protein Clec4f (Lavin *et al*., 2014a; Scott *et al*., 2016). The biological function of this surface marker on Kupffer cells remains elusive, while emerging studies indicate the absence of a human ortholog in humans (Taylor *et al*., 2019). The use of this marker combined with advanced fate mapping strategies is very useful for discriminating embryonic Kupffer cells (em-KC) from BM-derived macrophages (BM-MΦ) in various inflammatory models.

1.1.2 Dynamics and functions of macrophage subsets in the inflammatory liver

The origin and function of macrophages in the liver becomes more complicated during liver inflammation. This complexity can be explained by the presence of multiple progenies of macrophages simultaneously in the liver. In mice, depending on the severity and longevity of the liver injury (acute or chronic), the number of embryonic Kupffer cells decreases, followed by recruitment of $F4/80^+Ly6C^{hi}$ bone marrow-derived macrophages (Dambach *et al*., 2002; Holt *et al*., 2008; Karlmark *et al*., 2009; Zigmond *et al*., 2014). For instance, in experimental liver fibrosis, the physiological response of wound healing after injury, leads to the accumulation of extracellular matrix (ECM) and infiltration of bone marrow-derived macrophages ($F4/80^+Ly6C^{hi}$) which are linked to further progression of fibrosis in mice (Ehling *et al*., 2014; Mitchell *et al*., 2009; Wynn and Vannella, 2016). Similarly, in mouse models of acute liver injury, a single dose of a hepatotoxic carbon tetrachloride (CCl_4), promotes apoptosis of Kupffer cells and accumulation of $CD11b^+$ macrophages, which aggravate the hepatic injury (Karlmark *et al*., 2009).

In the context of infection, Kupffer cells play an important role in both clearance and capture of pathogens as well as apoptotic host cells. By phagocytosing activated and apoptotic neutrophils, KCs are regulating the course of liver inflammation (Shi *et al*., 2001; Shi *et al.*, 1996). Recruitment of other cell types into the liver can also be exhibited by KCs. Neutrophils that kill bacteria during *Listeria monocytogenes* infection are recruited to the liver by KC *via* macrophage inflammatory protein-2 (MIP-2) and other cytokines (Ebe *et al*., 1999).

Common features of the Kupffer cell dynamics are present independently of the liver disease model and source of injury. The repopulation or replenishment of KC by recruited bone marrow-derived monocytes that differentiate into KC is a field of intensive research. Using genetic tools of KC depletion and various infection models researchers showed that Kupffer cells are replenished by bone marrow-derived monocytes that are recruited to the liver and differentiate into KC (Blériot *et al.*, 2015; Borst *et al*., 2018; Scott *et al*., 2016). In the case of genetic depletion of KC, the repopulation of the niche is achieved through competition between proliferation of KC and bone marrow-derived macrophages. The recruited bone marrow-derived MΦ will gradually acquire the transcriptomic signature and a similar function with embryonic Kupffer cells, through signaling from the liver microenvironment (Scott *et al*., 2016).

The presence of phenotypically different populations of hepatic macrophages in the liver, translates into an altered contribution in the homeostatic functions. In many cases, such a disbalance can further elevate the progression and severity of a disease.

1.1.3 Pathology and triggers of obesity-induced liver inflammation

Diet-induced obesity is a type of mild metabolic inflammation (meta-flammation), targeting different organs, including the liver, that in turn can alter its physiological mechanisms.

Obesity is a fast-growing health concern, specifically characterizing western societies. According to statistics from the CDC in 2017-2018, the prevalence of obesity among US adults was 42.4%, whereas 9.2% were severely obese (Hales *et al*., 2017). The causes of this prevalence are related to increased intake of high fat and high sugar context of food, while a decreased physical activity characterizes some modern societies. Although obesity represents a reversible state, it can lead to serious health

complications in the long term, such as heart diseases and strokes, type II diabetes and some forms of cancer.

Among the mentioned above health complications, obesity leads to fat accumulation in the liver parenchyma affecting its function and leading to non-alcoholic fatty liver disease (NAFLD). The term NAFLD describes a spectrum of chronic liver disease ranging from simple steatosis to hepatic inflammation, hepatocellular ballooning degeneration (NASH) and can progress further to fibrosis and cirrhosis. Non-alcoholic fatty liver disease (NAFLD) and steatohepatitis (NASH) are correlating with the metabolic syndrome and as it is suggested by its name, this spectrum excludes all groups of patients with excessive consumption of alcohol. The hallmark of NAFLD is a transient triglycerides lipid accumulation in liver parenchymal cells in forms of micro or macro vesicular lipid droplets within the hepatocytes (steatosis). Although it was initially believed that steatosis is the first "hit" of NAFLD followed by a second hit of lipo-toxicity and necroinflammation (Day, 2006; Day and James, 1998), this dogma might be over-simplistic to characterize the progression of NAFLD. In fact, lipid droplets stored in hepatocytes seem to be the outcome rather the trigger. The increased uptake of fat and sugar results in an increased influx of free fatty acids (FFA´s) within the liver. This influx is the metabolic cargo that promotes lipo-toxicity and ER stress, associated with further progression of NAFLD (Özcan *et al.*, 2004; Pardo *et al*., 2015; Pfaffenbach *et al*., 2010). Followingly, the development of lipo-toxicity, reactive oxygen species (ROS), ER stress and cellular damage, trigger hepatocellular apoptosis and necrosis. Ultimately, when this state persists, it progresses to stellate cell activation and fibrogenesis. As a counterbalance mechanism, triglyceride accumulation occurs in hepatocytes, reflecting the ongoing metabolic changes and need for storing of potentially toxic FFAs in the form of triglyceride droplets (Neuschwander-Tetri, 2010).

On a molecular level, NAFLD leads to the release of damage-associated molecular patterns (DAMPs), upon cell death or injury. In the case of NAFLD and NASH, hepatocyte apoptosis followed by DAMPs release is a key sterile inflammation inducer (Csak *et al.*, 2011; Peverill *et al*., 2014). Some examples of DAMPs related to liver disease during obesity are the High-Mobility Group Box 1 (HMGB1), nuclear or mitochondrial DNA and ATP (Gan *et al*., 2014; Xiao *et al*., 2012).

In addition, pathogen-associated molecular patterns (PAMPs) play a significant role in the development and severity of liver disease during NAFLD. PAMPs are bacterial or viral products recognized by innate immune cells, promoting inflammatory responses that can amplify the severity of chronic liver inflammation and have been detected in NAFLD and NASH patients. The best characterized example of PAMPs involved in NAFLD is endotoxin (lipopolysaccharide/LPS). LPS is a product of the cellular membrane of Gram-negative bacteria that can reach the liver only in cases where disruption of the intestinal barrier has occurred. The tight junctions of the mucosal barrier are disrupted in NAFLD and NASH patients. Emerging data suggest a strong correlation between NAFLD and intestinal permeability, and this was attributed to hepatic injury and metabolic inflammation according to a metadata analysis of 5 different clinical studies (Luther *et al.*, 2015). The functional alterations that occur, have been found to be linked to decreased expression of Claudin proteins, which normally act as a mucosal barrier of the intestine (Ahmad *et al*., 2017; Garcia-Hernandez *et al.*, 2017). JAM-A (Junctional Adhesion Molecule A) is another important adhesion molecule, whose loss from the intestinal junctions leads to severely induced steatohepatitis in mice fed a high fat diet (Laukoetter *et al*., 2007; Rahman *et al*., 2016).

Supporting the studies of the structural identification of a leaky gut, studies in both mice and humans with NAFLD or NASH showed that significantly increased levels of LPS are translocating from the intestinal barrier and through the portal vein into the liver and can also be detected in the serum (Bergheim *et al*., 2008; Miele *et al.*, 2009; Sabaté *et al*., 2008).

1.1.4 Role of Kupffer cells in the progression of obesity-induced inflammation

Innate immune cells have a dynamic role in the pathogenesis as well as the progression of NAFLD. To begin with, the recognition of the previously mentioned PAMPs is initiated by innate immune cells, possessing pathogen recognition receptors (PRRs). Such receptors are Toll-like receptors (TLRs), C-type lectin receptors (CLRs), nucleotide-binding oligomerization domain-like receptors (NLRs), retinoic acid-inducible gene-I-like receptors (RLRs), and the AIM2-like receptor (ALR).

Depending on the type of stimulation and the presence of cytokines, the activation of macrophages was initially classified based on their differentiation stage to proinflammatory M1 macrophages and immunoregulatory M2 macrophages (Mills *et*

al., 2000). This view has changed over the years and proved today to be over-simplistic to reflect the spectrum of all tissue macrophages and their polarization upon different stimuli (Guillot *et al*., 2019).

In the liver tissue, TLR4 is one of the most studied KC receptors, associated with their activation and progression of NAFLD. Through TLR4, KC recognize LPS on their surface. The activation of TLR4 requires the co-receptors CD14 and MD-2 which then activate an inflammatory cascade (Akira and Takeda, 2004; Kim *et al*., 2007). The role of TLR4 in disease progression has been studied extensively in NAFLD murine models. Specifically, using a methionine choline-deficient diet (MCD), Rivera and colleagues (Rivera *et al*., 2007) showed an enhanced expression of TLR4 in the liver, alongside translocation of LPS from the intestine to the liver in MCD-fed mice. Moreover, genetic ablation of TLR4 has a protective effect against disease progression and reduced expression of fibrogenic markers *(Csak et al*., 2011).

The activation of TLR4 on KC surface favors an inflammatory phenotype characterized by the production of pro-inflammatory cytokines such as TNFα, IL-1β and IL-12. This kind of activation, which has been the old dogma of M1-activated macrophages, can further promote hepatic cell injury and release of DAMPs creating a feedback loop of macrophage activation and liver damage (Grunhut *et al*., 2018). This is in line with studies where significantly decreased inflammation was observed in obese mice where KC were depleted using clodronate liposomes (Duffield *et al.*, 2005; Huang *et al*., 2010). Of note, lipid storage in KC may also play a role in the activation and inflammatory phenotype of KC in NAFLD (Leroux *et al*., 2012).

1.1.5 Recruitment of bone marrow-derived macrophages in NAFLD

In homeostatic conditions, there is only a minimal contribution of BM-MΦ in the liver macrophage pool. Most macrophages in steady state are represented by Kupffer Cells, which can self-renew. However, during the ongoing inflammation in NAFLD, the activated embryonically derived KC have the potential of recruiting bone marrow-derived macrophages into the liver. Whether this recruitment is a result of KC death and the necessity for their replenishment or a mechanism to promote liver inflammation is under debate.

In a study using high fat diet-fed mice and bone marrow chimeras, Morinaga and colleagues (Morinaga *et al*., 2015) showed an increased expression of CCL2 chemokine on KC and at the same time 5-fold increase in the expression of the receptor CCR2 on the recruited liver monocytes. Increased influx of $CD11b^{+}Ly6C^{+}$ monocytes is followed by their rapid differentiation towards inflammatory macrophages, a process dependent on MYD88, giving rise to two different subpopulations of macrophages in the liver (Deng *et al.*, 2009). The findings above were also in line with a clinical study of obese individuals, where the severity of liver disease was positively correlated with the presence of $CCR2^{+}$ monocyte-derived cells (Krenkel *et al*., 2018).

1.2 Impact of obesity on the liver regenerative response to hepatectomy

Liver inflammation among NAFLD patients also affects the physiological function of the liver, while increasing the risk for progression to fibrosis, cirrhosis, and hepatocellular carcinoma (HCC). This type of cancer can occur in NASH patients with or without the presence of cirrhosis (Piscaglia *et al*., 2016). The prevalence of HCC occurring due to obesity in 2010 is estimated to be around 2.6% compared with 4% of the respective prevalence of the viral induced HCC, in the United States (Ascha *et al.*, 2010). This initially low percentage has already increased since 2010 and is estimated to further increase in the future, leading to an increased liver-related mortality among obese patients, according to epidemiologic models (Estes *et al*., 2018). Currently, HCC is the sixth most occurring type of cancer in the world while being the third most common cause of cancer-related mortality (McGlynn and London, 2011).

In the effort to prevent metastasis of HCC, the tumor is removed from the patients alongside healthy liver tissue surrounding the tumor. Depending on the size and number of tumors, partial or major hepatectomy can be employed. A major resection includes the removal of 5 or more liver segments during the operation (Morris-Stiff *et al*., 2016). The outcome of such an operation besides the removal of tumors, is the regeneration of the healthy liver tissue which is performed by the liver's unique regenerative capacity. This ability of the liver to regain its size and functionality, can be hampered by different factors and preconditions, including obesity and NAFLD. In both, human clinical studies and animal experiments, impaired regeneration of the liver after hepatectomy has been observed in obese individuals.

Impaired liver regeneration leading to liver failure is one of the most common complications and causes of death after such operation, while other operative complications that might arise (bleeding, etc.) are nowadays controlled (Rahbari *et al*., 2011; Yamamoto *et al*., 2016). Till date, different factors limited the generation of safe results concerning obese individuals and their outcome of liver regeneration after a liver insult. The underlying health conditions (HCC, etc.) may influence the regenerative capacity in clinical studies where the liver mass recovery of obese patients is compared with normal body weight patients. Additionally, a very often volumetric examination will be needed over a long period of time to track the mass restoration, even if it is not a necessary procedure for the well-being of the patient.

One of the first clinical studies addressing this matter was performed by Truant *et al*. (2013). This was a case-matched study of 84 patients split in 2 groups of obese and non-obese patients where the rate of liver volumetric gain 1 month and 6 month post hepatectomy was studied with respective computed tomography (CT) scans. Decreased percentage of liver volume gain was observed among obese patients in both timepoints (1 month and 6 months post-operatively). In a very similar study from 2016, overweight and obese patients demonstrated significantly decreased liver growth between 2 and 7 months after hepatectomy (Amini *et al*., 2016).

Hepatectomy is usually a routine operation with low post-operative morbidity. In a clinical study of 135 patients, Behrns *et al*. (1998) showed that hepatic steatosis is a risk factor during hepatic resection. In this study, higher morbidity and liver failure was observed among obese patients that underwent major hepatectomy. However, the classification of morbidity due to hepatic failure in the liver surgery field is very hard to define. The use of different classification systems by researchers to categorize cases of post-operative death as liver failure, morbidity, or post-operative complications, makes the literature interpretation a very hard task.

As surgeons around the world adopt currently a more aggressive approach towards tumor resection, that translates into achieving a larger extend of hepatic resection (Lin *et al*., 2011). The remnant liver fragments following hepatectomy have the crucial task of performing the postoperative liver function. With liver failure to be the most common cause of post- operative mortality (Vibert *et al*., 2014), prediction of such an event pre-operatively, has become of great importance. Researchers have used different tests to assess the outcome and prognosis of the operation to decrease complications. An

example is the LiMAx test developed at the Charité hospital in Berlin. This test is based on the hepatocyte metabolism of ^{13}C- labelled substrate by the P450 1A2 enzyme. After the injection of the substrate, it is metabolized into $^{13}CO_2$, which can be detected in the breath. Liver resection of a percentage of functional liver leads to equivalent decrease of the LiMAx value post-operatively (Stockmann *et al*., 2010). Therefore, this test is used to represent the capacity of liver function and to estimate liver mass growth after hepatectomy. Within the same study, significantly lower LiMAx values were obtained by deceased patients already from one day post hepatectomy compared with patients that survived the operation long-term. In that case, the cause of death among those patients was classified as post-operative liver failure.

The same group that has developed the LiMAx test, performed a study of obese and non-obese patients after hepatectomy. Strikingly, NAFLD and NASH patients have a significantly decreased LiMAX value 10 days after hepatectomy although the pre-operative values are equal (Hoppe *et al*., 2015). At a later timepoint after hepatectomy, decreased functionality of the liver of obese patients was observed even 12 weeks after, a timepoint at which non-obese individuals had fully restored their liver functionality (Lock *et al*., 2012).

In conclusion, although human clinical studies concerning obesity and liver regeneration have several limitations, there are indicators of impaired liver mass regeneration of NAFLD and NASH patients following hepatectomy. A reduced liver mass after hepatectomy in obese patients is of great importance since post-operative hepatic dysfunction is highly related to the value of residual liver volume at a given timepoint (Schindl *et al*., 2005). An increase in mortality of obese patients after operation often occurs due to impaired restoration of liver functionality which can lead to liver failure.

1.3 Liver regeneration in rodent models of partial hepatectomy

Some of the limitations in clinical models of obese patients undergoing hepatectomy were overcome with studies using animal models. Furthermore, studies in rodents have the advantage of a model where solely the influence of obesity (without underlying health conditions like HCC) can be determined on the outcome of liver regeneration.

The picture becomes clearer concerning the severe impact of obesity in liver regeneration using rodent models. Impaired liver mass regeneration, as well as decreased hepatocyte proliferation has been observed already decades ago in the hepatectomy model. Among the conclusions of many different studies with mouse and rat models using a high fat diet or genetic models of obesity (*ob/ob*) there was a significantly impaired liver mass regeneration, decreased ability of hepatocyte proliferation, higher incidence of liver failure and acute liver injury in obese rodents post-hepatectomy (DeAngelis *et al*., 2005; Leclercq *et al*., 2006; Selzner and Clavien, 2000). The mechanisms and pathways related to the impaired liver regeneration are diverse and include the involvement of IL-6, NF-kB or EGF.

In contrast to humans where the impaired liver regeneration among obese patients is identified from 10 days up to several months, in rodents, the significantly decreased mass of the liver is usually identified within the first 7 days post operation. In lean mice the liver has reached its initial pre-operative weight after 7 days (Michalopoulos and Bhushan, 2020). To understand the underlying mechanisms by which liver regeneration is initiated and liver mass is restored, animal models of Partial Hepatectomy (PhX) are being used. 2/3 PhX is a very well-established protocol in rodents, which has been used for decades (Higgins GM, 1931; Mitchell and Willenbring, 2008). Most of our current knowledge concerning the very complex mechanisms of liver regeneration is derived from the usage of different mouse reporter lines, knock-out lines, etc., in combination with PhX. This way the impact of immune and non-immune cells in liver regeneration and survival after PhX has been investigated.

During the 2/3 PhX protocol, a total of 3 lobes (2 median lobes and the left lateral) are resected and removed. Most of the hepatocytes from the remnant liver tissue are in the S phase of the cell cycle and initiating DNA replication between 36-42 hours post 2/3 PhX. Typically, and depending on the mouse strain, wild type mice regenerate the initial liver weight within 7 days post operation (Michalopoulos, 2007).

1.3.1 Kinetics of liver regeneration after partial hepatectomy

One of the most puzzling questions in regenerative medicine is: How is liver regeneration initiated? Additionally: Which signals enable the proliferation, regeneration and termination of these after the initial liver weight is obtained?

Among the different theories examined, Lorenz *et al*. (2018) proposed that liver sinusoidal endothelial cells (LSEC's) are mechanically stretched by blood perfusion and hence, increased blood pressure may act as a signal of liver growth and regeneration. However, this seems to mainly explain liver growth in the developing embryo but was not addressed extensively in the partial hepatectomy model. Although increased vessel dilation occurs in the liver few hours post PhX, this was not correlated with the initiation of hepatocyte proliferation and liver regeneration.

Using classical parabiosis experiments, where hepatectomized and non-operated animals were carotid-to-jugular cross circulated, liver regeneration cascade was also initiated in the non-operated animals (Moolten and Bucher, 1967). This fact already from 1967, shows that a humoral agent and/or circulating cells can act as the signal for liver regeneration. For this trigger, a coordinated fashion of the liver NPC's (Non-parenchymal cells) including LSECs, hepatic stellate cells (HSC's) and KC, act to control the regenerative phase. The most important cytokines and growth factors that play an unreplaceable role in liver regeneration are detailed in the following chapter.

1.3.2 Cytokines in partial hepatectomy-induced liver regeneration

In 1997 Yamada *et al*. showed the importance of TNFR-I signaling during partial hepatectomy by using TNFRI-KO animals. Specifically, those mice when undergoing PhX, have severely impaired DNA synthesis, inhibition of NF-κB and subsequent release of IL-6. In line with the impaired DNA synthesis, the restoration of a normal body weight/liver weight ratio is not reached even after two weeks post operation, whereas wild type mice restore it after 7 days. This work shows that during normal liver regeneration the activation of NF-κB by TNFα happens within minutes after hepatectomy. Downstream of NF-κB, activation of an IL-6-dependent pathway occurs, leading to activation of the STAT3 transcription factor in hepatocytes and their subsequent proliferation. Apart from the NF-κB activation-related function of TNFα, Webber and colleagues showed that TNFα has another potential role in liver regeneration by acting as a “primer” that sensitizes hepatocytes to respond to growth factors. On the contrary, hepatocytes do not respond to growth factors in the absence of TNFα (Webber *et al*., 1998).

TNFα is expressed within 30 minutes after partial hepatectomy by KC, which are induced to express this cytokine by sensing enteric-derived LPS detected in liver tissue

after hepatectomy (Cornell, 1985). The induction of Kupffer cells is reported to require the adaptor protein Myd88 since Myd88 KO mice have decreased levels of TNFα and IL-6, accompanied by a delayed regeneration of the liver (Campbell *et al*., 2006; Seki *et al*., 2005).

As indicated above, *il-6* is also strongly upregulated in hepatectomized animals shortly after operation. IL-6 is produced by Kupffer cells after partial hepatectomy and has multiple roles in regeneration by priming hepatocytes for proliferation and having an hepatoprotective function. The regulation of IL-6 is induced by LPS and Myd88. In an autocrine manner, TNFα is responsible for further elevating IL-6 production. Studies with IL6-KO animals showed impaired regeneration after partial hepatectomy, reduced survival after operation and increased necrosis of liver tissue (Cressman *et al*., 1996). In different series of experiments, where IL-6 was injected during partial hepatectomy, liver regeneration was successfully rescued in IL6-KO animals but also in TNFRI-KO animals (Cressman *et al*., 1996; Yamada *et al*., 1997). The latter findings show that the potential role of TNFα is to drive the production of IL-6 which in turn initiates liver regeneration.

Binding of Kupffer cell-derived IL-6 to hepatocytes, and specifically the IL-6 receptor, leads to the activation of the subunit glycoprotein 130 (gp130) which results in a tyrosine kinase activity that phosphorylates STAT3 on hepatocytes. As a result, almost 40% of the genes that are activated in this phase of liver regeneration, are induced by IL-6-enhancing hepatocyte proliferation. Interestingly, injection of hepatectomized animals with hyper-IL-6, a fusion protein of IL-6 and the soluble IL-6 receptor (sIL-6R), led to accelerated liver regeneration and earlier mitosis of hepatocytes (Streetz *et al*., 2000).

In a recent publication, Izumi *et al*. (2018), described a mechanism by which Kupffer cells can produce IL-6, promoting liver regeneration after partial hepatectomy. Specifically, the vagus nerve, which is part of the parasympathetic nervous system, releases acetylcholine, which is bound to Muscarinic receptors of Kupffer cells, promoting IL-6 production. The IL-6 consequently triggers the proliferation of hepatocytes through IL-6R/gp130 and expression of the transcription factor FOXM1 which enhances several pathways of cell cycle progression and progression to mitosis by transcription of different cyclins. Surgical removal of the hepatic vagus nerve while hepatectomy leads to decreased survival and liver regeneration.

In conclusion, IL-6 has a primary role in liver regeneration and subsequently Kupffer cells which produce IL-6. The importance of expression and release of IL-6 can be seen with the different mechanisms which in coordination enhance and trigger the expression of IL-6. Those include the LPS-mediated release of TNFα and IL-6 in an autocrine matter and the vagus nerve through acetylcholine release and triggering of IL-6 expression on Kupffer cells.

1.3.3 Growth factors in partial hepatectomy induced liver regeneration

Apart from the role of cytokines in liver regeneration, the function of growth factors has also been studied extensively. One of the most important growth factors that is upregulated after hepatectomy is the hepatocyte growth factor (HGF) which is normally present in the liver matrix and can bind hepatocytes through the c-Met receptor. Although mainly characterized *in vitro,* hepatocytes have a strong mitogenic response to HGF leading to their clonal expansion (Block *et al.*, 1996). Using *in vivo* models, genetic ablation of HGF or of its receptor c-Met impaired regeneration of the liver after hepatectomy (Borowiak *et al*., 2004; Huh *et al*., 2004).

Another important growth factor that contributes to liver regeneration is the receptor of the epidermal growth factor (EGFR) which is expressed on hepatocytes. The epidermal growth factor (EGF) is constantly available in the liver through the portal circulation, and it is derived from Brunner's glands of the duodenum (Böhm *et al*., 2010; Olsen *et al*., 1988). Activation of the EFGR occurs within 30-60 min post PhX, whereas increase of EGF post PhX has not been detected so far (Stolz *et al.*, 1999). At this point, it is important to mention that EGFR has multiple ligands such as EGF, *TGF*α and Heparin-binding EGF (HB-EGF). Mice lacking the EGF receptor have a decreased hepatic cell proliferation and a delayed liver regeneration post hepatectomy (Natarajan *et al*., 2007).

Heparin-binding EGF (HB-EGF) is a 20-30 kDa glycoprotein which is synthesized by macrophages and epithelial cells as a membrane bound precursor and becomes soluble after cleavage. There is an increase in soluble HB-EGF within 1.5 hours post partial hepatectomy. HB-EGF knockout animals have decreased hepatocyte DNA replication which leads to a delayed response in liver regeneration by playing a key role for the G1 to S transition in the cell cycle (Mitchell *et al*., 2005).

1.3.4 Hepatocyte proliferation in partial hepatectomy-induced liver regeneration

As compared to other models of acute liver injury, in the partial hepatectomy model there is no pronounced death of hepatocytes or histological injury in the residual liver tissue (Abu Rmilah *et al*., 2019). During resection, pericentral and periportal hepatocytes have the potential to proliferate and restore the liver mass loss. It is nowadays a field of discussion which subtypes of hepatocytes proliferate during liver regeneration.

For the investigation of pericentral and periportal hepatocytes and their proliferation during liver regeneration, two unique markers have been identified, Axin2 and mfs2da, respectively. Early discoveries showed $Axin2^+$ pericentral hepatocytes are having the ability to self-renew up to a period of 1 year by pulsing with tamoxifen the Axin2-CreERT2; Rosa26-$mTmG^{flox}$ mice (Wang *et al*., 2015) (Fig 1 A). In those mice, a portion of $Axin2^+$ cells are stochastically labelled permanently with green fluorescent protein (GFP) upon tamoxifen injection, allowing fate mapping of the pericentral hepatocytes.

However, during liver regeneration a follow up study showed that $mfs2da^+$ periportal hepatocytes are massively proliferating 2 days after PhX but at the same time have no ability of self-renewal (Pu *et al*., 2016). By using a fate mapping model of *Mfsd2a-CreER* mice crossed with *Rosa26-RFP*, this study showed that periportal hepatocytes repopulate the liver during liver regeneration after PhX, as well as in other models of liver injury such as the chronic CCl_4 and the bile duct ligation model. Although most proliferating hepatocytes are periportal, with Ki-67 staining of liver tissue 2 days post PhX, a proportion of pericentral hepatocytes are also able to proliferate but to a lesser extent. In line with the periportal hepatocyte proliferation, a recent study showed that homeostatic proliferation of hepatocytes is maintained throughout all zones of the liver lobule, while periportal and parenchymal hepatocytes proliferate at an early point (40 h) in response to partial hepatectomy (Sun *et al*., 2020) (Fig 1 A, B).

In summary, using animal models of liver regeneration, a very complex coordinated network of cytokines and growth factors involved has been described. Liver regeneration is a process of massive hepatocyte proliferation. Although there are significant data demonstrating that periportal hepatocytes have the upper hand in liver mass restoration, contribution of the pericentral proliferation cannot be excluded. This could also suggest different roles of the two types of hepatocytes, with the periportal

ones as an immediate mechanism of liver mass restoration and the pericentral hepatocytes involved in homeostatic replenishment of hepatocytes.

1.4 Regeneration of the liver from drug-induced acute liver injury

The function of the liver can be compromised by several different factors including alcohol, obesity, drugs, infections, and hepatocellular carcinoma. Apart from the important global burden of liver diseases, which account for appx. 2 million deaths worldwide (Asrani *et al*., 2019), a status of low life quality combined with a high economic impact arise. However, depending on the severity, source and the longevity of the insult, the liver can regenerate and regain its function.

Among liver diseases, drug-induced liver injuries (DILI) are usually caused by drug biotransformation in the liver into a reactive form that can cause oxidative stress and necrosis or apoptosis of liver cells. Widely used drugs such as paracetamol and amoxicillin can lead to liver injuries caused by overdose or by a non-dose dependent way (Andrade *et al.*, 2019).

Carbon tetrachloride (CCl_4) is a chemical compound in the group of haloalkanes. CCl_4 was commonly used in the past in industry and household as a detergent and solvent as well as a degreaser. The hepatotoxicity of CCl_4 has been elucidated in different species including rodents, non-human primates, and man. Nowadays, CCl_4 is being used in experimental models of hepatoxicity, including acute and chronic liver injury models (Weber *et al.*, 2003). CCl_4 exposure leads to pericentral hepatocyte necrosis (centrilobular). The metabolism of CCl_4 involves CYP2E1 that transforms CCl_4 to reactive CCl_3 (trichloromethyl) radical. Free radicals of CCl_3 cause lipid peroxidation and oxidative stress in hepatocytes leading to loss of membrane integrity and cell death (Manibusan *et al*., 2007). In experimental models of acute liver injury (ALI) animals treated with CCl_4 displayed many inflammatory sites, large necrotic areas located pericentrally going along with steatosis and ballooning of necrotic cells 24 hours post injection (Sun *et al*., 2001). Increased serum levels of the enzyme Alanin-aminotransferase (ALT) are detected from 24 to 36 hours after exposure to CCl_4 and is typically decreased to baseline levels after 5-7 days (Wang *et al.*, 2013). Exposure to CCl_4 induces the expression of pro-inflammatory cytokines such as TNFα by infiltrating liver macrophages (Sato *et al*., 2014). Liver-resident macrophages (KC) are

also stimulated and respond by producing cytokines and free radicals that further induce liver damage.

Various tools are currently being utilized to track the proliferation of hepatocytes following injury (e.g., Ki-67 staining and hepatocyte reporter mouse lines). In contrast to regeneration after PhX, an acute insult of mice with CCl_4 leads only to a partial replenishment by Mfsd2a$^+$ periportal hepatocytes (Fig 1 C). This replenishment of the pericentral hepatocytes, involves proliferation of periportal as well as pericentral hepatocytes (Font-Burgada *et al*., 2015; Pu *et al*., 2016; Sun *et al*., 2020).

Previous ongoing inflammation or liver injuries might affect the acute phase of liver damage (severity of injury), as well as the regeneration phase. On this note, delayed liver regeneration after CCl_4-mediated hepatotoxicity has been observed in obese mice. Depending on the severity of the insult, the liver typically regenerates within 7-10 days post carbon tetrachloride injury through restoration of the initial loss of liver tissue (Allman *et al*., 2010).

In conclusion, the acute carbon tetrachloride model of liver regeneration has some similarities, but also major differences from the partial hepatectomy model. Increased liver damage and pericentral necrosis characterize this model. In contrast to the partial hepatectomy model, both periportal and pericentral hepatocytes can proliferate to restore the damaged hepatocytes.

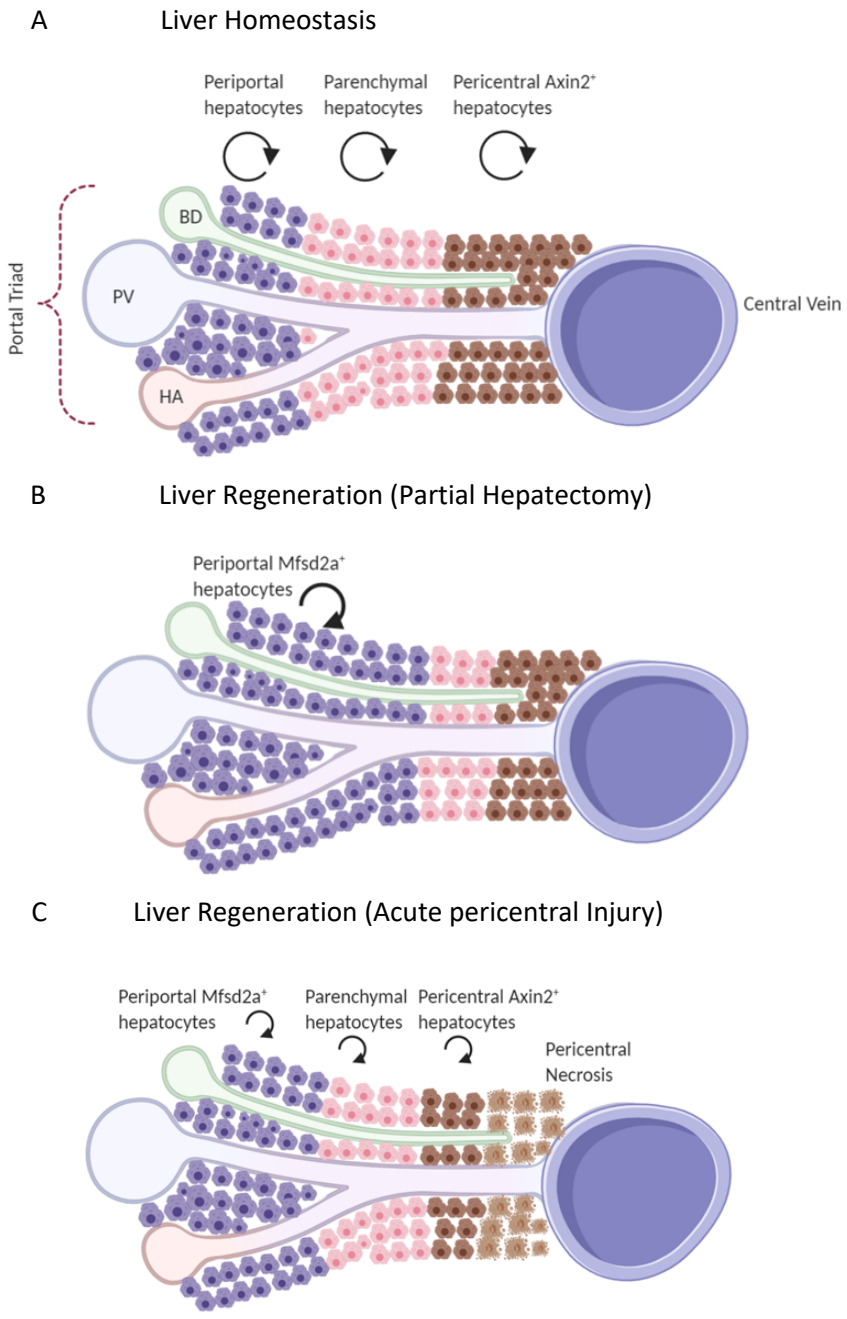

Figure 1: Mouse hepatic proliferation in homeostasis and after liver injury models, within the liver lobule. (A) During liver homeostasis, hepatocytes from periportal, parenchymal and pericentral zones can self-renew. Pericentral hepatocytes are characterised by Axin2 expression and have a limited contribution to homeostasis. PV=Portal vein, BD= Bile Duct, HA= Hepatic artery. (B) During liver regeneration after partial hepatectomy, Mfsd2a$^+$ periportal hepatocytes proliferate and contribute to the loss of the hepatic mass with pericentral hepatocytes having minimal contribution. (C) Regeneration of hepatocytes after an acute single injury with CCl_4 leads to pericentral necrosis. The replenishment of the hepatocyte loss is achieved with proliferation of hepatocytes from all different liver lobule zones. (Created with BioRender).

1.5 Aims of the study

Patients with NAFLD and NASH have an increased risk of impaired liver regeneration after resection, a situation that can lead to liver failure and post-operative death. Innate immune cells and specifically liver macrophages have been associated with both the gradual progression of inflammation during NAFLD, but also the recovery and regeneration of the liver after insult (hepatectomy, drug-induced liver injury). Throughout this thesis I aimed to examine the role of macrophages during liver injury and regeneration in more detail using the models of 2/3 partial hepatectomy and acute liver injury with CCl_4, to address the following questions:

What is the effect of metabolic inflammation in the liver macrophage phenotype and their homeostatic functions?

How do different macrophage progenies influence liver regeneration and post-hepatectomy morbidity?

What is the macrophage-associated mechanism of impaired liver regeneration in obese mice?

Which macrophage progeny/progenies inhabit the empty niche of the lean and obese regenerating liver?

2. Materials and Methods

2.1. Material

2.1.1. Equipment

Equipment	Name; Company.
γ-Irradiator	Biobeam2000; MCP-STS, Braunschweig, Germany
Autoclave	Belimed, Cologne, Germany
Stereo Microscope	Leica, Wetzlar, Germany
Cell counting chamber	Neubauer improved, Brand, Wertheim, Germany
Centrifuges	Centrifuge 5810R, Eppendorf, Hamburg Germany
Colibri retractor	Fine Science Tools GmbH, Heidelberg, Germany
Confocal Microscopy	Leica SP8 lightning, Leica, Wetzlar, Germany
Cryostat	Leica CM3050, Leica,Wetzlar, Germany
Flow cytometers	FACS CantoII, Fortessa; Becton, Dickinson, and Company, Franklin Lakes, NJ, USA
Freezers (-20°C)	Liebherr, Biberach, Germany
Freezers (-80°C)	Hera Freeze; Heraeus, Braunschweig, Germany
Heating block	ThermoStat plus; Eppendorf, Hamburg, Germany
Ice machine	Icematic Scotsman®; Frimont Bettolinc, Pogliano, Italy
Incubators	HERAcell; Heraeus, Braunschweig, Germany
IVC mice cages	Tecniplast, Hohenpeißenberg, Germany
ISOFLO Vaporizer	Eickemeyer, Tuttlingen, Germany
LightCycler	LightCycler 480 System, Roche, Manheim, Germany
Pipette-Boy	Integra Biosciences, Biebertal, Germany
Pipettes	Research plus 0.1-2.5, 0.5-10, 2-20, 20-200 and 100-1000 µl, Eppendorf, Hamburg, Germany
Preparation instruments	Labotec, Göttingen, Germany
Red light bulb	Infrafil; Phillips, Hamburg, Germany

Refrigerators (4°C)	Bosch, Stuttgart and Liebherr, Biberach, Germany
Tube roller	SRT6; Stuart, Stone, United Kingdom
Sieves, steel (small)	University of Bonn, Department Feinmechanik, Bonn, Germany
Sieves, steel (big)	Universitätsklinikum Bonn, Hauswerkstatt, Bonn, Germany
Shaver	Exacta, Aesculap, Suhl, Germany
Vortex	Genie 2 Bender & Hobein, Ismaning, Switzerland 20
Water bath (37°C)	TW8; Julabo, Seelbach, Germany
Water ion exchanger	EASYPURE®II; Thermo Fisher Scientific, Waltham, MA, USA
Workbench, sterile	HERAsafe; Heraeus, Braunschweig, German

2.1.2. Consumables

Equipment	Name; Company.
Cannula	22G; B. Braun, Melsungen, Germany
Cell Strainer Snap	Falcon® 5 ml; Corning, Corning, USA
FACS tubes	Polystyrene, 12/75 mm; Sarstedt, Nümbrecht, Germany
High Fat Diet (60 kJ%)	High fat diet for rodents with lard (& soybean oil), Ssniff Spezialdiäten GmbH, Soest, Germany
Injection needles	27G, 25G, 20G; BD Microlance, Becton, Dickinson and Company, Franklin Lakes, NJ, USA
Microscopy slides	Superfrost Plus, VWR, Darmstadt, Germany
Microtiter plates	6, 12, 24 & 96-well, round and flat bottom; TPP, Trasadingen, Switzerland
Normal Fat Diet (10 kJ%)	Low fat Control diet for rodents with lard (& soybean Ssniff Spezialdiäten GmbH, Soest, Germany
Parafilm	Parafilm “M” ®; American National Can TM, Greenwich, USA
Pasteur pipettes	150 mm and 230 mm; Roth, Karlsruhe, Germany
Petri dishes	10 cm; Greiner bio-one, Solingen, Germany
Pipette tips	10 µl, 200 µl, 1000 µl; Greiner bio-one, Solingen, Germany
Pipette tips	10/100/ µl, STARLAB, Hamburg, Germany

Plastic pipettes	5 ml, 10 ml, 25 ml; Sarstedt, Nümbrecht, Germany
Polypropylene tubes	15 ml and 50 ml; Greiner bio-one, Solingen, Germany
PVDF membranes	0.2 µm; Thermo Fisher Scientific, Waltham, MA, USA
Reaction tubes	0.5 ml, 1.5 ml, 2 ml; Eppendorf, Hamburg, Germany
Sieves, plastic	Falcon® 40µm,70,90µm Cell Strainers; Corning, Corning, USA
Silk sutures 6-0	PERMA-HAND Johnson&Johnson Medical GmbH Ethicon Deutschland, Norderstedt Germany
Syringes	1, 2, 5, 10, 20 ml BD Discardit™; Becton, Dickinson and Company, Franklin Lakes, NJ, USA
Tubes	15 ml and 50 ml; Greiner bio-one, Solingen, Germany

2.1.4. Chemicals and reagents

Reagent	Company
Ammonium chloride (NH_4Cl)	Merck, Darmstadt, Germany
AP20187 Dimerizer	R&D Systems
Blocking serum, human IgG	Sigma-Aldrich, St. Louis, MO, USA
Bovine serum albumin fraction V (BSA)	Roth, Karlsruhe, Germany
Bromphenol blue	Roth, Karlsruhe, Germany
Collagenase type IV	Roche, Mannheim, Germany
Dimethylsulfoxid (DMSO)	Roth, Karlsruhe, Germany
DNAse I	Roche, Mannheim, Germany
Ethanol, absolute	Merck, Darmstadt, Germany
Ethylene diamine tetraacetic acid (EDTA)	Merck, Darmstadt, Germany
Ethylene glycol tetraacetic acid (EGTA)	Merck, Darmstadt, Germany
Fetal calf serum (FCS)	Life Technologies, Carlsbad, CA, USA
Fluoromount G	eBioscience, San Diego, CA, USA
GBSS	PAN Biotech, Aidenbach, Germany
Foxp3 / Transcription Factor	eBioscience, San Diego, CA, USA
Clodronate liposomes / Control	FormuMax Scientific, Sunnyvale, CA, USA
Staining Buffer Set	

Glycine	Sigma-Aldrich, St. Louis, MO, USA,
Isoflurane	AbbVie, Wiesbaden, Germany
L-Glutamine (200 mM)	PAA, Cölbe, Germany
Liquid nitrogen	Linde, Wiesbaden, Germany
LIVE/DEAD Fixable Near-IR Dead Cell Stain Kit	Life Technologies, Carlsbad, CA, USA
Methanol	Sigma-Aldrich, St. Louis, MO, USA
Normal goat serum	Life Technologies, Carlsbad, CA, USA
Normal mouse serum	Life Technologies, Carlsbad, CA, USA
Olive Oil	Sigma-Aldrich, St. Louis, MO, USA
Penicillin/Streptomycin (P/S)	Gibco, Thermo Fisher Scientific, Waltham, MA USA
Phosphate buffered saline (PBS)	Life Technologies, Carlsbad, CA, USA
Potassium bicarbonate ($KHCO_3$)	Merck, Darmstadt, Germany
Propidium iodide	Sigma-Aldrich, St. Louis, MO, USA
Pierce Protein G Plus Agarose	Thermo Fisher Scientific, Waltham, MA, USA
RNase away spray	VWR, Darmstadt, Germany
RPMI 1640 medium	Invitrogen, Darmstadt, Germany
Sodium azide (NaN_3)	Roth, Karlsruhe, Germany
Sodium chloride (NaCl)	Sigma-Aldrich, St. Louis, MO, USA
Sodium periodate (NaIO4)	Sigma-Aldrich, St. Louis, MO, USA
TaqMan Gene Expression Mastermix	Applied Biosystems, Foster City, CA, USA
Tamoxifen (TAM)	Sigma
Trizol	Life Technologies, Carlsbad, CA, USA
Trizma® hydrochloride (Tris HCL)	Sigma-Aldrich, St. Louis, MO, USA
Trypan blue (0.4 %)	Lonza, Cologne, Germany
Triton X-100	Promega, Madison, WI, USA
Tween20	Roth, Karlsruhe, Germany

2.1.5. Buffers, media, and solutions

Buffer	Ingredients
ACK lysis buffer	Deionized water, 8.26 % ammonium chloride, 1 % potassium bicarbonate, 0.037 % EDTA; pH = 7.2
Blocking buffer	5% NDS (Normal Donkey Serum), 5% BSA, 1%GCWFS, 0.5% Triton-X, 0.1% NaN_3
Cell lysis buffer.	PBS, 0.5 % (v/v) NP-40, 20 mM Tris HCl pH 7.6, 150 mM NaCl, 1 mM EDTA pH 8.0, 1 mM EGTA pH 8.0
PFA solution	4 % (w/v) PFA in 1x PBS gradually heated (pH value 7.4)
Sucrose solution	30 % (w/v) Sucrose in PBS
FACS buffer	PBS, 3 % (v/v) FCS, 0.1% (v/v) NaN_3.
MACS buffer	PBS, 3 % (v/v) FCS, 2 mM EDTA.

2.1.5.1 Antibodies used for Immunofluorescence staining

The following directly-labelled antibodies were used for staining of liver tissue sections.

Antigen	Clone	Conjugate(s)	Company
CD11b	M1/70	Alexa Fluor 488	Biolegend
CD45.1	A20	Alexa Fluor 488	Biolegend
CD45.2	104	Pacific Blue	Biolegend
CD31	390	Alexa Fluor 647	Biolegend
F4/80	BM8	BV421	Biolegend
Tim4	RMT4-54	PE/Alexa Fluor 647	Biolegend

Anti-GFP	A-21311	Alexa Fluor 488	Thermofisher

Additionally, unconjugated primary antibodies were used that were stained with secondary antibodies.

Unconjugated Ab	Company	Secondary Ab	Company
CLEC4F	R&D Systems	Goat anti-rat IgG (H+L)	Invitrogen
F4/80	Abcam	Goat anti-rat IgG (H+L)	Invitrogen

2.1.5.2 Antibodies used for Flow Cytometry

Antigen	Clone	Conjugate(s)	Company
B220	RA3-6B2	APC-Cy7	BioLegend
CD3ε	145-2C11	eFluor450	eBioScience
CD11b	M1/70	Alexa Fluor 488	BioLegend
		BV 711	BioLegend
CD11c	N418	PE-Cy7	eBioscience
CD16/32 (FC-Block)	2.4G2	unlabeled	self-made
CD45.1	A20	PerCp-Cy5.5	BioLegend
		BV605	BioLegend
F4/80	BM8	BV421	BioLegend
Ly6C	HK1.4	PerCP5.5	BioLegend
	HK1.4	APC	BioLegend
Ly6G	1A8	APC-Cy7	Biolegend
	1A8	PE-Cy7	BioLegend
CD45		BUV395	BD
CD146	ME-9F1	PE	BioLegend
	ME-9F1	FITC	Miltenyi
Ki-67	SolA15	eF660	ThermoFisher

Tim4	RMT4-54	PE	Biolegend
		PE-Cy7	Biolegend
CLEC4F	polyclonal	-	R&D Systems
+ anti-rat IgG		Alexa fluor 647	.Invitrogen

2.1.6. q-PCR primers and probes

To perform the SYBR Green q-PCR protocol the following custom primers were purchased from Integrated DNA Technologies (Iowa, USA)

Primer	Forward (5' to 3')	Reverse (5' to 3')
Foxm1	GCTCCATAGAAATGTGACCATC	AACCTTCACTGAGGGCTGTAAC
Cdk1	AAGAACCTGGACGAGAACG	GTCATCAAAGTACGGGTGCT
Ccna2	CCTTAAGTACCTGCCTTCACTC	ACAAGGCTTAAGACTCTCCA
Il6	CGTGGAAATGAGAAAAGAGTTG	ATCCAGTTTGGTAGCATCCATC
Gapdh	CATCACTGCCACCCAGAAGACTG	ATGCCAGTGAGCTTCCCGTTCAG
Chrm3	GTCTGGCTTGGGTCATCTCCT	GCTGCTGCTGTGGTCTTGGTC

2.1.7. Mouse strains

C57BL/6J — C57BL/6J non-transgenic mice were used as wild type controls (WT). Purchased from Charles River

CD45.1 — B6.SJL-Ptprca Pepcb/BoyJ mice express the leukocyte marker CD45.1 (Shen *et al.*, 1985). As B6 mice express CD45.2 instead, these mice can be used for T-cell transfer experiments as donor and recipient cells can be easily distinguished by the differential expression of CD45.1 and CD45.2.

Cx3cr1creER x R26Confetti — Cx3cr1creER x R26Confetti mice express a Cre-ER fusion protein from endogenous *Cx3cr1* promoter/enhancer elements (Tay *et al*., 2017a). Following a tamoxifen (TAM) injection in Cx3cr1creER/+ R26RConfetti/+ mice, macrophages can stochastically express one of four possible fluorescent reporter proteins. Those are encoded within the Confetti construct and are the following: a

	green fluorescent protein (GFP) in the cell nucleus, a yellow fluorescent protein (YFP) and a red fluorescent protein (RFP) in the cytoplasm, and a membrane-tagged cyan fluorescent protein (mCFP).
Csf1r-EGFP-NGFR	The macrophage Fas-induced apoptosis (MaFIA) transgenic mice are characterized by fluorescence of cells expressing the receptor of Csf1. Additionally, mice have inducible Fas apoptotic system, which is Csf1r-driven, Transgene insert contains the mutant human protein FK506 (FKBP12) which bind dimerization drug AP20187 (Burnett *et al*., 2004) .

2.1.8. Software

Software	Company
FACS DIVA V6.1.1	Becton Dickinson, Franklin Lakes, NJ, USA
FlowJo V 10.7.1	Becton Dickinson, Franklin Lakes, NJ, USA
iMARIS V7.6.3	Bitplane, Zurich, Switzerland
Microsoft Office 365	Microsoft, Redmond, WA, USA
Prism V 8.0.1 GraphPad	La Jolla, CA, USA
Image J	National Institutes of health (NIH), Maryland, USA
Leica LAS X	Leica, Wetzlar, Germany
KNIME Analytics Platform	KNIME, Zurich, Switzerland
iRoCS Toolbox	University of Freiburg, Freiburg, Germany
Mendeley	Mendeley, London, UK

2.2. Methods

2.2.1. Experimental treatment of mice

Cells and reagents were adjusted in PBS for experimental injection. Intraperitoneal (i.p) injections were performed with a volume of 200 µl, intravenous (i.v) injections with 100 µl and subcutaneous (s.c) with 50 µl.

2.2.1.1. Induction of diet-induced obesity

Male, 6-week-old C57BL/6J were fed a high fat context diet (60 kJ%) with lard (& soybean oil) for 16 weeks to induce fatty liver disease. The weight of the mice was monitored every week and before proceeding to the different experimental setups, blood sample from tail vein was taken to determine the serum levels of ALT (week 15 after start of diet).

2.2.1.2 Generation of Bone marrow chimeras

Mice were anaesthetized with a Ketamine/xylazine cocktail (0.1mL/20g mouse) intraperitoneally and irradiated with 9 Gy, with the abdominal area covered using a lead shield. After 6 hours, $2x10^6$ total bone marrow cells isolated from donor mice, were transferred in PBS intravenously. After mouse recovery and engraftment for 6 weeks, blood $Ly6C^{hi}$ chimerism was determined by flow cytometry before the experiments were performed.

2.2.1.3 Partial hepatectomy

All operations were carried out with male 8-10week-old mice. Mice were initially shaved and injected with 0.1 mg/kg Buprenorphine. Inhalation of 2.5% isoflurane in 100% oxygen (v/v) was used to anesthetize the mice. Through midline laparotomy an initial midline incision was opened. For better access to all different liver lobes, a metal retractor was introduced to keep the incision stretched. Using sterile 6-0 silk sutures, manually folded knots were placed on the base of the left latter lobe and tightened firmly. Incision of the whole lobe was then performed with surgical scissors and the area was monitored for bleeding. The same procedure was performed for the two median lobes separately. The peritoneal cavity was rinsed with 100 µl 0.9% sterile NaCl solution. The incisions in the peritoneum and the skin were closed using two silk sutures. To prevent hypothermia, operated animals were placed in cages warmed up

by infrared lamps until they were fully awake. For the rest of the experiments, animals were transferred back into normal cages with unhindered access to food and water and were monitored closely. During the first 3 days after operation, all animals received additional s.c injections of 0.1 mg/kg Buprenorphine every 10 hours to reduce post-operative pain.

2.2.1.4 Acute liver damage with CCl_4

Male, 8-weeks-old B6 mice were orally-gavaged with CCl_4 to induce acute liver injury. Each mouse was weighted and administered 3.5 mL/kg CCl_4 mixed with olive oil 1:1. Control mice were treated with olive oil only at the same time points. Mice were let for a recovery period and were monitored closely till the start of the experiment.

2.2.1.5 In *vivo* depletion of macrophages

To deplete hepatic macrophages, mice were injected intra-peritoneally 140 µg/ body weight Clodronate or control liposomes 24 hours prior to partial hepatectomy or to validate the efficiency of depletion.

For depletion of bone marrow-derived macrophages in CSF1r-gfp chimeric mice, 10 mg/kg AP20187 solution was intravenously injected 24 hours prior to surgical operation with an additional injection every 24 hours to ensure depletion, till the day of the analysis.

2.2.2. Non-parenchymal cell isolation

For the isolation of non-parenchymal cells (NPC), livers of donor mice were perfused with pre-warmed Calcium-deprived buffer containing 0.08% Collagenase IV or VIII for 10 seconds and were removed afterwards. Perfused livers were then homogenized through a metal cell strainer and resuspended in 2.5 ml GBSS containing 0.04% Collagenase IV. Digestion was performed by storing resuspended homogenates for 17 min at 37°C shaking at 250 rpm. Collagenase activity was then stopped by adding 40 ml ice-cold GBSS and samples were pelleted by centrifugation (800 g / 4°C / 10 min). Pellets were washed with ice-cold PBS once and resuspended in 10ml ice-cold PBS. For each sample, a 50 ml Falcon containing 20 ml 25% Percoll underlayed with 15 ml 80% Percoll (50% Percoll when only myeloid cells were required) was prepared. Percoll gradient centrifugation was performed at 1349 g at

room temperature for 30 min without brake. After centrifugation, the interphase containing the NPC between the two Percoll layers was removed and diluted in 12 ml MACS buffer. Cells were pelleted again by centrifugation (800 g / 4°C / 10 min). Finally, NPC were resuspended in 2 ml MACS buffer.

2.2.3. Cell culture for apoptotic cell uptake assay

A total of 10^5 F4/80$^+$ macrophages from lean and obese mice were cultured into separate wells of a 96-well plate, together with $2x10^5$ CFSE-labeled apoptotic mouse embryo fibroblasts. Cells were incubated at 37^{o}C, 5% CO_2 for 1 hour pelleted by centrifugation (800 g, 5 min, 4°C) and supernatant was aspirated. Cells were then washed three times, trypsinized and further analyzed with flow cytometry.

2.2.4. Flow cytometry

2.2.4.1. Staining of surface molecules

To assess the expression of cell surface molecules, single cell suspensions of NPC's were transferred to 96-well plates, centrifuged (1600 rpm / 3 min / 4°C) and resuspended in 100 µl of FACS buffer containing the respective fluorochrome-coupled antibodies and blocking serum (1:100 dilution). Cells were stained for 20 min at 4°C. Excessive antibodies were removed by two washing steps followed by centrifugations (300 g / 2 min / 4°C). Pellets were resuspended in FACS buffer or FACS Fix buffer if analysis was to be performed the next day.

2.2.4.2. Staining of Ki-67 transcription factor

To determine the proliferation of non-parenchymal cells with flow cytometry, cells were first stained for surface markers and after two washing steps with PBS, pellets were fixed with 200 µl of the Foxp3 fixation buffer (eBiosciences). Cells were then incubated for 30 min at 4°C. Cells were permeabilized with Foxp3 permeabilization buffer and stained with Ki-67 antibody or the respective isotype controls. Cells were finally washed three times with permeabilization buffer and resuspended in FACS buffer.

2.2.5. Confocal Microscopy

2.2.5.1. Fixation of liver samples

Liver biopsies (resected lobes during PhX) or whole regenerated liver lobes were fixed in 14 ml of 4% PFA fixation buffer. Samples were then incubated at 4°C for 6 hours. Residual PFA was washed away by 4 times washing with 14 ml PBS. Finally, liver samples were placed in tubes with 15 ml 30% Sucrose for at least 36 hours at 4°C.

2.2.5.2. Staining of liver sections for confocal microscopy

60 µm sections of frozen liver tissue were cut at -17°C using a cryostat and were placed directly in PBS. Removal of PBS was followed by addition of 600 µl 0.1% Triton. Blocking buffer (described above) was added and sections were incubated at RT on a plate rotor for 1 h. Antibody master mixes were prepared in Blocking buffer and incubated overnight at 4°C. After the staining, excess antibodies were removed with 6 washing steps with PBS. Finally, the sections were mounted on Cryo-slides and stored in darkness at RT overnight. An additional DNA counterstain with DAPI was also performed as proof of cell-specific binding (Ki-67 stain) (Graefe *et al*., 2019). Similarly, DAPI staining contained in the mounting gel was used for the discrimination of cellular, cytoplasmic, etc. expression of fluorescence proteins in the microfetti mice.

2.2.5.3. Determination of clone areas in Cx3cr1creER x R26Confetti mice

For the determination of the clone area of tissue-resident Kupffer cell expansion, random multi-stack confocal images were acquired using the Leica SP8 lightning. Each confocal Leica image file (lif.) was imported to KNIME Analytics Platform where Kupffer cells were automatically labelled as (GFP^+ or RFP^+ or $Microffeti^-$). Labelled data were then converted with the use of the same software to coordinate in a 2-dimensional space. Labelling was validated manually using iRoCS toolbox, where $Microfetti^+$ macrophages were assigned, different labels based on the expression of a fluorescent protein. All possible labels include: YFP^+, GFP^+, CFP^+, RFP^+ or $Microfetti^-$ macrophages. The final lists of XY coordinates of each picture were then imported to Prism8 to measure the clone area. For clone area calculations, 3 or more daughter cells of same fluorescent protein expression were considered as the minimum size of a clone. The maximal migratory distance radius was set at 300 µm. Finally, the minimal radius of a circle that contains all the daughter cells of non-linear clones was measured and the area was determined in μm^2.

2.2.6. RNA extraction, cDNA-synthesis, and RT-PCR

Liver biopsies were homogenized in 1ml Quiazol or 1ml Trizol and total RNA was isolated using the RNeasy Lipid Tissue Kit. Afterwards, 2-5 µg of RNA was reverse transcribed into cDNA at 37°C for 2 hours using the High-Capacity cDNA Reverse Transcription Kit. cDNA was stored at -20°C and RT-PCR was performed later using SYBR green primers. Results were calculated with the ΔΔCt-method.

2.2.7. Statistical analysis

To determine statistical differences, a two-tailed unpaired or paired Student's t-test was used when two groups were compared. A multiple comparison two-way ANOVA was used when three or more groups were compared. Significance in survival curves were calculated using the Log-rank (Mantel-Cox test) analysis. For correlation analysis, the two-tailed Pearson correlation was utilized. Statistical analysis was executed with Prism V 8.0. Statistical significance is set in the margin of $p < 0.05$.

3. Results

3.1 Obesity impairs liver regeneration after hepatectomy and delays recovery after toxin-induced liver injury

Obesity and NAFLD are associated with impaired liver regeneration after hepatectomy and significant susceptibility to drug-induced liver injuries (Aubert *et al*., 2011; Begriche *et al*., 2011). Additionally, obese patients undergoing liver resection have increased likelihood of post-operative morbidity (Acosta *et al*., 2017). Hepatic macrophages have a dual role in obesity, not only by promoting obesity-induced liver inflammation, but also initiating responses of liver mass restoration through the production of cytokines. The origin of the hepatic macrophage pool includes mainly embryonically derived macrophages, but in the context of liver injury and inflammation, other origins of macrophages will likely have a different role in promoting or terminating inflammation. Our approach aims to identify the contribution of each macrophage origin in liver regeneration and the mechanism by which a diverse macrophage origin pool is influencing liver mass regeneration after hepatectomy.

3.1.1 Diet-induced obesity impairs liver regeneration of hepatectomised mice

Obesity was induced to laboratory C57BL7/6J mice by feeding with a highly enriched fat diet (HFD, 60 kcal%) for 16 weeks. This mouse model is being frequently used to mimic obesity-related diseases of humans as a preclinical model (Wang and Liao, 2012). Obese and lean mice (normal diet/ND) were subjected to 2/3 partial hepatectomy (PhX) and the liver growth was measured 2 and 7 days post PhX. The regenerated lobes (left lobe and caudate lobe) of the obese mice, appear fatty 7 days post-PhX with a reduced macroscopic elongation of the caudate lobe (Fig 2 A). Liver regeneration, measured as the ratio of the regenerated liver weight (LW_{reg}) to liver weight before hepatectomy (LW_{ref}) was significantly decreased already from the 2nd day post PhX and remained significantly lower till day 7 (Fig 2 A, B). Normal diet fed mice restored the initial liver weight at day 7, with the respective percentage of liver regeneration of obese mice to be ~60% of their initial liver weight before the operation (Fig 2 B). In line with our results, the decrease of liver weight regeneration is also reflected by the LW/BW (Liver weight/ Body weight) ratio, as same results were obtained at day 2 post PhX (Fig 2 C).

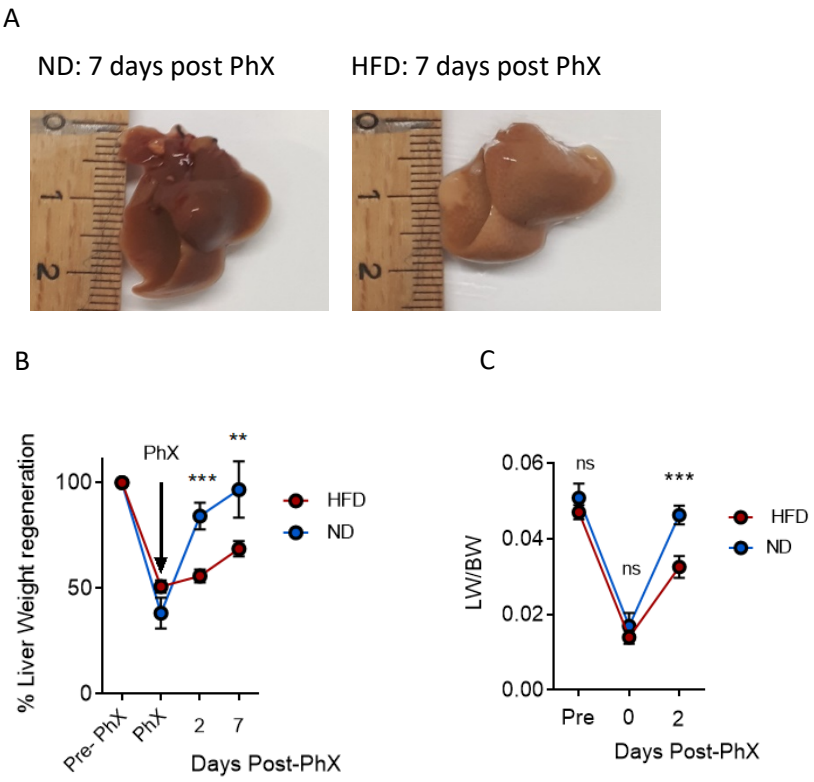

Figure 2: Impaired liver mass regeneration of obese mice following partial hepatectomy. Mice were fed a normal or high fat diet for 16 weeks. After progression of obesity accompanied with slightly elevated ALT levels (data not shown), mice were operated and a 2/3 Partial hepatectomy was performed. **(A)** Pictures of the regenerated lobes 7 days post PhX with ND mouse liver (left) and HFD fed harvested mouse liver (right). **(B)** Liver weight regeneration of ND and HFD fed mice 2 and 7 days post PhX. Liver weight regeneration was calculated as the percentage of remnant or regenerated liver weight divided by the pre-operative total liver weight (defined from reference animals). **(C)** Liver weight to Body weight ratio (LW/BW) of ND and HFD fed mice pre-Phx and 2 days post PhX. Mice were weighed for their BW and LW before (reference animals) and after PhX. Two-way ANOVA, Bonferroni's multiple comparison test, *P<0.05, **P<0.01, ***P<0.001, data were obtained from three independent experiments, (n=5 mice per group) (B, C)

3.1.2 Obesity leads to delayed resolution of inflammation and severe liver damage following acute CCl_4-induced liver injury

To gain more insight in the underlying mechanisms of how obesity affects physiological processes such as liver regeneration and recovery, we used the model of liver injury with CCl_4. In this model, CCl_4 was administrated orally, as a single "shot" of CCl_4 leading to pericentral necrosis of hepatocytes and inflammation 24 hours post injection (Fig 3 A). In those necrotic areas surrounding the central vein, infiltration of $CD11b^+$

cells and absence of F4/80^{+} macrophages were observed compared with the oil-treated mice (Fig 3 A). When obese mice were challenged with CCl_4, significantly higher levels of liver injury were observed 24 h post injection, as measured by the levels of Alanine Aminotransferase (ALT) (Fig 3 B). The levels of ALT remained elevated also 2 and 3 days (although not significant) post injury compared to the control group, indicating a delayed recovery and restoration of liver function in obese mice.

In summary, in our studied model, obese mice show reduced liver regeneration after PhX and a delayed restoration of liver function after CCl_4-induced liver injury.

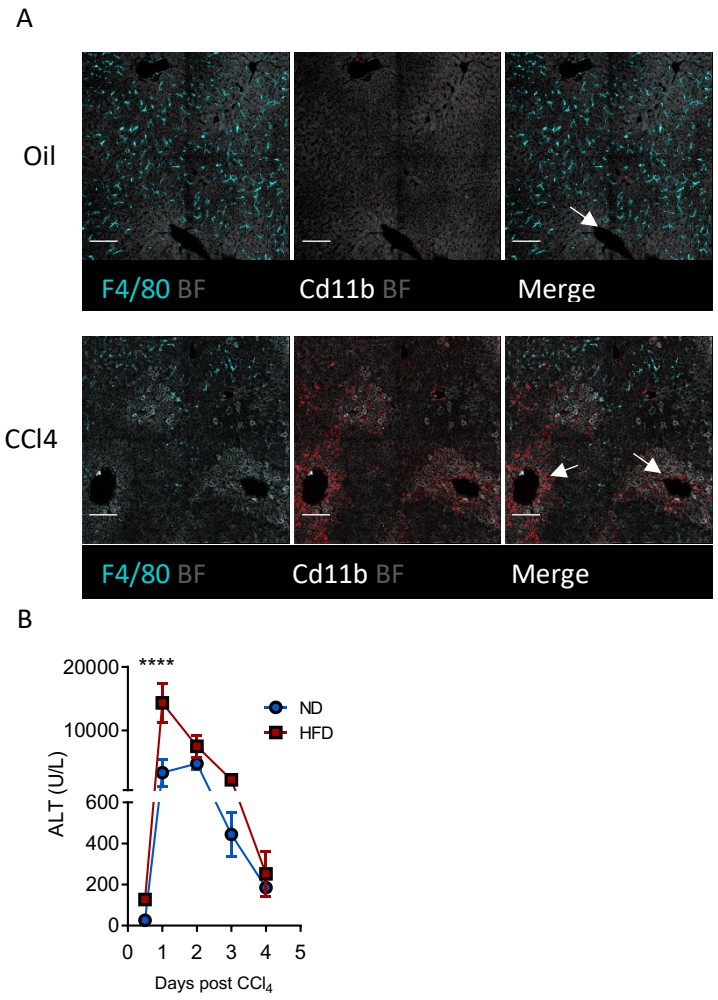

Figure 3: Increased liver damage and delayed resolution of inflammation in obese mice following liver injury with CCl_4. (A) Liver tissue biopsies from normal diet fed mice treated with CCl_4 or Oil were fixed and 30µm slices were stained with antibodies against F4/80 (cyan), CD11b (red). BF= Brightfield. The arrows represent the central veins of the liver lobules. Scale bars = 150 µm. (B) Mice were fed a high fat diet or a normal diet for 16 weeks before CCl_4 was administrated orally. ALT levels (U/L) were measured in the blood serum of the mice for 4 consecutive days. Two-way ANOVA, Bonferroni's multiple comparison test, *P<0.05, **P<0.01, ***P<0.001, data were obtained from two experiments (A, B), n=5 mice per group.

3.2 Obesity is associated with changes in the composition of hepatic innate immune cells and macrophage phenotype and function.

Metabolic inflammation or meta-inflammation is a term often used to describe the effects of obesity in the immune cell-mediated inflammation. This kind of inflammation depending on the organ, can result in disturbed physiological mechanisms. Here we aimed to address and enumerate the effect of obesity and the changes in the innate immune compartment of the liver, with a specific focus in liver macrophage subsets and their function. Using the diet-induced obesity model we characterized those phenotypic and functional differences, that influence liver homeostasis.

3.2.1 Obesity leads to innate immune cell infiltration in the liver

Liver non parenchymal cells (NPCs) were isolated from obese and lean mice and with a flow cytometry staining we enumerated the absolute number of innate immune cells. Our results suggest an increased liver inflammation as indicated by the elevated numbers of $Ly6C^{hi}$ monocytes, $Ly6G^{+}$ neutrophils and $Ly6C^{+}$ macrophages (Fig 4 A, B, D). On the contrary, $F4/80^{hi}$ Kupffer cells are significantly decreased in obese mice (Fig 4 C). Of note, the number of the whole $F4/80^{+}$ fraction including $Ly6C^{+}F4/80^{+}$ macrophages remained significantly decreased, with the number of inflammatory macrophages not making up for the number of the observed decrease of Kupffer cells (Fig 4 E).

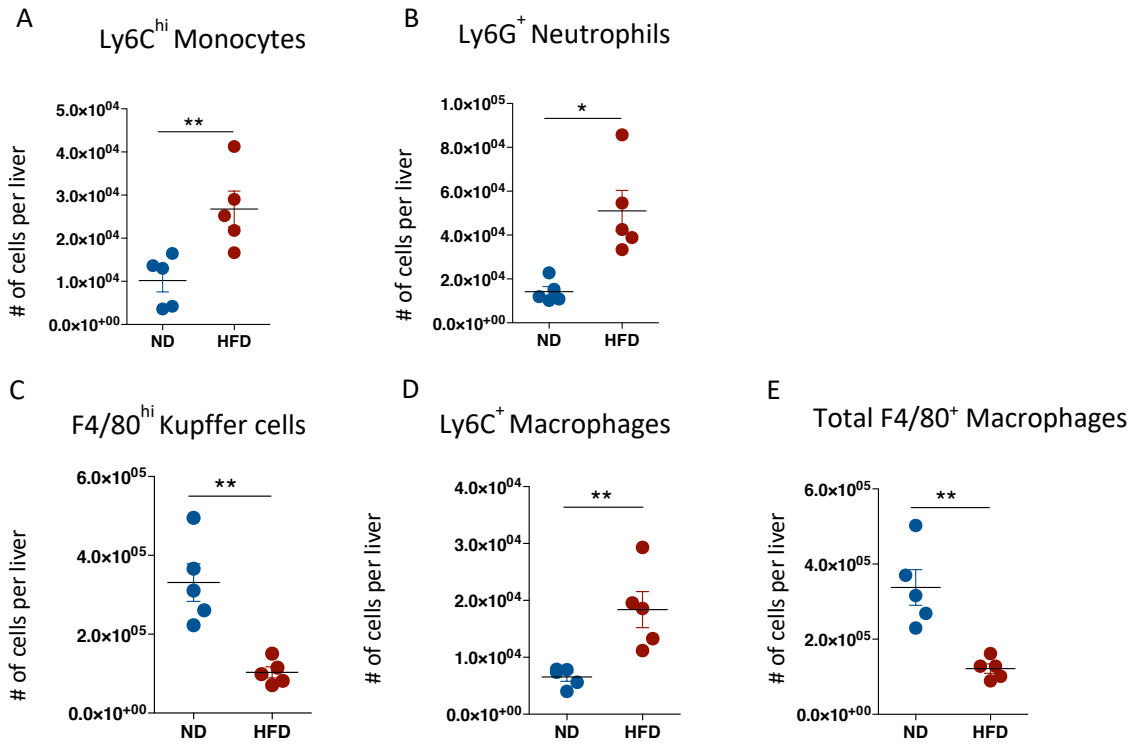

Figure 4: Innate immune cell infiltration and loss of F4/80^{hi} Kupffer cells in livers of obese mice. Number of (A) Ly6C^{hi} monocytes, (B) Ly6G^{+} neutrophils, (C) F4/80^{hi} Kupffer cells, (D) Ly6C^{+} F4/80^{+} inflammatory macrophages and (E) total F4/80^{+} macrophages per liver, determined by flow cytometry. *P<0.05, **P<0.01, ***P<0.001 Student's t-test (A-E), , *P<0.05, **P<0.01, ***P<0.001, data were obtained from three experiments, n=5 mice per group.

3.2.2 Obesity leads to a loss of the embryonic Kupffer cell phenotype and their phagocytic function.

Next, we isolated macrophages from lean and obese mice and performed flow cytometric analysis to test the expression of markers typically expressed in embryonic Kupffer cells or bone marrow-derived macrophages. Among the various markers studied, the expression of T-cell immunoglobulin mucin protein 4 (TIM4), was significantly decreased in F4/80^{+} liver cells of obese mice (Fig 5 A, B). Typically, this marker is highly expressed in tissue-resident macrophages, but not in bone marrow-derived macrophages *(Sakai et al.*, 2019; Scott *et al.*, 2016). The absence of Tim4 expression, also validated through immune fluorescence microscopy (Fig 5 C), suggests a loss of embryonic Kupffer cells and an infiltration of bone marrow-derived macrophages. Of note, the possibility of Kupffer cells downregulating TIM4 was excluded based on our results in fate-mapping models of

various inflammatory models. The main function of Tim4 is the apoptotic cell engulfment, which comes in line with our results of significantly reduced uptake of CFSE-labelled apoptotic mouse embryo fibroblasts (MEF) by total F4/80$^+$ liver macrophages of obese mice (Fig 5 D).

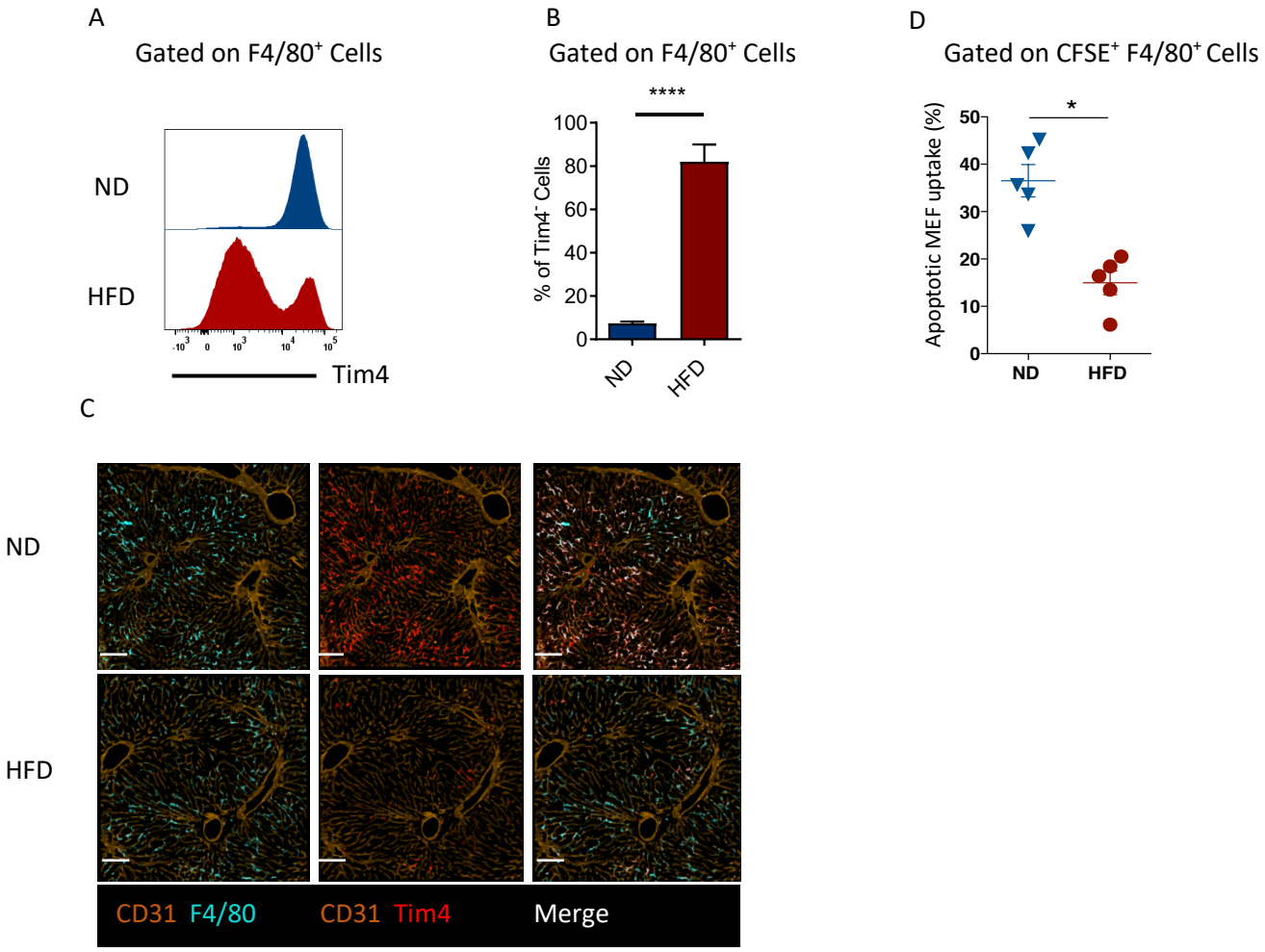

Figure 5: Phenotypic and functional changes of liver macrophages in obese mice. (A) Tim4 expression histogram of F4/80$^+$ macrophages from obese vs. lean mice. (B) Percentage of Tim4$^-$ liver macrophages from obese and lean mice. (C) Liver tissue biopsies from lean and obese mice were fixed and 30µm slices were stained with antibodies against macrophages: F4/80 (cyan), Tim4 (red) and endothelial cells: CD31 (orange). Scale bars= 150µm. (D) Mouse embryo fibroblasts were labelled with CFSE and followingly treated with UV. The apoptotic MEFs were then incubated with F4/80$^+$ cells from lean and obese mice. Apoptotic cell uptake was detected with flow cytometry. *P<0.05, **P<0.01, ***P<0.001 Student's t-test were obtained from two (A, B) and one (D) experiment, n=5 mice per group.

3.2.3 Bone marrow-derived macrophages in the fatty liver tissue are divided in two subtypes depending on Clec4f expression.

An emerging unique marker which is specifically expressed only in embryonic Kupffer cells has been identified (Lavin *et al*., 2014; Yang *et al*., 2013). The C-Type Lectin Domain Family 4 Member F marker (Clec4f) is expressed only on Kupffer cells of rodents and is involved in alpha-galactosylceramide (α-GalCer) presentation in liver and platelet clearance (Jiang *et al*., 2021). It is now understood that during the early stages of BM-MΦ infiltration in the liver microenvironment, they initially do not express Clec4f. However, the longevity of those macrophages in the liver tissue initiates their differentiation towards a Kupffer cell-like phenotype upregulating the expression of Clec4f and other signature KC markers (Scott *et al*., 2016).

We isolated liver macrophages from obese and lean mice and performed flow cytometric analysis. Three different subpopulations were identified in the obese mice based on the expression of Tim4 and Clec4f. Most of fatty liver macrophages are represented by expression of Clec4f and no expression of the marker Tim4 which is specified as population P2 (Fig 6 A, B). In contrast, lean mice liver macrophages are represented by a KC phenotype with expression of both Clec4f and Tim4 (P1). Moreover, an increased frequency of $Tim4^{-}$ $Clec4f^{-}$ (P3) Macrophages which are the “recently” infiltrated BM-MΦ were observed in obese mice although not significant.

The localization of the different subtypes of macrophages in the liver lobule had no specific pattern towards pericentral or periportal areas, with the fatty liver having mixed heterogenous liver macrophages subsets (Fig 6 C, D) as identified with immune fluorescence microscopy.

In conclusion, obesity leads to inflammation in the liver which is represented as an increased infiltration of innate immune cells and alters the steady state composition of hepatic macrophage phenotypes. Those changes have a direct impact on basic homeostatic functions of hepatic macrophages in the liver.

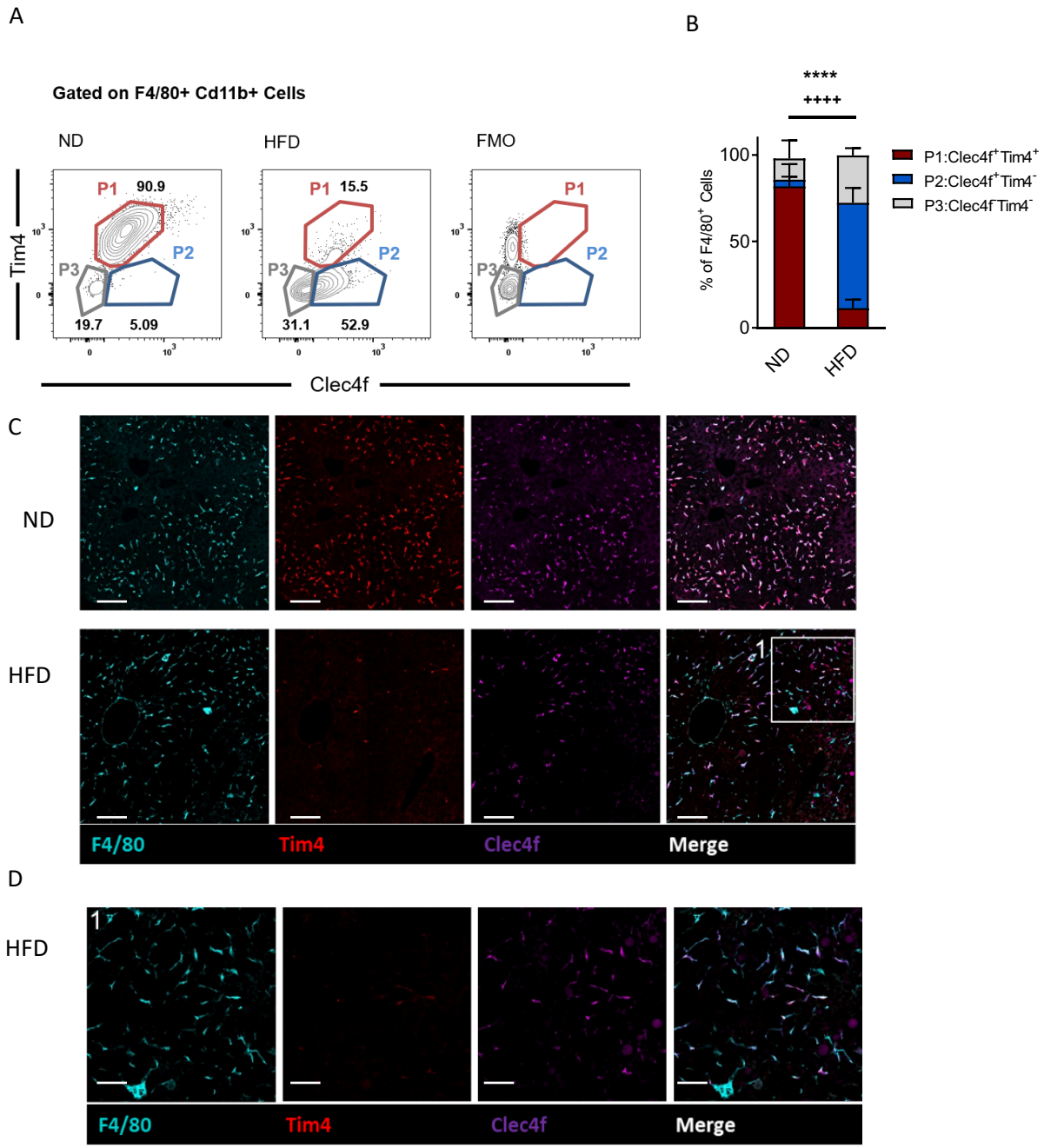

Figure 6: Different subtypes of bone marrow-derived macrophages in fatty livers of obese mice. (A) Tim4 and Clec4f expression plots of F4/80^{+} macrophages from obese vs. lean mice. (B) Percentage of P1 (Clec4f^{+} Tim4^{+}), P2 (Clec4f^{+} Tim4^{-}), and P3 (Clec4f^{-} Tim4^{-}) of F4/80^{+} liver macrophages from obese and lean mice. (C, D) Liver tissue biopsies from lean and obese mice were fixed and 30µm slices were stained with antibodies against F4/80 (cyan), Tim4 (red) and Clec4f (purple). (D) Zoom in area (1) shown in C. Scale bars = 100µm (C) and 50µm (D). *P<0.05, **P<0.01, ***P<0.001 for P1 (ND vs. HFD), $^{+}$P<0.05, $^{++}$P<0.01, $^{+++}$P<0.001 for P2 (ND vs. HFD), Two-way ANOVA, Bonferroni's multiple comparison test, were obtained from two experiments, n=5 mice per group.

3.3 Embryonic KC play a vital role in regeneration, with their expansion occurring during liver weight restoration.

In steady state conditions, there is a minimal contribution of BM-MΦ in the liver macrophage pool, with most macrophages having an embryonic origin, able to self-renew, rather be replenished by monocytes. However, during tissue injury and depletion of embryonic macrophages, BM macrophages contribute to this macrophage pool (Beattie *et al*., 2016; Ikarashi *et al*., 2013). The partial hepatectomy model differs from other types of liver insults, since embryonic macrophages are present in the remnant liver, which followingly regenerates. Interestingly, despite the presence of embryonic Kupffer cells, reports have indicated the presence of BM-derived macrophages in the liver after hepatectomy (Nishiyama *et al*., 2015), however, their role in liver regeneration remains to be fully elucidated. Therefore, to investigate the role of the macrophage pool in liver regeneration we examined the impact and dynamics of both progenies of macrophages (embryonic and bone marrow-derived) in the regenerating liver environment.

3.3.1 Embryonic Kupffer cells are essential for liver regeneration.

As our data suggest, the liver macrophages are among the most altered components of the liver innate immune system during obesity. To examine if this liver macrophage changes could translate to the impaired liver regeneration observed in obese mice, we first focused on understanding the main role of macrophages in liver regeneration under steady state conditions. To investigate this, we depleted liver macrophages of lean mice and performed partial hepatectomy.

For the experiments with depletion of liver macrophages, we injected clodronate or control liposomes intraperitoneally to mice, 24 h prior to surgical liver hepatectomy. $F4/80^{+}$ cells are depleted 24 hours post injection of clodronate liposomes (Fig 7 A, B). The post-operative survival of mice treated with clodronate liposomes decreased dramatically between 2 and 4 days after operation (Fig 7 C). The post-operative (resected) LW/BW ratio of the clodronate-treated group was significantly higher than the control-treated group, which led to a very similar LW/BW ratio 7 days after operation (Fig 7 D). Therefore, the fold increase of LW was calculated to compare the liver regeneration between the control and clodronate liposome-treated mice. Control mice 7 days after PhX had a 4-fold higher increase of LW compared to clodronate-treated mice (Fig 7 E).

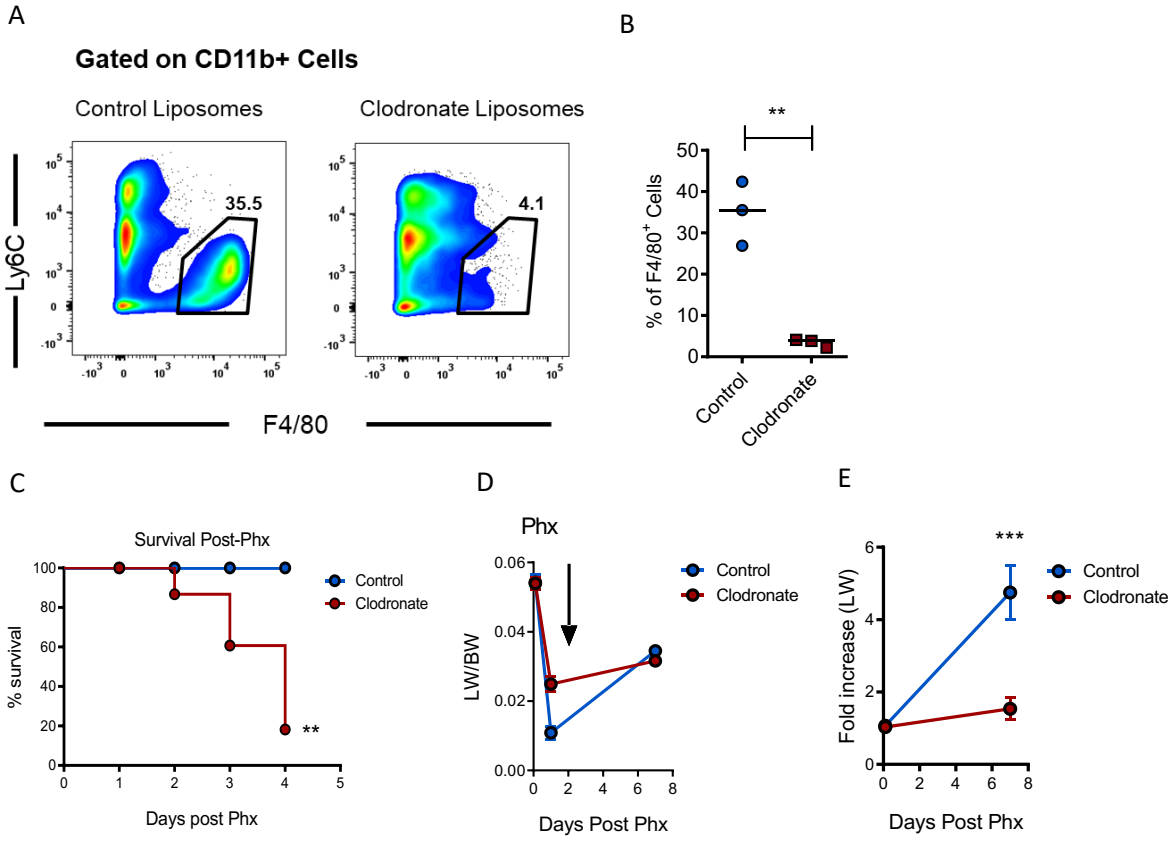

Figure 7: Embryonic Kupffer cells are essential for survival and Liver regeneration following partial hepatectomy. Mice were injected with control or clodronate liposomes 24 h prior to liver PhX. (A) Efficiency of depletion of $CD11b^{+}$ $F4/80^{+}$ macrophages. (B) Frequency of $F4/80^{+}$ cells after depletion with clodronate liposomes. (C) Post-operative survival of mice that were injected with control or clodronate liposomes 24 h prior to partial hepatectomy. (D) LW/BW ratio of control- and clodronate-treated mice post-operatively. (E) Fold increase of liver weight (LW) following partial hepatectomy. The 7-day fold increase was calculated through the initial resected and remnant LW of operated and non - operated animals (reference), respectively. *P<0.05, **P<0.01, ***P<0.001 Student's t-test (B), Log rank survival curve analysis test (C), Two-way ANOVA, Bonferroni's multiple comparison test (D-E), data were obtained from two experiments (C-E), n=3 (A,B) and 5 (C-E) mice per group.

3.3.2 Superior expansion of Embryonic - Tim4^{+} Kupffer cells in the regenerated liver tissue after hepatectomy.

Our findings support the idea that the presence of embryonic macrophages in the remnant liver after resection, is essential for liver growth. However, given that the process of regeneration involves a 7-8-day timeframe of dynamic changes and massive cell proliferation, we investigated the dynamics and expansion of the different macrophage progenies in a regenerating liver microenvironment.

Previous studies using animal and mathematical models have shown that the total liver macrophage density correlates with the liver restoration rate during regeneration (Zafarnia *et al*., 2019). Others proposed that only the BM-derived macrophages are likely related with the liver weight restoration (Melgar-Lesmes and Edelman, 2015). The approach that we utilized to solve discrepancies in literature, was based on using bone marrow chimeras that underwent PhX and analyzed the density of the macrophage progenies with flow cytometry at various timepoints after PhX (Fig 8 A).

To determine the fate and the origin of macrophages that occupy the new “niche” because of liver regeneration, we irradiated C57BL/6J – CD45.2 mice and followingly injected BM from CD45.1 donors (Fig 8 A). Six weeks after reconstitution mice underwent 2/3 partial hepatectomy, and macrophages were isolated at different timepoints after PhX. The chimerism of Ly6C^{hi} monocytes which give rise to bone marrow-derived macrophages is represented in Fig 8 B. Additionally, because of the full body irradiation, which leads to macrophage loss (data not shown), CD45.1^{+} macrophages contribute to the ~50% of the liver macrophages 6 weeks after irradiation (Fig 8 C). With a flow cytometric staining of Tim4 marker expression in combination with CD45.1, three different macrophage populations were present in the liver at steady state. The CD45.1^{-}Tim4^{+} which are the classic embryonic Kupffer cells (KC), CD45.1^{+}Tim4^{-} bone marrow-derived macrophages (BM-MΦ) and CD45.1^{+}Tim4^{+} bone marrow-derived macrophages differentiating towards Kupffer cells (BM-KC) probably after longevity of the BM-MΦ in the liver microenvironment. Of note, there were no Tim4^{-} CD45.1^{-} macrophages present which indicates no significant contamination of residual CD45.2^{+} Ly6C^{hi} Monocytes and no downregulation of TIM4 on KCs (Fig 8 C). Furthermore, we compared the proliferating capacity of CD45.2^{+} Tim4^{+} KC with CD45.1^{+} bone marrow-derived macrophages in lean

mice. Resected liver biopsies and regenerated liver lobes were used for NPC isolation and intracellular flow-cytometric staining for the proliferation marker Ki-67. In resected liver pieces of mice that underwent partial hepatectomy, we observed a significantly higher turnover rate of embryonic Tim4^{+} macrophages compared to bone marrow-derived Tim4^{-} macrophages (Fig 8 D, E). However, both macrophage progenies can proliferate equally 2 and 5 days after liver regeneration. Finally, 7 days after the initial weight of the liver has been restored, embryonic KC remain superior in their proliferating capacity.

As the Ki-67 marker is only an indicator of the cell proliferation, we also calculated the absolute number of the different macrophage populations in the neo-synthesized liver tissue. An increase of BM-derived macrophages at day 2, although not significant, has been observed (Fig 8 F). Strikingly, between day 2-5 post PhX, embryonic Kupffer cells show a 5-6-fold increase in absolute number in the regenerated tissue (Fig 8 F).

Finally, using the Pearson correlation coefficient, we compared the correlation between the absolute number of the different macrophage populations (per gram of liver tissue) with the liver weight growth (LW_{reg}). Interestingly, only in the case of true em-KC (CD45.2^{+} Tim4^{+}) we have a strong correlation (r=0,9878).

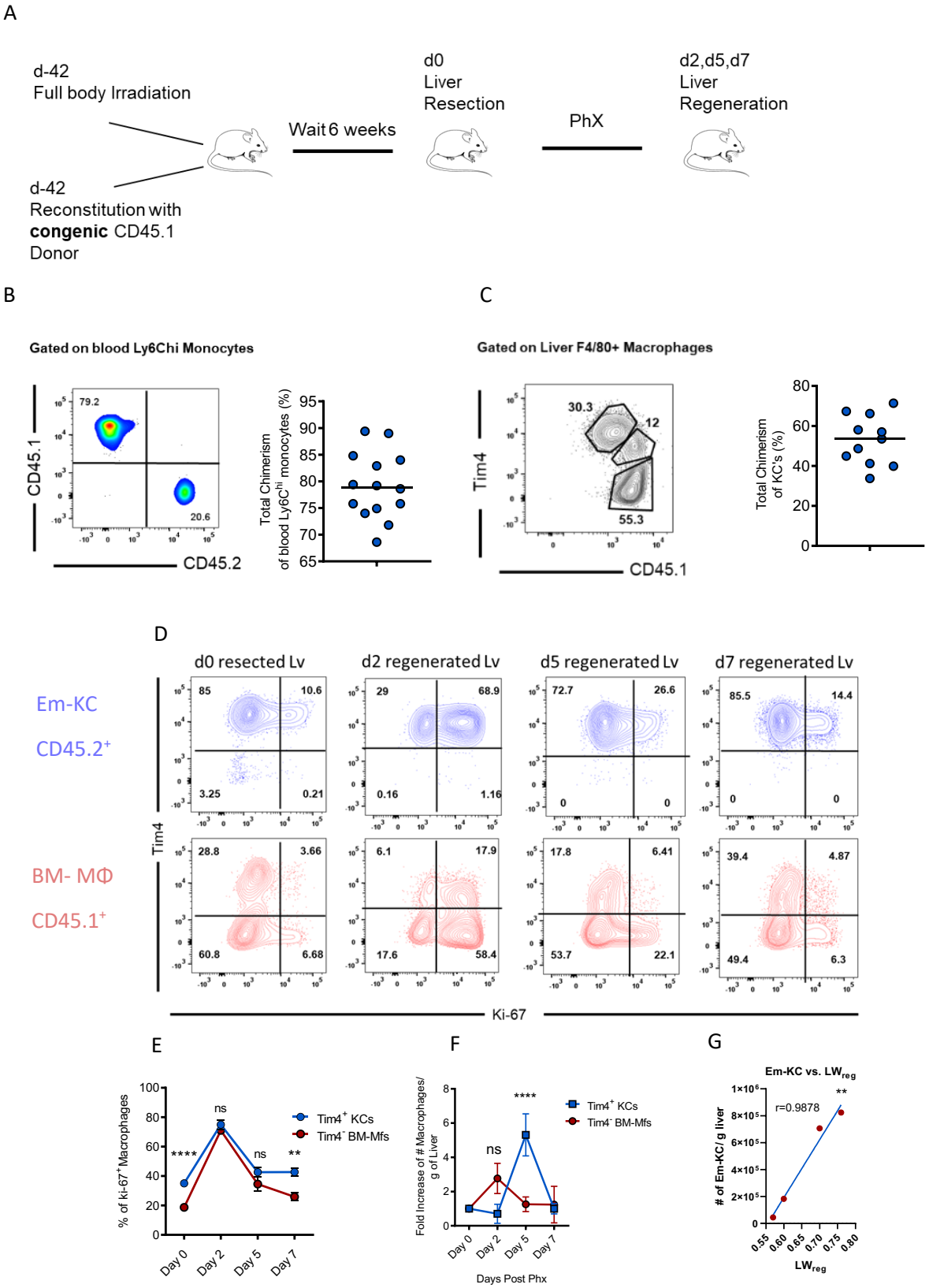

Figure 8: Proliferation and expansion of embryonic KC and bone marrow-derived macrophages in the regenerated tissue. Bone marrow chimeras (CD45.1/2) underwent partial hepatectomy. (A) Schematic representation of the experiment. (B) Chimerism of

Ly6C^{hi} monocytes in the blood of mice after 6 weeks of receiving BM transplant. (C) Chimerism of CD45.1/2 Kupffer cells isolated from the liver of mice. (D) Proliferation of Kupffer cells in the resected and regenerated liver. Blue=Embryonic CD45.2^{+} KC, Red= BM-derived macrophages. (E) % of Ki-67* macrophages among Tim4^{+} (blue) and Tim4^{-} (red). (F) Fold increase of absolute numbers of macrophages / g of liver. (G) Correlation between Em-KC number and restored LW. *P<0.05, **P<0.01, ***P<0.001 Two-way ANOVA, Bonferroni's multiple comparison test, data were obtained from two experiments (E, F). *P<0.05, **P<0.01, ***P<0.001, calculation of Pearson Correlation Coefficient test (G), n=5 mice per group.

To further understand the dynamics of KC expansion upon liver regeneration we utilized the "Microfetti" reporter mice kindly offered by AG Prinz (Tay *et al*., 2017). These mice are a cross between the tamoxifen-induced Cx3cr1-CreERT2 and R26RConfetti mouse lines. A tamoxifen (TAM) injection induces the expression of a random fluorescent protein in CX3CR1^{+} cells encoded by this construct. The four stochastically expressed proteins are a nuclear green fluorescent protein (nGFP), a cytoplasmic yellow fluorescent protein (YFP), a cytoplasmic red fluorescent protein (RFP), or a membrane-tagged cyan fluorescent protein (mCFP) (Fig 9 A). In this mouse model, the embryonic or postnatal age at which tamoxifen is injected, results to potential recombination of different macrophage origins and percentage of recombined cells.

To selectively recombine a low percentage of the resident Kupffer cells, we injected OH-Tamoxifen in Microfetti pups at P1 (1st day after birth). By this, a proportion of Kupffer cells is recombined while avoiding the recombination of CD11b^{hi} CX3CR1^{+} originating from definitive hematopoiesis (Hagemeyer *et al*.,2018). The relatively low percentage of recombination of Kupffer cells makes this tool suitable for the study of single cell clonal expansion.

At the age of 6 weeks, mice underwent partial hepatectomy (Fig 9 A). The resected liver lobes as well as the regenerated liver lobes were analyzed at day 7 by immune fluorescence microscopy to visualize the expansion of Kupffer cells in the form of clones expressing a fluorescent protein. Whole resected and regenerated liver lobes were fixed, stained and patches (clones) of GFP and RFP could be detected in both liver lobes (Fig 9 B). By imaging single clones in high resolution, we used the KNIME data analytics platform to automatically label all F4/80^{+} macrophages and F4/80^{+}Microfetti^{+} cells. Based

on the cellular localization of the GFP signal (counterstained with anti-GFP antibody) and by using DAPI to stain the nucleus we discriminated YFP^+ from $nGFP^+$ and $mCFP^+$. All labelled cells were conversed to a two-dimensional space, where *x* and *y* are representing the coordinates in μm (Fig 9 C). The process followed for an image of a resected liver from a Microfetti mouse is shown in (Fig 9 C). We next analyzed a high number of clones from the resected vs regenerated liver sections. Followingly, we measured the radius of the morphologically spherical clones which contain more than 4 cells (2 division) of the same fluorescent protein and a maximal radius of 300 μm as the maximum migratory distance travelled by a daughter cell after division (Tay *et al*., 2017). With a given radius, the area of expansion of a clone was calculated. The regenerating liver lobes have a significant increased area of expansion compared to resected liver lobes (Fig 9 D, E). This result shows the pronounced expansion of embryonically-derived Kupffer cells and the occupation of the new regenerated liver niche. Of note, the increased area of clones in the resected liver tissue might be related with macrophage homeostatic proliferation.

In summary, embryonic macrophages expand and proliferate in the regenerating liver in the new empty niche contributing to the KC pool in the new homeostatic state.

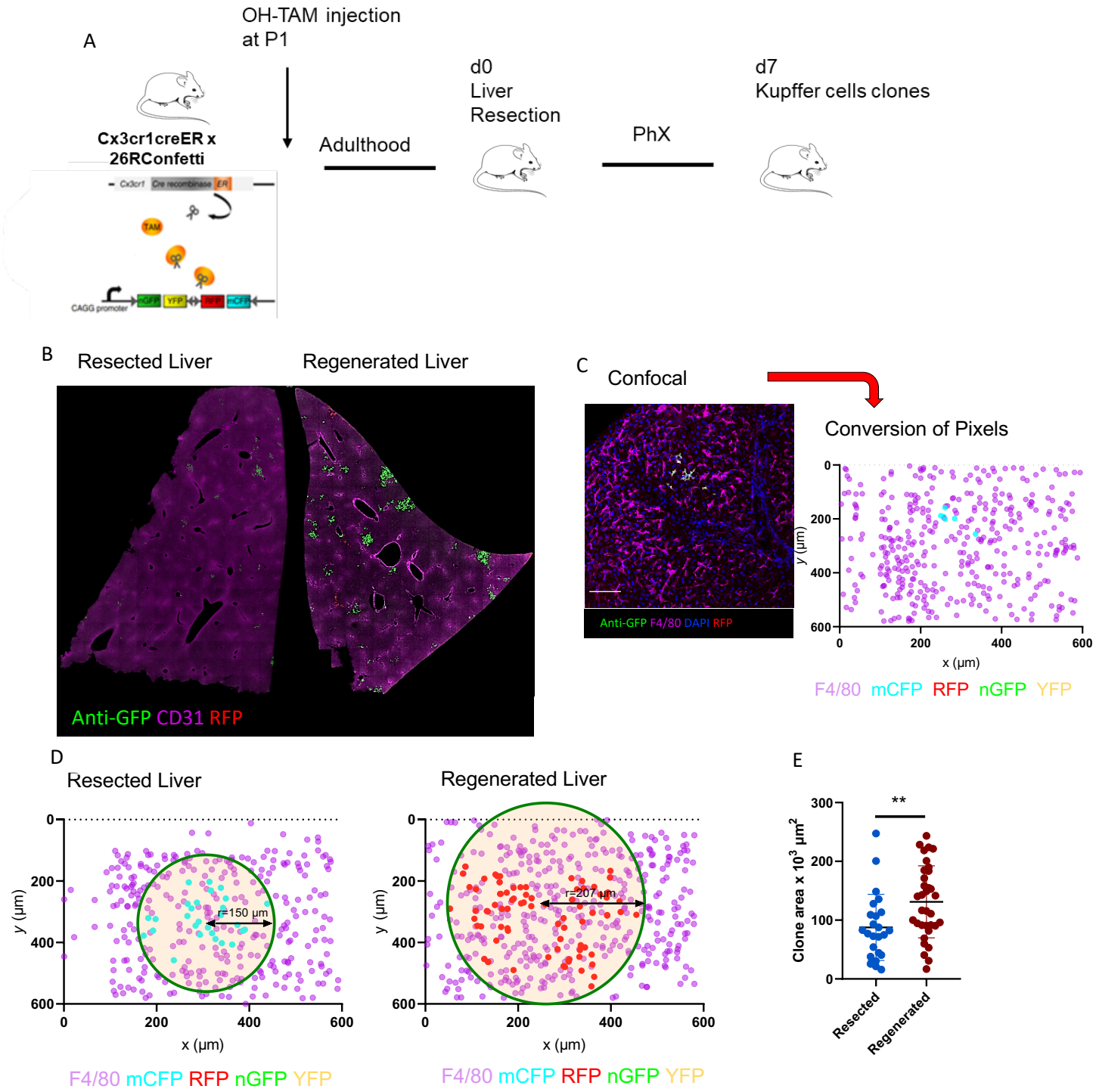

Figure 9: Expansion of embryonic Kupffer cells after PhX in the microfetti mouse model. (A) Schematical representation of experimental setup. Cx3cr1-CreERT2 26RConfetti mice (Microfetti) were injected OH-Tamoxifen at P1. 6 weeks after, mice underwent PhX and resected with regenerated liver lobes were used for

immunofluorescence microscopy and detection of fluorescent protein Kupffer cell clones. (B) Whole liver lobe IF microscopy stained with anti-GFP, CD31. Scale bars = 500 μm. (C) Conversion of a confocal image from a resected liver (scale bars= 150 μm) to a labelled 2D space with x,y the distances in μm. (D) 2D representation of resected and regenerated liver lobes from microfetti mice. Measurement of r=radius of spherical clones of the same fluorescent protein. (E) Area of clones (μm^2) from confocal images from resected and regenerated livers. *P<0.05, **P<0.01, ***P<0.001 Student's t-test (E), data were obtained from one experiment, n=5 mice per group.

3.3.3 Depletion of BM-derived MΦ does not affect liver regeneration and survival post hepatectomy

The infiltration and proliferation of bone marrow-derived macrophages in the regenerated liver have been observed at day 2 post Phx (Fig 8 F). We have shown that liver macrophages are essential for the survival post-operatively and their expansion correlates with liver regeneration, however, the role of the bone marrow-derived macrophages in regeneration has not been investigated yet. For this, we generated bone marrow chimeras by injecting bone marrow from Csf1r-GFP (MaFIA) animals into C57/BL6J mice after shielded irradiation. The abdomens of mice were covered with a lead shield to protect the liver from irradiation damage and prevent embryonic (WT) Kupffer cell loss. 6 weeks post irradiation we examined the chimerism of the $Ly6C^{hi}$ monocytes. Due to the partial bone cover with the lead shield, a lower ~60-70% of chimerism was accomplished (Fig 10 A, B). The MAFIA mice have an inducible Fas suicide/ apoptotic system driven by the mouse *Csf1r*, colony stimulating factor 1 receptor promoter. This transgene construct includes a human mutation of the FKBP12 protein, which binds a dimerization drug AP20187. An i.v injection of the dimerizer AP20187, induces apoptosis in macrophages (Burnett *et al.*, 2004).

Interestingly, a single injection of AP20187 leads to depletion of $Ly6C^{hi}$ monocytes in the bloodstream of the bone marrow chimeras (Fig 10 C, D). However, this depletion of monocytes did not affect the liver growth, the survival of the animals (data not shown) and the LW/BW ratio 3 days after performing PhX (Fig 1 E, F). In the absence of $Ly6C^{hi}$ monocytes which also equals absence of bone marrow macrophages, liver regeneration was not impaired.

In summary, liver macrophages have a profound role in liver regeneration and survival post-PhX. In the regenerating liver microenvironment, both embryonic proliferate and expand. The expansion of em-KC might play an important role in liver regeneration with which it strongly correlates, but this needs further investigation. Moreover, we showed no indication of BM-MΦs having an influence in the liver regeneration process despite their definitive infiltration in the tissue.

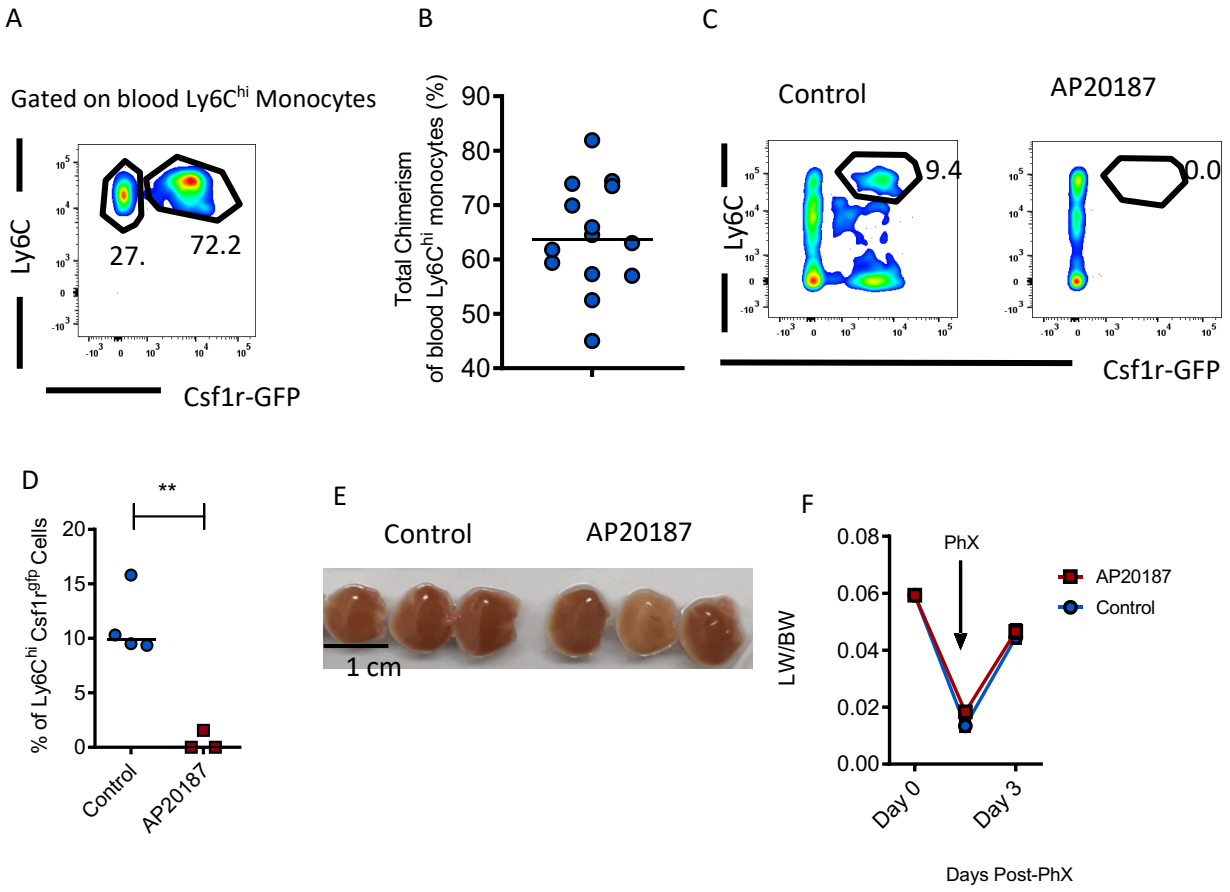

Figure 10: Depletion of bone marrow-derived macrophages does not impair liver regeneration. (A) Plot of Ly6C^{hi} monocytes chimerism in the bloodstream of BL6/Csf1r-gfp bone marrow chimeras (B) % of chimerism of blood Ly6C^{hi} monocytes. (C) Plots of depletion of GFP^{+} cells in the bloodstream with injection of AP20187. (D) Statistical analysis of depleted Ly6C^{hi}GFP^{+} monocytes post AP20187 injection. (E) Pictures of regenerated liver lobes 3 days post PhX. (F) LW/BW ratio of regenerated liver lobes between PBS and AP20187 injected mice 3 days post PhX. *P<0.05, **P<0.01, ***P<0.001 Two-way ANOVA, Bonferroni's multiple comparison test. Data were obtained from two experiments, n=4 mice per group.

3.4 Pericentral Tim4$^-$ MΦ and a decreased KC proliferation, define the regenerating liver lobule of obese mice.

The localization and expansion of the different progenies of macrophages in the regenerating liver has not been studied yet. We have previously observed that em-KC expand in the regenerating liver in the steady state. However, the situation is different in obese mice, where loss of embryonic macrophages and replenishment by BM-derived macrophages occurs. Whether the proliferation and expansion of liver macrophages follow the same pattern as in the steady state will give us insights about the impaired liver regeneration of obese mice.

3.4.1 Tim4$^+$ embryonic Kupffer cells expand in the periportal regions of obese mouse livers.

Liver regeneration after hepatectomy aims at restoring its complete function from the remnant liver after resection. Interestingly, in this process new liver lobules are not formed, rather pre-existing liver lobules grow by proliferation of their cell components (e.g. hepatocytes) from a periportal to a pericentral direction (Elchaninov *et al.*, 2018; Rabes, 2008). During this physiological process it is notable that liver macrophages also proliferate. To track the expansion of macrophages we examined the liver lobules of ND and HFD-fed mice after regeneration with immune fluorescence microscopy.

To begin with, C57BL/6J mice were fed a ND or a HFD and underwent partial hepatectomy. Both, resected and regenerated liver sections were imaged. Liver macrophages from lean mice remained Tim4$^+$ 7d post PhX but showed visual differences of increased macrophage density in liver lobules of regenerating liver lobes (Fig 11 A). On the contrary, resected livers of obese mice, contain only few Tim4$^+$ macrophages with the majority of F4/80$^+$ cells being Tim4$^-$ (Fig 11 B). However, 7 days after liver regeneration, there is an increase of Tim4$^+$ macrophage density, surrounding the periportal regions of the liver lobules, while Tim4$^-$ macrophages are localized in the center of the liver lobule around the central vein (Fig 11 B).

A ND (Resected Liver)

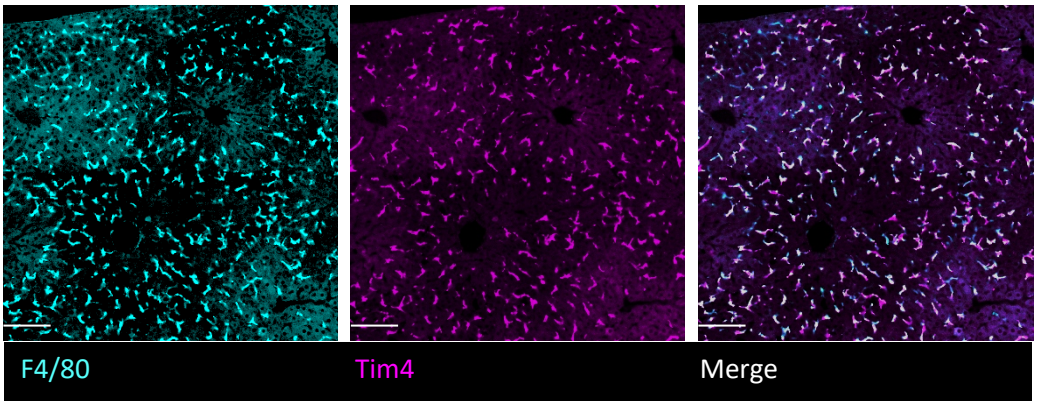

B ND (Regenerated Liver)

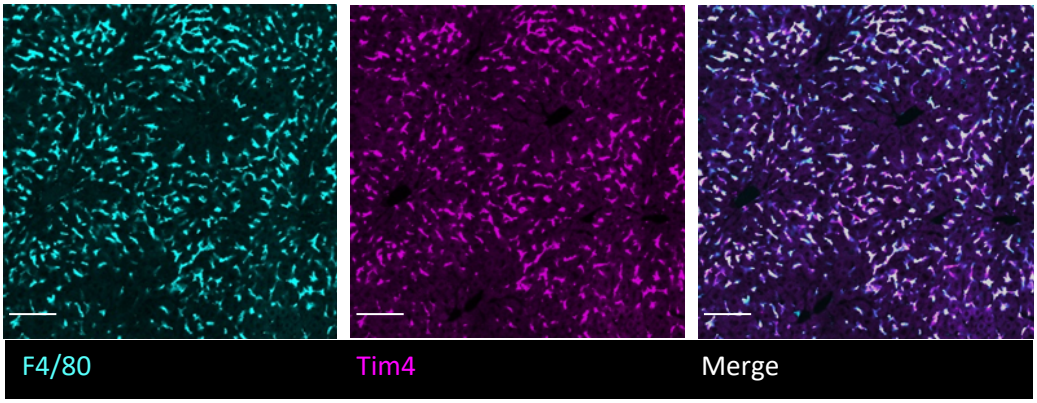

C HFD (Resected Liver)

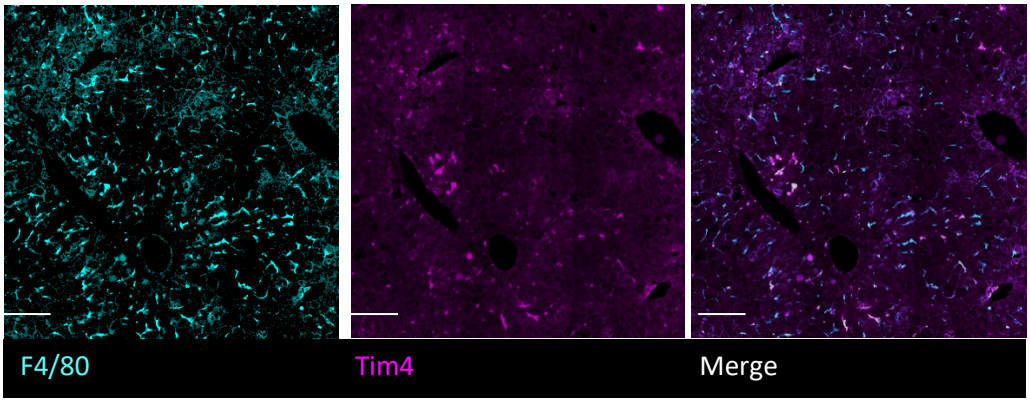

D HFD (Regenerated Liver)

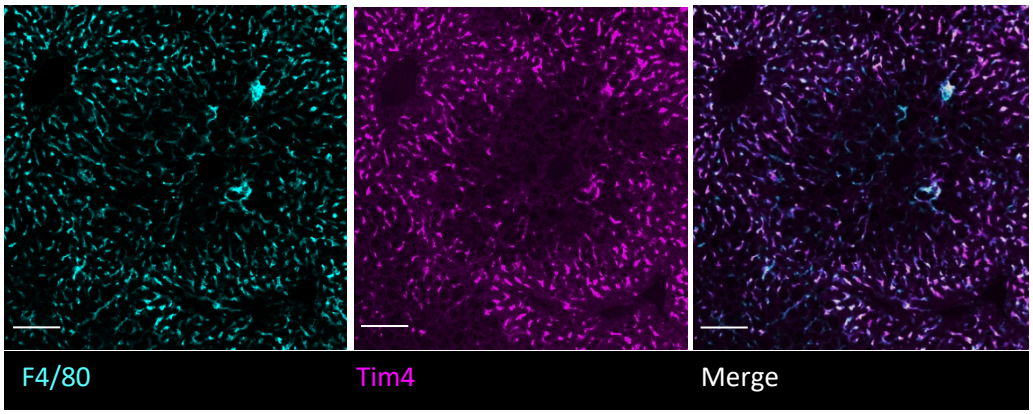

Figure 11: Phenotype of macrophage in lean and obese regenerating livers. Liver tissue biopsies from lean and obese mice were fixed and 30µm slices were stained with antibodies against F4/80 (cyan), Tim4 (red). (A) Lean mice liver tissue resected during partial hepatectomy. (B) Regenerated lean mice liver lobes were harvested and stained 7 days after PhX. (C) Obese mice liver tissue resected during partial hepatectomy. (D) Regenerated liver lobes from obese mice were harvested 7 days after PhX. Scale bars = 100 µm. Pictures are representative from 5 mice and experiment was performed 3 times.

3.4.2 Tim4$^-$ macrophages of obese mice have a bone marrow-derived origin

With this view of liver macrophage dynamics after regeneration, we sought to investigate the distribution of the macrophage progenies in the liver lobule of obese mice. As the expression of the Tim4 marker can be upregulated by BM-MΦ, to confirm the origin of Tim4$^-$ macrophages, we generated bone marrow chimeras. CD45.2 mice were shield irradiated and followingly injected with bone marrow from CD45.1 mice. In the livers of those mice, all embryonically-derived macrophages are CD45.2$^+$ and bone marrow-derived macrophages express CD45.1. Those chimeric mice were fed a normal and a high fat diet for 16 weeks and underwent partial hepatectomy afterwards. We harvested the regenerating livers of those mice and using immunofluorescence we compared the Tim4 marker expression in combination with expression of CD45.1 and CD45.2. Hepatic macrophages of lean mice post-PhX have embryonic origin with co-expression of CD45.2 and Tim4 (Fig 12 A). However, obese mice contain two origins of hepatic macrophages. Surrounding periportal areas, the embryonic Kupffer cells which are exclusively Tim4$^+$ CD45.2$^+$ and the BM-derived macrophages, which are either Tim4$^-$ or Tim4$^+$ CD45.1$^+$. The Tim4$^-$ CD45.1$^+$ are the “recently” infiltrated BM-MΦ and the Tim4$^+$ CD45.1$^+$ the macrophages with bone marrow origin differentiating towards Kupffer (BM-KC). Of note, Tim4$^-$ macrophages have a definitive BM origin, since Tim4$^-$CD45.2$^+$ macrophages are not present (Fig 12 B), indicating a clear distinction of bone marrow-derived macrophages based on their absence of Tim4 expression.

A

CD45.1/2 ND (Regenerated Liver)

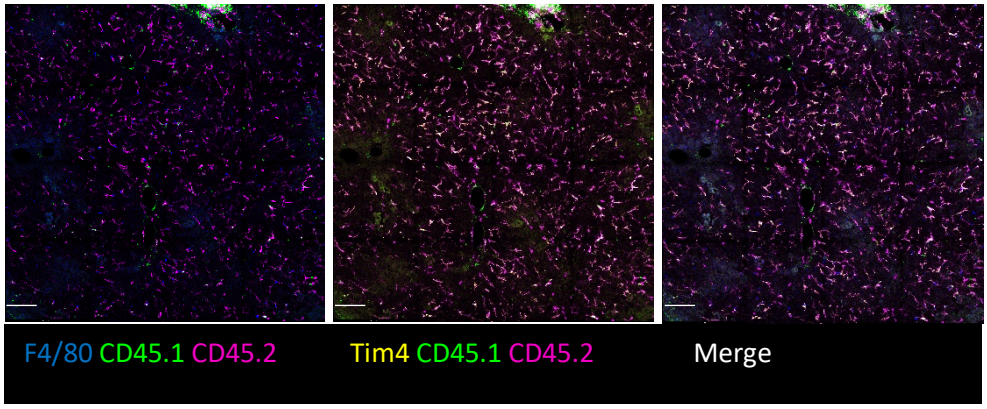

B

CD45.1/2 HFD (Regenerated Liver)

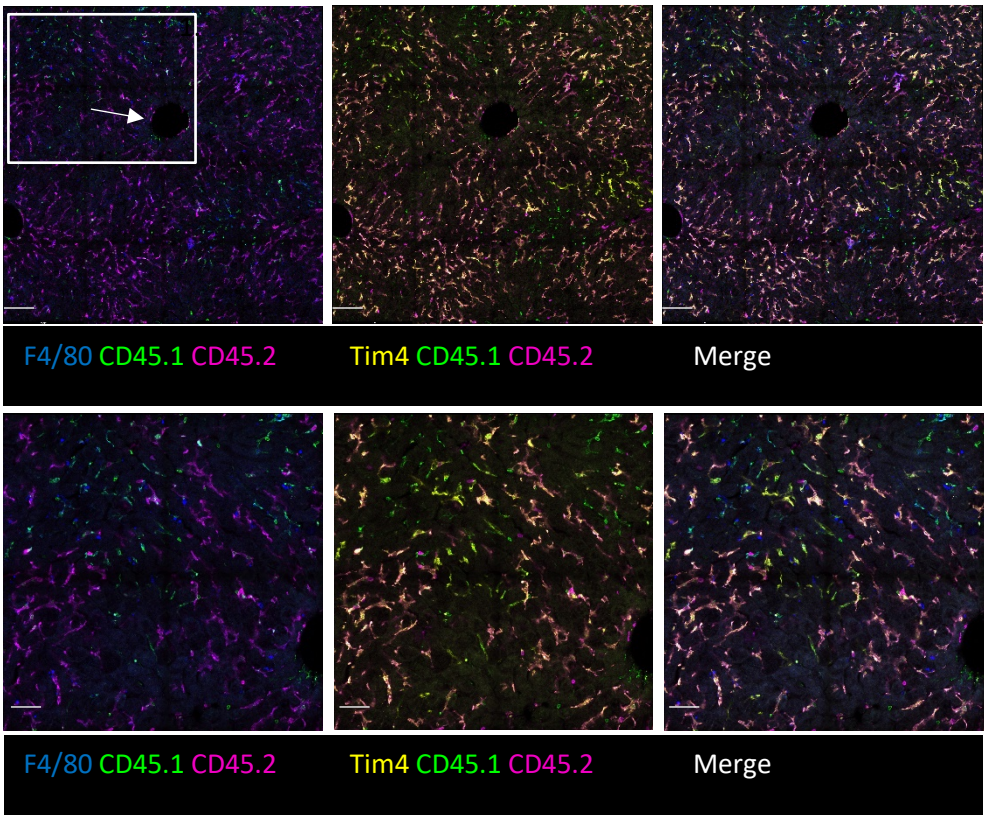

1.

Figure 12: Bone marrow origin of Tim4$^-$ macrophages of obese mice. Liver tissue biopsies from lean and obese CD45.1/2 chimeric mice were fixed, cut and 50µm slices were followingly stained with antibodies against F4/80 (blue), Tim4 (yellow), CD45.1 (green), CD45.2 (magenta). (A) Lean mice liver tissue 7 days post-PhX. (B) Regenerated lobes of obese mice livers were harvested and stained 7 days after PhX. Rectangle represents pericentral area of liver lobule. Arrow=Central Vein, Scale bars = 150 µm (A,B) and 50 µm (B_1, zoom of B upper panel). Pictures are representative from 5 mice and experiment was performed 3 times.

3.4.3 Impaired proliferation of embryonic-derived macrophages in the regenerating livers of obese and lean mice

The significance of embryonic macrophage proliferation in regeneration led us to conduct experiments to analyze the proliferation of embryonic and BM-derived macrophages in the liver of obese and lean mice post PhX. The proliferation was studied in $Tim4^+$ and $Tim4^-$ macrophages of lean and obese mice 48 hours post PhX, a timepoint at which the proliferation of macrophages typically begins (Elchaninov *et al.*, 2018). Additionally, the resected livers during PhX were analyzed with flow cytometric staining.

Firstly, obese mice exhibit an increased frequency of $Ly6C^{hi}$ monocytes (Fig 13 A) in line with the ongoing inflammation and replenishment of embryonic Kupffer cells by BM macrophages, originating from $Ly6C^{hi}$ monocytes. This is also reflected by the total percentage of $Tim4^-$ BM-MΦ which is significantly increased in HFD fed mice (Fig 13 B).

In the regenerating liver lobes of mice, $Tim4^+$ embryonic Kupffer cells are mainly the proliferating macrophages as indicated by the Ki-67 staining. In contrast, $Tim4^-$ bone marrow-derived macrophages have limited capacity of proliferation in both, lean and obese mice (Fig 13 C, D). The embryonic Kupffer cells from obese mice have also a reduced proliferating capacity when compared with those from lean mice (Fig 13 E). Of note, the proliferation of LSECs which happens in identical timeframe as the macrophages is significantly impaired in obese mice (Fig 13 F).

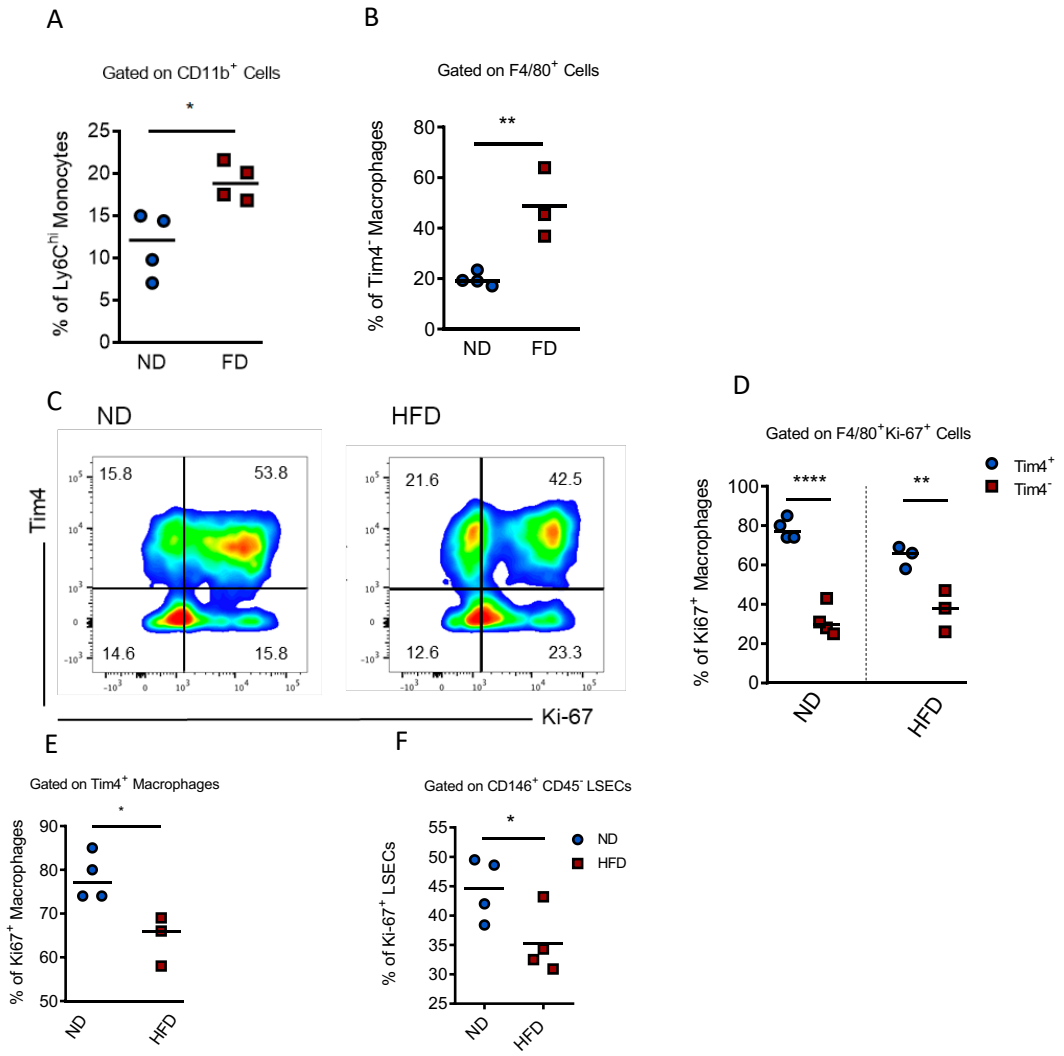

Figure 13: Proliferation of embryonic (Tim4$^+$) and bone marrow-derived (Tim4$^-$) macrophages in regenerating livers of lean and obese mice. (A) % of Ly6C^{hi} monocytes in liver tissue of lean and obese BL6 mice. (B) % of Tim4$^-$ macrophages previously gated on CD11b$^+$F4/80$^+$ macrophages isolated from livers of obese and lean mice. (C) Flow cytometry plots of CD11b$^+$F4/80$^+$ macrophages stained with Tim4, and the proliferation marker Ki-67, 48 hours post PhX (ND vs HFD). (D) % of Ki-67$^+$ macrophages among Tim4$^+$ (blue) and Tim4$^-$ (red) cell population. Comparison between ND vs. HFD fed mice. (E) % of proliferating Ki-67$^+$ Tim4$^+$ embryonic macrophages 2 days after PhX in lean and obese mice. (F) % of proliferating Ki-67$^+$ CD146$^+$ LSECs 2 days after PhX in lean and obese mice *P<0.05, **P<0.01, ***P<0.001 Two-way ANOVA, Bonferroni's multiple comparison test. Data were obtained from one experiment. Student's t-test (A,B,E,F), data were obtained from two experiments, n=4 mice per group.

Altogether, our data suggest that obesity alters the composition of hepatic macrophages in the liver by recruitment of bone marrow-derived macrophages which replenish the loss of embryonic origin Kupffer cells. In response to partial hepatectomy followed by liver regeneration, $Tim4^{+}$ embryonic macrophages have decreased proliferative capacity in obese mice, but nevertheless expand around periportal regions, where also the proliferation of hepatocytes occurs. $Tim4^{-}$ bone marrow-derived macrophages have a limited proliferation in livers of lean and obese mice and no direct effect or correlation with regeneration.

3.5. Obesity alters the early response of liver macrophages to initiate liver regeneration

We hypothesized that following liver resection, Kupffer cells from the remnant liver lobes will be the first “responders” to initiate liver regeneration. Indeed, KC are responding as early as 6 h post PhX by producing IL-6 and other cytokines such as TNFα. Till date, the cause of impaired liver regeneration in obese mice remains incompletely understood. We therefore also examined the possibility of a disrupted downstream signaling of KC “responders” in obese mice, due to the changes in their liver macrophage pool.

3.5.1 Reduced expression of *il-6* and hepatocyte proliferation-associated genes in obese mice

To investigate further the mechanism by which the imbalance of hepatic embryonic/BM-derived macrophages in obese mice leads to an impaired regenerative response, we analyzed the expression of genes shortly after performing partial hepatectomy.

The earliest response of Kupffer cells to partial hepatectomy is the expression and production of interleukin IL-6. According to Izumi *et al*. (2018), IL-6 is produced solely by Kupffer cells as early as 6 h post PhX. The increase of liver IL-6 leads to downstream expression of FoxM1, CDK1 and CCNA2 by hepatocytes which enter the cell cycle and proliferate, restoring the loss of liver mass. The initial signal that triggers the expression of IL-6 by KC is a subject of debate. The vagus nerve of the liver has been identified as the source of acetylcholine which, by binding to receptors on KCs, leads to the expression of IL-6.

As it has been previously shown, loss of embryonic Tim4^{+} Kupffer cells followed by BM-derived Tim4^{-} macrophages occurs in obese mice. The impact of this imbalance of macrophage progenies in obese mice was evaluated by the gene expression of *il-6* in the liver tissue before and after PhX. Indeed, 6 h post PhX, obese mice have a significantly decreased expression of *il-6* compared to ND fed mice (Fig 14 A). The expression of *il-6* returns to baseline levels 72 hours post PhX. Target genes downstream of *il-6*, by binding to the IL6R-gp130 on hepatocytes, is the transcription factor Forkhead box protein M1 (FoxM1) which was analyzed 3 days post PhX. The expression of *Foxm1* with its role in cell cycle progression is significantly decreased in obese mice 3 days post PhX (Fig 14 B). The same transcription factor regulates the expression of several G2/M cycle genes such as *cdk1* and *ccna2* which were also analyzed. The Cyclin-dependent kinase-1 CDK1 is strongly downregulated in obese mice 3 days post PhX compared to lean mice (Fig 14 C). However, no significant differences were observed in the expression of the Cyclin A2 (CCNA2, Fig 14 D). We also examined the expression of different acetylcholine receptors in the liver. The expression of Cholinergic Muscarinic Receptor 3 (*Chrm3*) showed a tendency of decrease on obese mouse livers pre PhX, although not significant (Fig 14 E).

In summary, the early responses in the liver post PhX which include the expression of *il-6* in macrophages and subsequent expression of cell cycle genes on hepatocytes are impaired in obese mice. This leads to a notable impaired liver regeneration in obese mice post PhX. Furthermore, no significant differences were identified concerning the expression of acetylcholine receptors on macrophages, but this subject needs further investigation.

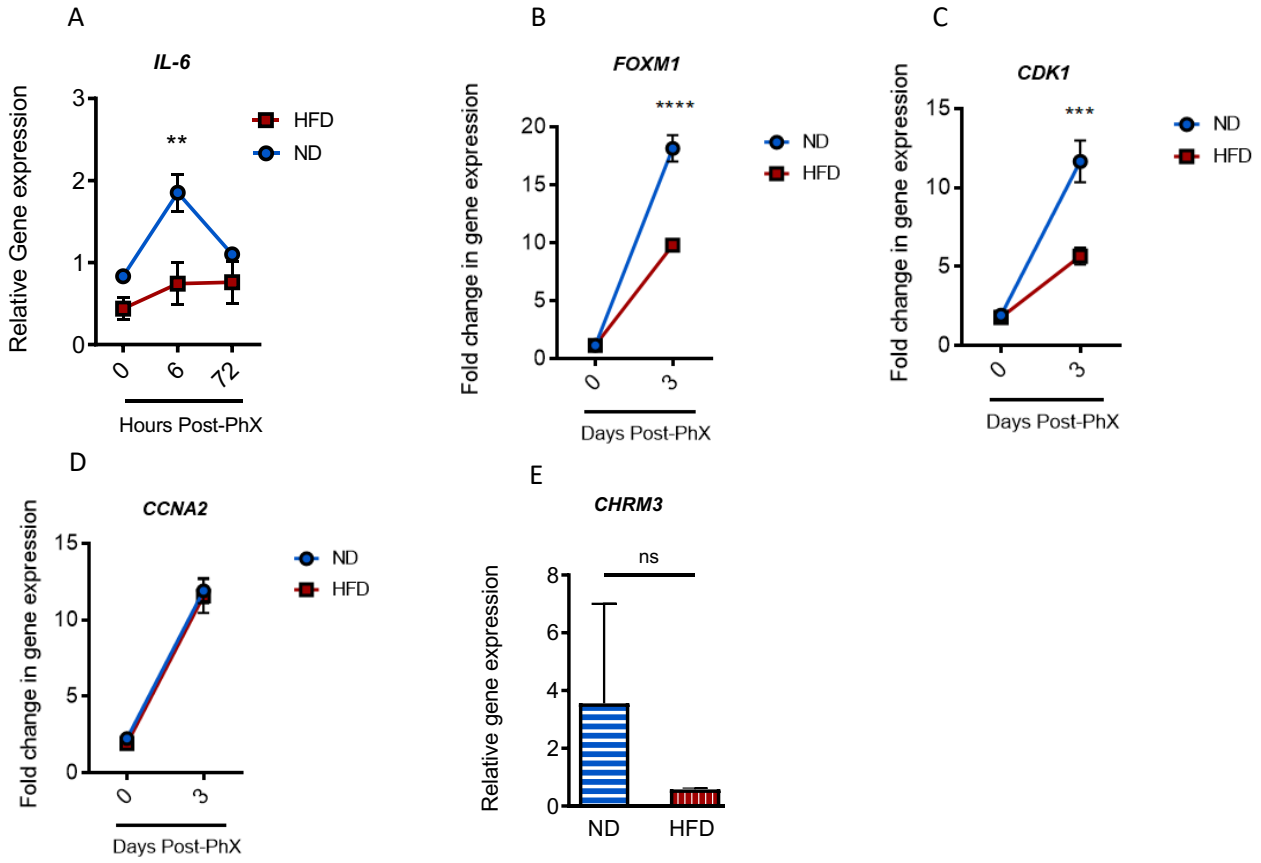

Figure 14: Early gene expression of *il-6* and cell cycle-associated genes in ND and HFD mice post PhX. (A) Relative gene expression of *IL-6* in biopsies of liver tissue of lean and obese BL6 mice after the course of 6- and 72-hours Post PhX. (B) Fold change in gene expression of *FOXM1* (B)*, CDK1* (C) and *CCNA2* (D from liver biopsies of obese and lean mice before and 3 days Post-PhX. (E) Relative gene expression of *CHRM3* of obese and lean livers before PhX. *P<0.05, **P<0.01, ***P<0.001 Student's t-test (E), Two-way ANOVA, Bonferroni's multiple comparison test (A-D), data were obtained from three experiments, n=4 mice per group.

3.6 Em-KC expand after recovery from acute liver damage with CCl_4

So far, we have studied the expansion and role of liver macrophages in liver regeneration after resection (PhX). Given that in the hepatectomy model remnant liver macrophages are present to initiate their expansion and drive regeneration, we examined a model of liver injury where liver macrophages are undergoing cell death. We studied the fate and dynamics of liver macrophages after long term recovery from acute liver injury with CCl_4.

3.6.1 Replenishment of em-KC and BM-MΦ after long term recovery from CCl_4-induced acute liver damage

The impaired liver regeneration of obese mice is also observed after toxin-induced acute liver injury with CCl_4 (Fig 3 B). This type of liver injury leads to pericentral necrosis and loss of liver macrophages. In our experimental setup we used C57BL/6J mice, that were orally gavaged with oil (control) or CCl_4. 24 hours post injury, livers were harvested and used for NPC isolation and a flow-cytometric staining. CCl_4-treated mice exhibit a significant loss of liver $F4/80^+Tim4^+$ macrophages compared to oil-treated mice (Fig 15 A, B).

Following the macrophage loss, we investigated the long-term replenishment of the latter, 30 days post CCl_4 injection in CD45.1/2 bone marrow chimeras. Interestingly, 30 days after complete loss of liver macrophages, those are replenished not only by BM-derived macrophages ($F4/80^+$ $Tim4^-$ $CD45.1^+$) but also by KC ($F4/80^+$ $Tim4^+$ $CD45.1^-$) (Fig 15 C, D). Of note, there were no differences in bone marrow-derived macrophages differentiating towards Kupffer cells (BM-KC), meaning only few BM macrophages upregulated Tim4 in the liver, 30 days post injury (Fig 15 D).

To study the long-term replenishment of liver macrophages from obese mice, we induced acute liver injury in ND and HFD fed mice and examined the phenotype of macrophages 30 days post injury. Surprisingly, a significantly higher percentage of embryonic macrophages was observed 30 days after recovery from liver injury compared to the oil-treated obese mice (Fig 15 E, F). This higher prevalence of em-KC might be explained by the expansion of the latter, similar to the one observed in the partial hepatectomy model of liver regeneration.

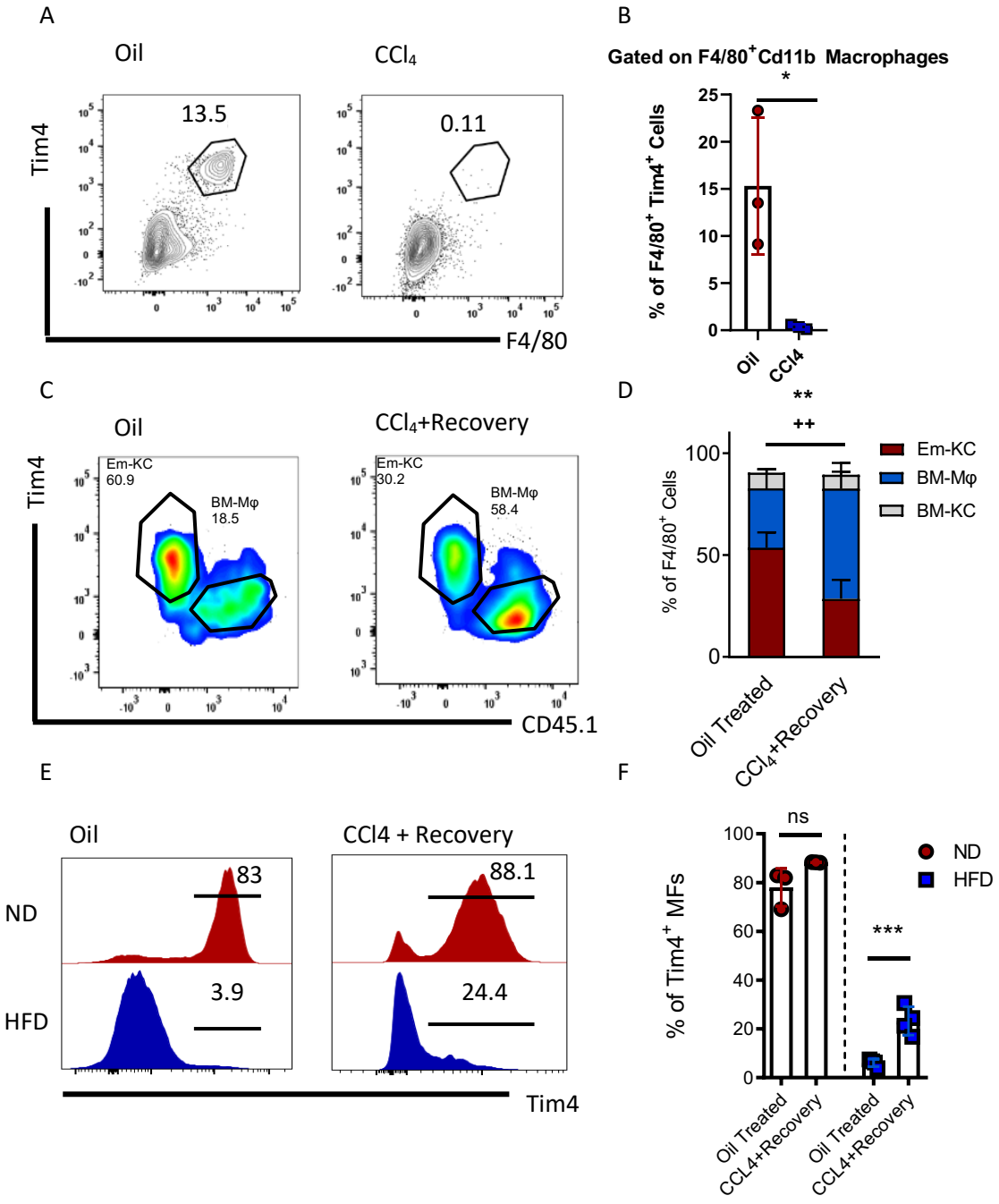

Figure 15: Replenishment of liver macrophages after acute liver injury with CCl_4. (A, B) FACS plots and % of F4/80$^+$Tim4$^+$ macrophages 24 hours post CCl_4 liver injury and oil-treated control. (C) Plots of liver macrophages (F4/80$^+$) isolated from BM chimeras (CD45.1/2) 30 days after treatment with CCl_4 or oil control. (D) % of liver macrophage origins based on Tim4 expression, 30 days after treatment with CCl_4 or oil control. (E) Overlaid histograms of Tim4 expression on liver macrophages (F4/80$^+$) in ND and HFD fed mice, 30 days after treatment with CCl_4 or oil control. (F) % of Tim4 macrophages in ND and HFD fed mice, 30 days after treatment with CCl_4 or oil control. *P<0.05, **P<0.01, ***P<0.001 for BM-Mφ (oil vs. CCl_4 + recovery), $^+$P<0.05, $^{++}$P<0.01, $^{+++}$P<0.001 for em-KC (oil vs. CCl_4 + recovery), Two-way ANOVA, Bonferroni's multiple comparison test, data were obtained from two (A) and one (C, D, E, F) experiment, n=3 and 4 mice per group respectively.

4.Discussion

Obese liver donors that undergo major liver resection for liver transplantation, have a significantly decreased regenerative response leading to an impaired post-operative liver function (Allaire and Gilgenkrantz, 2020; Caldez *et al*., 2020). A loss of liver function in the post-operative timeframe can advance to liver failure, the most common complication after a hepatectomy operation leading to death (Belghiti *et al*., 2000; Van Den Broek *et al*., 2008; Kaibori *et al*., 2008). The exact mechanisms resulting in a slower regenerative mass recovery of the remnant liver of NAFLD patients remain unknown. Finding the mechanisms is hampered by the complexity of the signaling pathways, cell types, cytokines, and growth factors involved in homeostatic regeneration.

The liver is the organ that contains the largest population of tissue-resident macrophages (Kupffer cells). It is understood that liver macrophages have opposing roles by promoting both the progression and resolution of NAFLD related inflammation (Endo-Umeda and Makishima, 2019; Gadd *et al*., 2014; Lanthier *et al*., 2011). To examine the potential role of liver macrophages during homeostatic and inadequate (obesity-related) regeneration, we utilized a pre-clinical mouse model of diet-induced obesity and examined liver regeneration after liver resection (hepatectomy) and chemically-induced liver damage.

Within this study, we demonstrated the high fat diet-induced changes in the innate immune system, specifically the macrophages. Changes in macrophage function and phenotype in obese mice, are related to the replenishment of embryonic Kupffer cells by BM-derived macrophages. By performing regeneration studies in steady state, we elucidated the major role of em-KC in survival and regeneration post hepatectomy. While both em-KC and BM-MΦ proliferate in the remnant regenerating liver, em-KC are superior in expansion and their density correlates with the liver recovery growth. BM-MΦ from obese mice also expand, but to a lesser degree, in both PhX and CCl_4 injury models.

Finally, the altered macrophage pool of obese mice influences the early regenerative response, by impairing *il-6* gene expression and the downstream signaling of hepatocyte proliferation leading to an impaired regenerative potential.

4.1 Tim4^{-} BM-derived macrophages invade the liver macrophage pool and disrupt homeostatic functions

In the present study, specific focus was given to identify the different progenies of macrophages in the livers of obese mice. Using BM-chimeras and Tim4 receptor staining, we firstly showed that Tim4^{-} macrophages have an exclusively bone marrow origin. In agreement with recent studies *(*Devisscher *et al.,* 2017; Remmerie *et al.,* 2020; Tran *et al*., 2020), we observed a loss of the embryonic KC in obese mice, while Tim4^{-} BM macrophages append the liver macrophage pool. The cause of the em-KC death/loss remains elusive till date (Zigmond and Varol, 2020). In a different context, KC-depletion in *Clec4f*-DTR mice and replenishment has been previously described (Scott *et al*., 2016). There, upon depletion of em-KC, Ly6C^{hi} monocytes infiltrate the liver, becoming BM-MΦ (Clec4f^{-} Tim4^{-}) and after their persistence in the tissue, they differentiate towards BM-KC (Clec4f^{+} Tim4^{-}) a highly similar phenotype with the em-KC.

In our findings, we observed a pronounced loss of em-KC and a replenishment by BM-Tim4^{-} macrophages. The baseline proliferation of Em-KC was similar in both diets, but in obese mise there was increased proliferation of BM-MΦ. The results indicate that despite the constant loss of em-KC in obese mice, the latter do not enhance their proliferation and renewal to compensate their own loss, rather BM-MΦ gain the ability to proliferate and replace the em-KC. This hypothesis is in line with Remmerie *et al.* (2020), showing no alteration of the proliferative profile of em-KC 26 weeks after Western diet.

Although BM-KC of obese mice are in process of transitioning toward a KC-like phenotype, we reported impaired homeostatic functions of the obese liver macrophage pool. Specifically, our sorted F4/80^{+} macrophages from obese mice have a significantly impaired function in apoptotic mouse embryonic fibroblast uptake. This is interpretated by taking in consideration that an F4/80^{+} macrophage pool is constituted by a phenotypically different population in obese mice. Those phenotypical differences account for a potential altered function. For instance, the necessity of the phosphatidylserine apoptotic cell receptor Tim4 for macrophage phagocytosis has been previously reported *(*Miyanishi *et al*., 2007; Roberts *et al*., 2017). The pronounced loss of Tim4 we observed in HFD mice could potentially explain the inability for apoptotic cell uptake by the macrophages. However, many different receptors and components can be potentially involved in the

apoptotic cell uptake by macrophages. The expression of genes associated with apoptotic cell receptors pathways between KC and BM-MΦ has been recently published in the Gene expression omnibus (GEO). The most differentially expressed apoptotic cell receptor was Tim4 while other candidate genes for recognition of phosphatidylserine (PS) such as stabilin-1,2 (Park *et al*., 2008), CD300 (Tian *et al*., 2014) do not differ in expression between KC and BM-MΦ.

In summary, macrophages in the liver are responsible for the clearance of blood and uptake of apoptotic cells and translocated gut microbiota (Balmer *et al.*, 2014). A loss of such a crucial function may be detrimental for recovery and regeneration after liver tissue injury. Future research is needed to establish the liver macrophage function in *in vivo* experimental setups.

4.2 Embryonic Kupffer cells are the drivers of liver regeneration

To address the role of liver macrophages in liver regeneration, we performed a series of experiments in the steady state (lean mice). Depletion of Tim4^{+} Kupffer cells led to post-operative death and defective regenerative response. Our liver macrophage kinetic studies during regeneration showed infiltration of BM macrophages followed by proliferation of both, em-KC and BM-MΦ. However, we observed increased expansion (absolute number related) and self-renewal only among em-KC and not BM-MΦ. In line with this, depletion of BM-macrophages did not affect survival or regeneration.

The initial events following a liver resection are characterized by dynamic changes and proliferation of all liver cells. In the context of liver macrophage kinetic changes, our results are in line with others, reporting an infiltration of BM-derived macrophages occurring within 48 hours post liver resection. However, our results contradict the same study where it was demonstrated that CD11b^{+} BM macrophages accelerate liver regeneration *(*Nishiyama *et al*., 2015). The authors considered non shielded irradiation as a model to deplete only BM-derived macrophages and examined liver regeneration after PhX. Shown with our experiments approximately half of the embryonic Kupffer cells are replenished by bone marrow macrophages after a non-shielded irradiation. Therefore, the observed impaired liver regeneration by the authors was not a result of BM-macrophage absence, rather em-KC loss after non-shielded irradiation. In our experiments we observed no significant

decrease in the early regenerative response after depletion of Ly6C^{hi} monocytes. However, due to shielded irradiation, a proportion of endogenous Ly6C^{hi} monocyte remains in circulation, therefore an alternative approach of eliminating monocytes is needed.

The self-renewal ability of em-KC is a part of their identity that is imprinted from the liver microenvironment and cell interactions. When both em-KC and BM-MΦ co-exist in the liver tissue (non-shielded irradiated chimeras), only em-KC retain this ability. Our hypothesis suggests that the em-KC is the progeny of macrophages that expands and occupies the newly regenerated liver after hepatectomy and has the ability to self-renew throughout life. One of the few studies in the context of competition between em-KC and BM-MΦ, Scott *et al*. (2016) showed that KC depletion using the Clec4f-DTR mice, is followed by a competition between BM-MΦ and em-KCs for the KC niche repopulation. Our view on this suggests that depending on the necessity for liver macrophage replenishment and the source or type of liver injury it might or might not lead to competition of em-KC and BM-MΦ. Specifically, in the hepatectomy model that we used, remnant liver macrophages are still present in the liver before initiation of the regeneration. This might be their advantage over BM-MΦ to repopulate the liver microenvironment. In other models where apoptosis or necrosis of KC occurs (such as KC depletion or chemical injury), BM macrophages have a more important role and are participating in the replenishment of the liver macrophage pool. This might suggest an emerging role of BM-MΦ as a supportive measure to combat inflammation and promote macrophage replenishment.

As the liver regenerates, cells proliferate to reach the preoperative liver size. Hepatocytes proliferate first, to restore the hepatic mass and therefore the function of the liver. Followingly, non-parenchymal cells (LSEC, KC, HSC) proliferate and contribute to the original liver size. In line with others (Zafarnia *et al.*, 2019) we observed significantly increased density of em-KC after regeneration. In this study, the liver weight recovery was also correlated with the total number of liver macrophages. By using fate mapping models, we were able not only confirm these data, but also to narrow it down to the density of a specific progeny which are the em-KC. With this finding we hypothesize that em-KC expand as part of the liver regeneration process, contributing partially to the liver weight recovery.

4.3 Impaired early *il-6* expression drives defective proliferative potential of hepatocytes in obese mice.

Among our observations in the above mentioned steady state experiments, was that the time-window of post-operative mouse mortality of KC-depleted mice, aligns with previous studies reporting mortality of IL6-KO mice. In both cases mortality occurs between 2-5 days post PhX. In addition, defective hepatocyte proliferation and liver failure of IL-6 KO mice after PhX has also been described (Blindenbacher *et al*., 2003).

Recently, a potential mechanistic link between the hepatic vagus nerve, the production of IL-6 by macrophages and subsequent hepatocyte proliferation was characterized (Izumi *et al*., 2018). Since macrophages are the main source of IL-6 in the liver, we examined *il-6* expression few hours post-PhX in ND and HFD mice. Here we showed that the normal increase of IL-6 in the regenerative microenvironment, is absent in obese mice. This was followed by a decreased expression of proliferative markers of liver cells, which is associated with an impaired liver regeneration. The decreased release of IL-6 is likely related to the decreased expression of acetylcholine receptor on macrophages by which macrophages respond to vagus nerval signals to release IL-6 post PhX. However, many different types and subtypes of receptors can bind acetylcholine. It is in our future interest to identify the expression of acetylcholine receptors expressed on the different subsets of macrophages in lean and obese mice.

Since we showed a pronounced role of embryonic Kupffer cells in regeneration, we hypothesized that their loss in obese mice led to a macrophage pool unable to receive and initiate signals to promote successful liver regeneration. Interestingly, pre-operatively, obese mice exhibit a decreased expression of *il-6* compared to lean mice. This result is in line with recent RNA-seq data showing that one of the most upregulated genes in em-KC compared to BM macrophages is *il-6* (GEO). In addition to this, within the same study it was also shown that the few em-KC in mice fed a Western diet, have a decreased expression of *il-6* during steady state (Remmerie *et al*., 2020).

In summary, our research indicates that loss of embryonic Kupffer cells and the decrease of *Il-6* expression from the whole macrophage pool leads to decreased hepatocyte proliferation and impaired liver restoration in obese mice. Whether this is mechanistically related to the hepatic nerve is something in need of further investigation.

4.4 Impaired proliferation of KCs and LSECs in the hepatic niche of obese mice after hepatectomy.

Apart from the early regenerative response, where IL-6 has a crucial role in triggering the early proliferation of hepatocytes, proliferation of liver non-parenchymal cells (NPCs) occurs in a different timeframe. Hepatocytes undergo the first round of DNA synthesis within the first 36 hours post hepatectomy (in mice). Subsequently, endothelial cells (LSECs) and KC proliferate starting 2–3 days till 4–5 days after PhX (Sato *et al.*, 2001). The existence of different waves of proliferation regarding the liver cell populations is the signature of the complex mechanisms underlying liver regeneration. It should be underlined that the complete restoration of the lost hepatic mass, includes not only adult hepatocyte proliferation but also proliferation of different types of cells contained within the structure of the liver lobule. In that case, the proliferation of LSECs (angiogenesis) is establishing the new sinusoidal network in the regenerating liver having a significant contribution to liver mass restoration (Drixler *et al*., 2002; Uda *et al*., 2013). Angiogenesis in the partial hepatectomy model is reported to be solely mediated by proliferation of resident ECs and not from bone marrow-derived mononuclear cells (Singhal *et al*., 2018).

Liver macrophages as inhabitants of the sinusoidal network expand in the regenerating liver lobule. Using fate mapping models in lean mice, we showed an advantage of em-KC for expansion compared to BM-derived macrophages. This might suggest that the imprinted identity of em- KC is more potent to occupy the new empty niche. The absolute number of the expanding em-KC correlates with the LW gain, a fact that indicates that restoration of the sinusoidal and macrophage pool network contributes to the liver mass recovery as well.

Regarding the liver lobule structure, the direction of hepatocyte proliferation after partial hepatectomy is initiated from periportal to pericentral areas. The exact same direction of proliferation was observed for LSECs and KC in the regenerating empty cluster of hepatocytes (Andez and Amenta, 1995; Taniguchi *et al*., 2001). By tracing the kinetics of liver macrophages in the regenerating liver lobules of obese and lean mice, we identified expansion of $Tim4^{+}$ KC in periportal areas of both obese and lean mice 7 days post hepatectomy. This confirms our previous results of superiority of em-KC by occupying the

regenerating periportal regions through expansion. BM-derived macrophages, in the case of obese mice, are restricted to deeper parenchymal zones, neighboring pericentral areas.

Expansion of $Tim4^+$ KCs was also observed in the acute liver injury of pericentral necrosis. This model is accompanied by KC loss and pericentral hepatocyte necrosis. During liver regeneration similarly with the PhX model, periportal hepatocytes proliferate. In obese mice em-KC increased their frequency after long term recovery from CCl_4 injury. This potentially indicates that after a total loss of the MΦ pool, loss and regeneration of hepatocytes, $Tim4^+$ and $Tim4^-$ macrophages will expand in the long term and occupy the newly regenerated liver. Those results are in line with findings in KC replenishment after depletion in the Clec4f-DTR mice, where em-KC and BM-MΦ compete for the reconstitution of the macrophage pool.

The presence of $Ly6C^{hi}$ monocytes in livers of obese mice indicates the ongoing inflammation and the differentiation towards $Tim4^-$ BM macrophages. During the proliferation phase of NPCs (48 hours post PhX), in the regenerating liver, $Tim4^-$ BM macrophages have limited proliferation capacity in both ND and HFD fed mice. In addition to this, em-KC and LSECs of HFD mice have decreased proliferative potential 48 hours post hepatectomy.

In summary, we hypothesize that the initial defective hepatocyte proliferation of obese mice post PhX (*via* IL-6), gives rise to a smaller new niche, which is then the scaffold for em-KC proliferation and angiogenesis through LSEC proliferation. As a result, decreased proliferation of KCs and LSECs is observed following the impaired hepatocyte proliferation, contributing further to the slow liver mass recovery post PhX in obese mice.

4.5 Implications of the two-step influence of em-KC in liver regeneration after hepatectomy.

In summary, the data presented in this study improve our understanding of the liver macrophage role in liver regeneration through IL-6 production and subsequent hepatocyte mass restoration, as well as their own proliferation during liver mass regeneration and angiogenesis. In NAFLD, decreased early IL-6 production and impaired proliferation of em-KC and LSECs, lead to impaired regenerative responses post PhX.

The IL-6 pathway is a very potent initiator of liver regeneration and should be considered in the future as a therapeutic target to prevent liver failure in obese patients undergoing major hepatectomy as well as for the regeneration of liver transplant from obese donors to other recipients.

5. Abstract

Obesity-associated liver disease represents a continuously increasing health concern. Besides the risk of obese individuals towards liver dysfunction, cirrhosis and hepatocellular carcinoma, an increased risk for defective liver regeneration post hepatic resection contributes to post-operative morbidity and mortality. Failure of hepatic regeneration, which can ultimately lead to liver failure, is a result of impaired hepatic cell proliferation. Hepatic macrophages have multiple roles in the liver, both in homeostasis and disease progression. However, their exact role and kinetics during physiological and impaired liver regeneration, as seen with non-alcoholic fatty liver disease (NAFLD), is not well understood.

In this study, the role of macrophage progenies during liver regeneration was analyzed by using rodent models of diet-induced obesity followed by models of partial hepatectomy or toxin-induced liver injury.

In our set of experiments, obese mice appeared to have impaired liver regeneration and delayed resolution of inflammation after hepatectomy and acute liver injury, respectively. Macrophages in the fatty liver are among the most altered innate immune populations, with loss of Kupffer cells and recruitment of bone marrow-derived macrophages. Kupffer cells are important for survival and normal liver regeneration of the remnant liver post hepatectomy, while bone marrow-derived macrophages do not exhibit a significant role in this process.

Early post-operative intrahepatic gene expression of *il-6* is impaired in obese mice, which followingly disrupts the expression of cell cycle genes associated with liver cell proliferation and regeneration. Proliferation of hepatocytes, LSECs and embryonic Kupffer cells is decreased post hepatectomy, which leads to a reduced liver regenerative capacity.

These results highlight the importance of embryonic Kupffer cells for liver regeneration through the production of IL-6, which drives a cascade proliferation of liver cells to restore the loss of liver tissue. Obesity strongly impairs the liver regeneration through loss of embryonic Kupffer cells and replenishment by bone marrow-derived macrophages which leads to a defective liver cell proliferation.

6. List of Figures

7. References

Abu Rmilah, A., Zhou, W., Nelson, E., Lin, L., Amiot, B., Nyberg, S. L. Understanding the marvels behind liver regeneration. Wiley interdisciplinary reviews developmental biology 2019; 8: 340

Acosta, L.F., Garcia, C.R., Dugan, A., Marti, F., Davenport, D., Gedaly, R. Impact of super obesity on perioperative outcomes after hepatectomy: The weight of the risk. Surgery (United States) 2017; 162: 1026–1031.

Ahmad, R., Rah, B., Bastola, D., Dhawan, P., Singh, A.B. Obesity-induces Organ and Tissue Specific Tight Junction Restructuring and Barrier Deregulation by Claudin Switching /631/80/79/1987 /692/699/1702/393 /96/63 /14/19 /82/29 /64/60 /141 article. Scientific Reports 2017; 7:.

Akira, S., Takeda, K. Toll-like receptor signalling. Nature Reviews Immunology 2004; 4: 499–511.

Allaire, M., Gilgenkrantz, H. The impact of steatosis on liver regeneration, 2020.

Allman, M., Gaskin, L., Rivera, C.A. CCl_4 -induced hepatic injury in mice fed a Western diet is associated with blunted healing. Journal of Gastroenterology and Hepatology 2010; 25: 635–643.

Amini, N., Margonis, G.A., Buttner, S., et al. Liver regeneration after major liver hepatectomy: Impact of body mass index. Surgery (United States). pp. 81–91. Mosby Inc. (2016).

Andez, A.M., Amenta, P.S. The extracellular matrix in hepatic regeneration. The FASEB Journal 1995; 9: 1401–1410.

Andrade, R.J., Aithal, G.P., Björnsson, E.S., et al. EASL Clinical Practice Guidelines: Drug-induced liver injury. Journal of Hepatology 2019; 70: 1222–1261.

Ascha, M.S., Hanouneh, I.A., Lopez, R., Tamimi, T.A.R., Feldstein, A.F., Zein, N.N. The incidence and risk factors of hepatocellular carcinoma in patients with nonalcoholic steatohepatitis. Hepatology 2010; 51: 1972–1978.

Asrani, S.K., Devarbhavi, H., Eaton, J., Kamath, P.S. Burden of liver diseases in the

world. Journal of Hepatology 2019; 70: 151–171.

Aubert, J., Begriche, K., Knockaert, L., Robin, M.A., Fromenty, B. Increased expression of cytochrome P450 2E1 in nonalcoholic fatty liver disease: Mechanisms and pathophysiological role. Clinics and Research in Hepatology and Gastroenterology 2011; 35: 630–637.

Balmer, M.L., Slack, E., De Gottardi, A., et al. The liver may act as a firewall mediating mutualism between the host and its gut commensal microbiota. Science Translational Medicine 2014; 6: 237ra66-237ra66.

Beattie, L., Sawtell, A., Mann, J., et al. Bone marrow-derived and resident liver macrophages display unique transcriptomic signatures but similar biological functions. Journal of Hepatology 2016; 65: 758–768.

Begriche, K., Massart, J., Robin, M.A., Borgne-Sanchez, A., Fromenty, B. Drug-induced toxicity on mitochondria and lipid metabolism: Mechanistic diversity and deleterious consequences for the liver. Journal of Hepatology 2011; 54: 773–794.

Behrns, K.E., Tsiotos, G.G., DeSouza, N.F., Krishna, M.K., Ludwig, J., Nagorney, D.M. Hepatic Steatosis as a Potential Risk Factor for Major Hepatic Resection. Journal of Gastrointestinal Surgery 1998; 2: 292–298.

Belghiti, J., Hiramatsu, K., Benoist, S., Massault, P.P., Sauvanet, A., Farges, O. Seven hundred forty-seven hepatectomies in the 1990s: An update to evaluate the actual risk of liver resection. Journal of the American College of Surgeons 2000; 191: 38–46.

Bergheim, I., Weber, S., Vos, M., et al. Antibiotics protect against fructose-induced hepatic lipid accumulation in mice: Role of endotoxin. Journal of Hepatology 2008; 48: 983–992.

Blériot, C., Dupuis, T., Jouvion, G., Eberl, G., Disson, O., Lecuit, M. Liver-Resident Macrophage Necroptosis Orchestrates Type 1 Microbicidal Inflammation and Type-2-Mediated Tissue Repair during Bacterial Infection. Immunity 2015; 42: 145–158.

Blindenbacher, A., Wang, X., Langer, I., Savino, R., Terracciano, L., Heim, M.H. Interleukin 6 is important for survival after partial hepatectomy in mice. Hepatology 2003; 38: 674–682.

Block, G.D., Locker, J., Bowen, W.C., et al. Population expansion, clonal growth, and specific differentiation patterns in primary cultures of hepatocytes induced by HGF/SF, EGF and TGFα in a chemically defined (HGM) medium. Journal of Cell Biology 1996; 132: 1133–1149.

Böhm, F., Köhler, U.A., Speicher, T., Werner, S. Regulation of liver regeneration by growth factors and cytokines. EMBO Molecular Medicine 2010; 2: 294–305.

Bonnardel, J., T'jonck, W., Elewaut, D., Saeys, Y., Guilliams Correspondence, M. Stellate Cells, Hepatocytes, and Endothelial Cells Imprint the Kupffer Cell Identity on Monocytes Colonizing the Liver Macrophage Niche. Immunity 2019; 51: 638–654.

Borowiak, M., Garratt, A.N., Wüstefeld, T., Strehle, M., Trautwein, C., Birchmeier, C. Met provides essential signals for liver regeneration. Proceedings of the National Academy of Sciences of the United States of America 2004; 101: 10608–10613.

Borst, K., Frenz, T., Spanier, J., et al. Type I interferon receptor signaling delays Kupffer cell replenishment during acute fulminant viral hepatitis. Journal of hepatology 2018; 68: 682–690.

Bouwens, L., Baekeland, M., de Zanger, R., Wisse, E. Quantitation, tissue distribution and proliferation kinetics of kupffer cells in normal rat liver. Hepatology 1986; 6: 718–722.

Van Den Broek, M.A.J., Olde Damink, S.W.M., Dejong, C.H.C., et al. Liver failure after partial hepatic resection: Definition, pathophysiology, risk factors and treatment, https://pubmed.ncbi.nlm.nih.gov/18647141/, 2008.

Burnett, S.H., Kershen, E.J., Zhang, J., et al. Conditional macrophage ablation in transgenic mice expressing a Fas-based suicide gene. Journal of Leukocyte Biology 2004; 75: 612–623.

Caldez, M.J., Bjorklund, M., Kaldis, P. Cell cycle regulation in NAFLD: when imbalanced metabolism limits cell division, 2020.

Campbell, J.S., Riehle, K.J., Brooling, J.T., Bauer, R.L., Mitchell, C., Fausto, N. Proinflammatory Cytokine Production in Liver Regeneration Is Myd88 -Dependent, but Independent of Cd14 , Tlr2 , and Tlr4 . The Journal of Immunology 2006; 176: 2522–

2528.

Cornell, R.P. Gut-derived endotoxin elicits hepatotrophic factor secretion for liver regeneration. American Journal of Physiology - Regulatory Integrative and Comparative Physiology 1985; 18:.

Cressman, D.E., Greenbaum, L.E., DeAngelis, R.A., et al. Liver failure and defective hepatocyte regeneration in interleukin-6- deficient mice. Science 1996; 274: 1379–1383.

Csak, T., Ganz, M., Pespisa, J., Kodys, K., Dolganiuc, A., Szabo, G. Fatty acid and endotoxin activate inflammasomes in mouse hepatocytes that release danger signals to stimulate immune cells. Hepatology 2011a; 54: 133–144.

Csak, T., Velayudham, A., Hritz, I., et al. Deficiency in myeloid differentiation factor-2 and toll-like receptor 4 expression attenuates nonalcoholic steatohepatitis and fibrosis in mice. American Journal of Physiology - Gastrointestinal and Liver Physiology 2011b; 300: 433–441.

Dambach, D.M., Watson, L.M., Gray, K.R., Durham, S.K., Laskin, D.L. Role of CCR2 in macrophage migration into the liver during acetaminophen-induced hepatotoxicity in the mouse. Hepatology 2002;

Day, C.P. From fat to inflammation. Gastroenterology 2006; 130: 207–210.

Day, C.P., James, O.F.W. Steatohepatitis: A tale of two “Hits”?, https://linkinghub.elsevier.com/retrieve/pii/S0016508598705992, 1998.

DeAngelis, R.A., Markiewski, M.M., Taub, R., Lambris, J.D. A high-fat diet impairs liver regeneration in C57BL/6 mice through overexpression of the NF-κB inhibitor, IκBα. Hepatology 2005; 42: 1148–1157.

Deng, Z. Bin, Liu, Y., Liu, C., et al. Immature myeloid cells induced by a high-fat diet contribute to liver inflammation. Hepatology 2009; 50: 1412–1420.

Devisscher, L., Scott, C.L., Lefere, S., et al. Non-alcoholic steatohepatitis induces transient changes within the liver macrophage pool. Cellular Immunology 2017; 322: 74–83.

Drixler, T.A., Vogten, M.J., Ritchie, E.D., et al. Liver regeneration is an angiogenesis-

associated phenomenon. Annals of Surgery 2002; 236: 703–712.

Duffield, J.S., Forbes, S.J., Constandinou, C.M., et al. Selective depletion of macrophages reveals distinct, opposing roles during liver injury and repair. Journal of Clinical Investigation 2005; 115: 56–65.

Ebe, Y., Hasegawa, G., Takatsuka, H., et al. The role of Kupffer cells and regulation of neutrophil migration into the liver by macrophage inflammatory protein-2 in primary listeriosis in mice. Pathology International 1999; 49: 519–532.

Ehling, J., Bartneck, M., Wei, X., et al. CCL2-dependent infiltrating macrophages promote angiogenesis in progressive liver fibrosis. Gut 2014; 63: 1960–1971.

Elchaninov, A. V., Fatkhudinov, T.K., Usman, N.Y., et al. Dynamics of macrophage populations of the liver after subtotal hepatectomy in rats. BMC Immunology 2018; 19: 23.

Endo-Umeda, K., Makishima, M. Liver X receptors regulate cholesterol metabolism and immunity in hepatic nonparenchymal cells. International Journal of Molecular Sciences 2019; 20:.

Estes, C., Razavi, H., Loomba, R., Younossi, Z., Sanyal, A.J. Modeling the epidemic of nonalcoholic fatty liver disease demonstrates an exponential increase in burden of disease. Hepatology 2018; 67: 123–133.

Font-Burgada, J., Shalapour, S., Ramaswamy, S., Deisseroth, K., Verma, I.M., Karin, M. Hybrid Periportal Hepatocytes Regenerate the Injured Liver without Giving Rise to Cancer. Cell 2015; 162: 766–779.

Frevert, U., Usynin, I., Baer, K., Klotz, C. Nomadic or sessile: can Kupffer cells function as portals for malaria sporozoites to the liver? Cellular Microbiology 2006; 8: 1537–1546.

Gadd, V.L., Skoien, R., Powell, E.E., et al. The portal inflammatory infiltrate and ductular reaction in human nonalcoholic fatty liver disease. Hepatology 2014;

Gan, L.T., Van Rooyen, D.M., Koina, M.E., McCuskey, R.S., Teoh, N.C., Farrell, G.C. Hepatocyte free cholesterol lipotoxicity results from JNK1-mediated mitochondrial injury and is HMGB1 and TLR4-dependent. Journal of Hepatology 2014; 61: 1376–1384.

Garcia-Hernandez, V., Quiros, M., Nusrat, A. Intestinal epithelial claudins: Expression and regulation in homeostasis and inflammation. Annals of the New York Academy of Sciences 2017; 1397: 66–79.

Gomez Perdiguero, E., Klapproth, K., Schulz, C., et al. Tissue-resident macrophages originate from yolk-sac-derived erythro-myeloid progenitors. Nature 2015; 518: 547–551.

Graefe, C., Eichhorn, L., Wurst, P., et al. Optimized Ki-67 staining in murine cells: a tool to determine cell proliferation. Molecular Biology Reports 2019; 46:.

Grunhut, J., Wang, W., Aykut, B., Gakhal, I., Torres-Hernandez, A., Miller, G. Macrophages in Nonalcoholic Steatohepatitis: Friend or Foe? European medical journal. Hepatology 2018; 6: 100–109.

Guillot A, Tacke F. Liver Macrophages: Old Dogmas and New Insights. Hepatol Commun 2019; 22:730-743.

Hagemeyer, N., Kierdorf, K., Frenzel, K., et al. Transcriptome-based profiling of yolk sac-derived macrophages reveals a role for Irf8 in macrophage maturation. The EMBO Journal 2016; 35: 1730–1744.

Hales, C.M., Carroll, M.D., Fryar, C.D., Ogden, C.L. Prevalence of Obesity and Severe Obesity Among Adults: United States, 2017-2018 Key findings Data from the National Health and Nutrition Examination Survey. , 2017.

Hashimoto, D., Chow, A., Noizat, C., et al. Tissue-resident macrophages self-maintain locally throughout adult life with minimal contribution from circulating monocytes. Immunity 2013; 38: 792–804.

Heinz, S., Braspenning, J. Measurement of Blood Coagulation Factor Synthesis in Cultures of Human Hepatocytes. Methods in molecular biology (Clifton, N.J.) 2015; 1250: 309–316.

Heymann, F., Peusquens, J., Ludwig-Portugall, I., et al. Liver Inflammation Abrogates Immunological Tolerance Induced by Kupffer Cells. Hepatology 2015; 62: 279–291.

Higgins GM, A.R. Experimental pathology of the liver. I. Restoration of the liver of the white rat following partial surgical removal. Arch Pathol 1931; 186–202.

Hoeffel, G., Wang, Y., Greter, M., et al. Adult Langerhans cells derive predominantly from embryonic fetal liver monocytes with a minor contribution of yolk sac-derived macrophages. Journal of Experimental Medicine 2012; 209: 1167–1181.

Holt, M.P., Cheng, L., Ju, C. Identification and characterization of infiltrating macrophages in acetaminophen-induced liver injury. Journal of Leukocyte Biology 2008;

Hoppe, S., Von Loeffelholz, C., Lock, J.F., et al. Nonalcoholic steatohepatits and liver steatosis modify partial hepatectomy recovery. Journal of Investigative Surgery 2015; 28: 24–31.

Huang, W., Metlakunta, A., Dedousis, N., et al. Depletion of liver kupffer cells prevents the development of diet-induced hepatic steatosis and insulin resistance. Diabetes 2010; 59: 347–357.

Huh, C.G., Factor, V.M., Sánchez, A., Uchida, K., Conner, E.A., Thorgeirsson, S.S. Hepatocyte growth factor/c-met signaling pathway is required for efficient liver regeneration and repair. Proceedings of the National Academy of Sciences of the United States of America 2004; 101: 4477–4482.

Ikarashi, M., Nakashima, H., Kinoshita, M., et al. Distinct development and functions of resident and recruited liver Kupffer cells/macrophages. Journal of Leukocyte Biology 2013; 94: 1325–1336.

Izumi, T., Imai, J., Yamamoto, J., et al. Vagus-macrophage-hepatocyte link promotes post-injury liver regeneration and whole-body survival through hepatic FoxM1 activation. Nature Communications 2018; 9: 1–13.

Jiang, Y., Tang, Y., Hoover, C., et al. Kupffer cell receptor CLEC4F is important for the destruction of desialylated platelets in mice. Cell Death and Differentiation 2021;

Joseph, S.B., Castrillo, A., Laffitte, B.A., Mangelsdorf, D.J., Tontonoz, P. Reciprocal regulation of inflammation and lipid metabolism by liver X receptors. Nature Medicine 2003; 9: 213–219.

Kaibori, M., Ha-Kawa, S.K., Uchida, Y., et al. Liver regeneration in donors evaluated by Tc-99m-GSA scintigraphy after living donor liver transplantation. Digestive Diseases and Sciences 2008; 53: 850–855.

Karlmark, K.R., Weiskirchen, R., Zimmermann, H.W., et al. Hepatic Recruitment of the Inflammatory Gr1 Monocyte Subset Upon Liver Injury Promotes Hepatic Fibrosis. HEPATOLOGY 2009; 50: 261–274.

Kim, H.M., Park, B.S., Kim, J.I., et al. Crystal Structure of the TLR4-MD-2 Complex with Bound Endotoxin Antagonist Eritoran. Cell 2007; 130: 906–917.

Krenkel, O., Puengel, T., Govaere, O., et al. Therapeutic inhibition of inflammatory monocyte recruitment reduces steatohepatitis and liver fibrosis. Hepatology 2018; 67: 1270–1283.

Lanthier, N., Molendi-Coste, O., Cani, P.D., Rooijen, N., Horsmans, Y., Leclercq, I.A. Kupffer cell depletion prevents but has no therapeutic effect on metabolic and inflammatory changes induced by a high-fat diet. The FASEB Journal 2011; 25: 4301–4311.

Laukoetter, M.G., Nava, P., Lee, W.Y., et al. JAM-A regulates permeability and inflammation in the intestine in vivo. Journal of Experimental Medicine 2007; 204: 3067–3076.

Lavin, Y., Winter, D., Blecher-Gonen, R., et al. Tissue-resident macrophage enhancer landscapes are shaped by the local microenvironment. Cell 2014a; 159: 1312–1326.

Lavin, Y., Winter, D., Blecher-Gonen, R., et al. Tissue-resident macrophage enhancer landscapes are shaped by the local microenvironment. Cell 2014b; 159: 1312–1326.

Leclercq, I.A., Vansteenberghe, M., Lebrun, V.B., et al. Defective hepatic regeneration after partial hepatectomy in leptin-deficient mice is not rescued by exogenous leptin. Laboratory Investigation 2006; 86: 1161–1171.

Leroux, A., Ferrere, G., Godie, V., et al. Toxic lipids stored by Kupffer cells correlates with their pro-inflammatory phenotype at an early stage of steatohepatitis. Journal of Hepatology 2012; 57: 141–149.

Lin, DX., Zhang, QY., Li, X. et al. An aggressive approach leads to improved survival in hepatocellular carcinoma patients with portal vein tumor thrombus. J Cancer Res Clin Oncol 2011; 137: 139–149.

Lock, J.F., Malinowski, M., Seehofer, D., et al. Function and volume recovery after partial hepatectomy: Influence of preoperative liver function, residual liver volume, and obesity. Langenbeck's Archives of Surgery 2012; 397: 1297–1304.

Lorenz, L., Axnick, J., Buschmann, T., et al. Mechanosensing by β1 integrin induces angiocrine signals for liver growth and survival. Nature 2018; 562: 128–132.

Luther, J., Garber, J.J., Khalili, H., et al. Hepatic Injury in Nonalcoholic Steatohepatitis Contributes to Altered Intestinal Permeability. CMGH 2015; 1: 222-232.e2.

Manibusan, M.K., Odin, M., Eastmond, D.A. Postulated carbon tetrachloride mode of action: A review. Journal of Environmental Science and Health - Part C Environmental Carcinogenesis and Ecotoxicology Reviews 2007; 25: 185–209.

Mass, E., Ballesteros, I., Farlik, M., et al. Specification of tissue-resident macrophages during organogenesis. Science 2016; 353:.

McGlynn, K.A., London, W.T. The Global Epidemiology of Hepatocellular Carcinoma: Present and Future. Clinics in Liver Disease 2011; 15: 223–243.

Melgar-Lesmes, P., Edelman, E.R. Monocyte-endothelial cell interactions in the regulation of vascular sprouting and liver regeneration in mouse. Journal of Hepatology 2015; 63: 917–925.

Michalopoulos, G.K. Liver regeneration. Journal of Cellular Physiology 2007; 213: 286–300.

Michalopoulos, G.K., Bhushan, B. Liver regeneration: biological and pathological mechanisms and implications, http://www.nature.com/articles/s41575-020-0342-4, 2020.

Miele, L., Valenza, V., La Torre, G., et al. Increased intestinal permeability and tight junction alterations in nonalcoholic fatty liver disease. Hepatology 2009; 49: 1877–1887.

Mills, C. D., Kincaid, K., Alt, J. M., Heilman, M. J.,Hill, A. M. M-1/M-2 Macrophages and the Th1/Th2 Paradigm. The Journal of Immunology 2000; 164: 6166–6173.

Mitchell, C., Couton, D., Couty, J.P., et al. Dual role of CCR2 in the constitution and the resolution of liver fibrosis in mice. American Journal of Pathology 2009; 174: 1766–1775.

Mitchell, C., Nivison, M., Jackson, L.F., et al. Heparin-binding epidermal growth factor-like growth factor links hepatocyte priming with cell cycle progression during liver regeneration. Journal of Biological Chemistry 2005; 280: 2562–2568.

Mitchell, C., Willenbring, H. A reproducible and well-tolerated method for 2/3 partial hepatectomy in mice. Nature Protocols 2008; 3: 1167–1170.

Miyanishi, M., Tada, K., Koike, M., Uchiyama, Y., Kitamura, T., Nagata, S. Identification of Tim4 as a phosphatidylserine receptor. Nature 2007; 450: 435–439.

Moolten, F.L., Bucher, N.L.R. Regeneration of rat liver: Transfer of humoral agent by cross circulation. Science 1967; 158: 272–274.

Morinaga, H., Mayoral, R., Heinrichsdorff, J., et al. Characterization of distinct subpopulations of hepatic macrophages in HFD/obese mice. Diabetes 2015; 64: 1120–1130.

Morris-Stiff, G., Marangoni, G., Hakeem, A., et al. Redefining major hepatic resection for colorectal liver metastases: Analysis of 1111 liver resections. International Journal of Surgery 2016; 25: 172–177.

Motta, P.M. The Three-Dimensional Microanatomy of the Liver. Archivum histologicum japonicum 1984; 47: 1–30.

Natarajan, A., Wagner, B., Sibilia, M. The EGF receptor is required for efficient liver regeneration. Proceedings of the National Academy of Sciences of the United States of America 2007; 104: 17081–17086

Neuschwander-Tetri, B.A. Hepatic lipotoxicity and the pathogenesis of nonalcoholic steatohepatitis: The central role of nontriglyceride fatty acid metabolites. Hepatology 2010; 52: 774–788.

Nguyen-Lefebvre, A.T., Horuzsko, A. Kupffer Cell Metabolism and Function. Journal of enzymology and metabolism 2015; 1: 101.

Nishiyama, K., Nakashima, H., Ikarashi, M., et al. Mouse CD11b+Kupffer cells recruited from bone marrow accelerate liver regeneration after partial hepatectomy. PLoS ONE 2015; 10:.

Olsen, P.S., Boesby, S., Kirkegaard, P., et al. Influence of epidermal growth factor on liver regeneration after partial hepatectomy in rats. Hepatology 1988; 8: 992–996.

Özcan, U., Cao, Q., Yilmaz, E., et al. Endoplasmic reticulum stress links obesity, insulin action, and type 2 diabetes. Science 2004; 306: 457–461.

Pardo, V., González-Rodríguez, Á., Muntané, J., Kozma, S.C., Valverde, Á.M. Role of hepatocyte S6K1 in palmitic acid-induced endoplasmic reticulum stress, lipotoxicity, insulin resistance and in oleic acid-induced protection. Food and Chemical Toxicology 2015; 80: 298–309.

Park, S.Y., Jung, M.Y., Kim, H.J., et al. Rapid cell corpse clearance by stabilin-2, a membrane phosphatidylserine receptor. Cell Death and Differentiation 2008; 15: 192–201.

Peverill, W., Powell, L.W., Skoien, R. Evolving concepts in the pathogenesis of NASH: Beyond steatosis and inflammation. International Journal of Molecular Sciences 2014; 15: 8591–8638.

Pfaffenbach, K.T., Gentile, C.L., Nivala, A.M., Wang, D., Wei, Y., Pagliassotti, M.J. Linking endoplasmic reticulum stress to cell death in hepatocytes: Roles of C/EBP homologous protein and chemical chaperones in palmitate-mediated cell death. American Journal of Physiology - Endocrinology and Metabolism 2010; 298:.

Piscaglia, F., Svegliati-Baroni, G., Barchetti, A., et al. Clinical patterns of hepatocellular carcinoma in nonalcoholic fatty liver disease: A multicenter prospective study. Hepatology 2016; 63: 827–838.

Pu, W., Zhang, H., Huang, X., et al. Mfsd2a+ hepatocytes repopulate the liver during injury and regeneration. Nature Communications 2016; 7: 1–15.

Rabes, H.M. Kinetics of Hepatocellular Proliferation as a Function of the Microvascular Structure and Functional State of the Liver. Ciba Foundation symposium. pp. 31–59. John Wiley & Sons, Ltd (2008).

Rahbari, N.N., Garden, O.J., Padbury, R., et al. Posthepatectomy liver failure: A definition and grading by the International Study Group of Liver Surgery (ISGLS). Surgery 2011; 149: 713–724.

Rahman, K., Desai, C., Iyer, S.S., et al. Loss of Junctional Adhesion Molecule A Promotes Severe Steatohepatitis in Mice on a Diet High in Saturated Fat, Fructose, and Cholesterol. Gastroenterology 2016; 151: 733-746.e12.

Remmerie, A., Martens, L., Thoné, T., et al. Osteopontin Expression Identifies a Subset of Recruited Macrophages Distinct from Kupffer Cells in the Fatty Liver. Immunity 2020; 53: 641-657.e14.

Rivera, C.A., Adegboyega, P., van Rooijen, N., Tagalicud, A., Allman, M., Wallace, M. Toll-like receptor-4 signaling and Kupffer cells play pivotal roles in the pathogenesis of non-alcoholic steatohepatitis. Journal of Hepatology 2007; 47: 571–579.

Roberts, A.W., Lee, B.L., Deguine, J., John, S., Shlomchik, M.J., Barton, G.M. Tissue-Resident Macrophages Are Locally Programmed for Silent Clearance of Apoptotic Cells. Immunity 2017; 47: 913-927.e6.

Robinson, M.W., Harmon, C., O'Farrelly, C. Liver immunology and its role in inflammation and homeostasis, www.nature.com/cmi, 2016.

Sabaté, J.M., Jouët, P., Harnois, F., et al. High prevalence of small intestinal bacterial overgrowth in patients with morbid obesity: A contributor to severe hepatic steatosis. Obesity Surgery 2008; 18: 371–377.

Sakai, M., Troutman, T.D., Seidman, J.S., et al. Liver-Derived Signals Sequentially Reprogram Myeloid Enhancers to Initiate and Maintain Kupffer Cell Identity. Immunity 2019;

Sato, A., Nakashima, H., Nakashima, M., et al. Involvement of the TNF and fasl produced by CD11b kupffer cells/macrophages in CCl4-induced acute hepatic injury. PLoS ONE 2014; 9:.

Sato, T., El-Assal, O.N., Ono, T., Yamanoi, A., Kumar Dhar, D., Nagasue, N. Sinusoidal endothelial cell proliferation and expression of angiopoietin/Tie family in regenerating rat liver. Journal of Hepatology 2001; 34: 690–698.

Schindl, M.J., Redhead, D.N., Fearon, K.C.H., Garden, O.J., Wigmore, S.J. The value of residual liver volume as a predictor of hepatic dysfunction and infection after major liver resection. Gut 2005; 54: 289–296.

Schulz, C., Perdiguero, E.G., Chorro, L., et al. A lineage of myeloid cells independent of myb and hematopoietic stem cells. Science 2012; 335: 86–90.

Scott, C.L., Zheng, F., De Baetselier, P., et al. Bone marrow-derived monocytes give rise to self-renewing and fully differentiated Kupffer cells. Nature Communications 2016a; 7: 1–10.

Seki, E., Tsutsui, H., Iimuro, Y., et al. Contribution of Toll-like receptor/myeloid differentiation factor 88 signaling to murine liver regeneration. Hepatology 2005; 41: 443–450.

Selzner, M., Clavien, P.A. Failure of regeneration of the steatotic rat liver: Disruption at two different levels in the regeneration pathway. Hepatology 2000; 31: 35–42.

Shen, F.W., Saga, Y., Litman, G., et al. Cloning of Ly-5 cDNA. Proceedings of the National Academy of Sciences of the United States of America 1985; 82: 7360–7363.

Sheng, J., Ruedl, C., Karjalainen, K. Most Tissue-Resident Macrophages Except Microglia Are Derived from Fetal Hematopoietic Stem Cells. Immunity 2015a; 43: 382–393.

Sheng, J., Ruedl, C., Karjalainen, K. Most Tissue-Resident Macrophages Except Microglia Are Derived from Fetal Hematopoietic Stem Cells. Immunity 2015b; 43: 382–393.

Shi, J., Fujieda, H., Kokubo, Y., Wake, K. Apoptosis of neutrophils and their elimination by Kupffer cells in rat liver. Hepatology 1996; 24: 1256–1263.

Shi, J., Gilbert, G.E., Kokubo, Y., Ohashi, T. Role of the liver in regulating numbers of circulating neutrophils. Blood 2001; 98: 1226–1230.

Singhal, M., Liu, X., Inverso, D., et al. Endothelial cell fitness dictates the source of regenerating liver vasculature. The Journal of experimental medicine 2018; 215: 2497–2508.

Sørensen KK, Simon-Santamaria J, McCuskey RS, Smedsrød B. Liver Sinusoidal Endothelial Cells. Compr Physiol 2015; 5(4):1751-74.

Stockmann, M., Lock, J.F., Malinowski, M., Niehues, S.M., Seehofer, D., Neuhaus, P.

The LiMAx test: A new liver function test for predicting postoperative outcome in liver surgery. HPB 2010; 12: 139–146.

Stolz, D.B., Mars, W.M., Petersen, B.E., Kim, T.H., Michalopoulos, G.K. Growth factor signal transduction immediately after two-thirds partial hepatectomy in the rat. Cancer research 1999; 59: 3954–3960.

Streetz, K.L., Luedde, T., Manns, M.P., Trautwein, C. Interleukin 6 and liver regeneration. Gut 2000; 47: 309–312.

Stremmel, C., Schuchert, R., Wagner, F., et al. Yolk sac macrophage progenitors traffic to the embryo during defined stages of development. Nature Communications 2018;

Sun, F., Hamagawa, E., Tsutsui, C., Ono, Y., Ogiri, Y., Kojo, S. Evaluation of oxidative stress during apoptosis and necrosis caused by carbon tetrachloride in rat liver. Biochimica et Biophysica Acta - Molecular Basis of Disease 2001; 1535: 186–191.

Sun, T., Pikiolek, M., Orsini, V., et al. AXIN2+ Pericentral Hepatocytes Have Limited Contributions to Liver Homeostasis and Regeneration. Cell Stem Cell 2020; 26: 97-107.e6.

Taniguchi, E., Sakisaka, S., Matsuo, K., Tanikawa, K., Sata, M. Expression and role of vascular endothelial growth factor in liver regeneration after partial hepatectomy in rats. Journal of Histochemistry and Cytochemistry 2001; 49: 121–129.

Tay, T.L., Mai, D., Dautzenberg, J., et al. A new fate mapping system reveals context-dependent random or clonal expansion of microglia. Nature Neuroscience 2017a; 20: 793–803.

Tay, T.L., Mai, D., Dautzenberg, J., et al. A new fate mapping system reveals context-dependent random or clonal expansion of microglia. Nature Neuroscience 2017b; 20: 793–803.

Taylor, M.E., Snelling, T., Smith, D.F., Drickamer, K. Absence of a human ortholog of rodent Kupffer cell galactose-binding receptor encoded by the CLEC4f gene. Glycobiology 2019; 29: 332–345.

Tian, L., Choi, S.C., Murakami, Y., et al. P85α recruitment by the CD300f

phosphatidylserine receptor mediates apoptotic cell clearance required for autoimmunity suppression. Nature Communications 2014; 5:.

Tran, S., Baba, I., Poupel, L., et al. Impaired Kupffer Cell Self-Renewal Alters the Liver Response to Lipid Overload during Non-alcoholic Steatohepatitis. Immunity 2020; 53: 627-640.e5.

Truant, S., Bouras, A.F., Petrovai, G., et al. Volumetric gain of the liver after major hepatectomy in obese patients: A case-matched study in 84 patients. Annals of Surgery 2013; 258: 696–704.

Uda, Y., Hirano, T., Son, G., et al. Angiogenesis is crucial for liver regeneration after partial hepatectomy. Surgery (United States) 2013; 153: 70–77.

Vibert, E., Pittau, G., Gelli, M., et al. Actual incidence and long-term consequences of posthepatectomy liver failure after hepatectomy for colorectal liver metastases. Surgery (United States) 2014; 155: 94–105.

Wang, B., Zhao, L., Fish, M., Logan, C.Y., Nusse, R. Self-renewing diploid Axin2 + cells fuel homeostatic renewal of the liver. Nature 2015; 524: 180–185.

Wang, C.Y., Liao, J.K. A mouse model of diet-induced obesity and insulin resistance. Methods in Molecular Biology 2012; 821: 421–433.

Wang, D.H., Wang, Y.N., Ge, J.Y., et al. Role of activin A in carbon tetrachloride-induced acute liver injury. World Journal of Gastroenterology 2013; 19: 3802–3809.

Webber, E.M., Bruix, J., Pierce, R.H., Fausto, N. Tumor necrosis factor primes hepatocytes for DNA replication in the rat. Hepatology 1998; 28: 1226–1234.

Weber, L.W.D., Boll, M., Stampfl, A. Hepatotoxicity and mechanism of action of haloalkanes: Carbon tetrachloride as a toxicological model. Critical Reviews in Toxicology 2003; 33: 105–136.

Wynn, T.A., Vannella, K.M. Macrophages in Tissue Repair, Regeneration, and Fibrosis, /pmc/articles/PMC4794754/?report=abstract, 2016.

Xiao, F., Waldrop, S.L., Khimji, A.K., Kilic, G. Pannexin1 contributes to pathophysiological ATP release in lipoapoptosis induced by saturated free fatty acids in

liver cells. American Journal of Physiology - Cell Physiology 2012; 303: C1034.

Yamada, Y., Kirillova, I., Peschon, J.J., Fausto, N. Initiation of liver growth by tumor necrosis factor: Deficient liver regeneration in mice lacking type I tumor necrosis factor receptor. Proceedings of the National Academy of Sciences of the United States of America 1997; 94: 1441–1446.

Yamamoto, K.N., Ishii, M., Inoue, Y., et al. Prediction of postoperative liver regeneration from clinical information using a data-led mathematical model. Scientific Reports 2016; 6: 1–9.

Yang, C.Y., Chen, J.B., Tsai, T.F., et al. CLEC4F Is an Inducible C-Type Lectin in F4/80-Positive Cells and Is Involved in Alpha-Galactosylceramide Presentation in Liver. PLoS ONE 2013; 8:.

Yona, S., Kim, K.W., Wolf, Y., et al. Fate Mapping Reveals Origins and Dynamics of Monocytes and Tissue Macrophages under Homeostasis. Immunity 2013; 38: 79–91.

Zafarnia, S., Mrugalla, A., Rix, A., et al. Non-invasive imaging and modeling of liver regeneration after partial hepatectomy. Frontiers in Physiology 2019; 10: 904.

Zigmond, E., Samia-Grinberg, S., Pasmanik-Chor, M., et al. Infiltrating Monocyte-Derived Macrophages and Resident Kupffer Cells Display Different Ontogeny and Functions in Acute Liver Injury. The Journal of Immunology 2014;

Zigmond, E., Varol, C. Two Roads Diverge in the Sick Liver, Monocytes Travel Both. Immunity 2020; 53: 479–481.

8. Acknowledgements

First and foremost, I want to thank Prof. Zeinab Abdullah who gave me the opportunity to do my PhD studies in her group. Her exceptionally good supervision and support in each direction was pivotal for this thesis and my education during the past years. Thank you for your continuous support, encouragement and challenges!

I would also like to thank the other members of my graduation committee consisting of Prof. Natalio Garbi, Prof. Katrin Paeschke and Prof. Irmgard Foerster who were unhesitant to take the duty of reviewing my thesis.

I thank Prof. Kurts who made it possible to convey this study in his institute and provided new ideas and important scientific input for this project.

Special thanks go to the other members of our Institute and specifically Sabrina, Sarah, Rebecca, Alissa and Lisa on whose support I could always count!

Within the last years, many of my colleagues became friends and shared many precious moments with me. Thanks to my friends who supported me and encouraged me also during the difficult phases of my PhD studies. Thank you for being there!

Most importantly, I want to thank my partner and my family for backing me up and providing confidence! This thesis would not have been possible without your support! Thank you very much!